



**HAL**  
open science

## The 2018 unrest phase at La Soufrière of Guadeloupe (French West Indies) andesitic volcano: Scrutiny of a failed but prodromal phreatic eruption

Roberto Moretti, Jean-Christophe Komorowski, Guillaume Ucciani, Séverine Moune, David Jessop, Jean-Bernard de Chabalier, François Beauducel, Magali Bonifacie, Arnaud Burtin, Martin Vallee, et al.

### ► To cite this version:

Roberto Moretti, Jean-Christophe Komorowski, Guillaume Ucciani, Séverine Moune, David Jessop, et al.. The 2018 unrest phase at La Soufrière of Guadeloupe (French West Indies) andesitic volcano: Scrutiny of a failed but prodromal phreatic eruption. *Journal of Volcanology and Geothermal Research*, 2020, 393, pp.106769. 10.1016/j.jvolgeores.2020.106769 . insu-02440761

**HAL Id: insu-02440761**

**<https://insu.hal.science/insu-02440761>**

Submitted on 15 Jan 2020

**HAL** is a multi-disciplinary open access archive for the deposit and dissemination of scientific research documents, whether they are published or not. The documents may come from teaching and research institutions in France or abroad, or from public or private research centers.

L'archive ouverte pluridisciplinaire **HAL**, est destinée au dépôt et à la diffusion de documents scientifiques de niveau recherche, publiés ou non, émanant des établissements d'enseignement et de recherche français ou étrangers, des laboratoires publics ou privés.

## Journal Pre-proof

The 2018 unrest phase at La Soufrière of Guadeloupe (French West Indies) andesitic volcano: Scrutiny of a failed but prodromal phreatic eruption



Roberto Moretti, Jean-Christophe Komorowski, Guillaume Ucciani, Séverine Moune, David Jessop, Jean-Bernard de Chabalière, François Beauducel, Magali Bonifacie, Arnaud Burtin, Martin Vallée, Sébastien Deroussi, Vincent Robert, Dominique Gibert, Tristan Didier, Thierry Kitou, Nathalie Feuillet, Patrick Allard, Giancarlo Tamburello, Tara Shreve, Jean-Marie Saurel, Arnaud Lemarchand, Marina Rosas-Carbajal, Pierre Agrinier, Anne Le Friant, Marc Chaussidon

PII: S0377-0273(19)30339-7

DOI: <https://doi.org/10.1016/j.jvolgeores.2020.106769>

Reference: VOLGEO 106769

To appear in: *Journal of Volcanology and Geothermal Research*

Received date: 17 June 2019

Revised date: 3 January 2020

Accepted date: 4 January 2020

Please cite this article as: R. Moretti, J.-C. Komorowski, G. Ucciani, et al., The 2018 unrest phase at La Soufrière of Guadeloupe (French West Indies) andesitic volcano: Scrutiny of a failed but prodromal phreatic eruption, *Journal of Volcanology and Geothermal Research*(2020), <https://doi.org/10.1016/j.jvolgeores.2020.106769>

This is a PDF file of an article that has undergone enhancements after acceptance, such as the addition of a cover page and metadata, and formatting for readability, but it is not yet the definitive version of record. This version will undergo additional copyediting, typesetting and review before it is published in its final form, but we are providing this version to give early visibility of the article. Please note that, during the production process, errors may be discovered which could affect the content, and all legal disclaimers that apply to the journal pertain.



## The 2018 unrest phase at La Soufrière of Guadeloupe (French West Indies) andesitic volcano: scrutiny of a failed but prodromal phreatic eruption

Roberto Moretti (1,2), Jean-Christophe Komorowski (1), Guillaume Ucciani (1,2), Séverine Moune (1,2,3), David Jessop (1,2,3), Jean-Bernard de Chabalière (1), François Beauducel (1,4), Magali Bonifacie (1,2), Arnaud Burtin (1,2), Martin Vallée (1), Sébastien Deroussi (1,2), Vincent Robert (1,2), Dominique Gibert (5), Tristan Didier (1,2), Thierry Kitou (1,2), Nathalie Feuillet (1), Patrick Allard (1), Giancarlo Tamburello (6), Tara Shreve (1), Jean-Marie Saurel (1), Arnaud Lemarchand (1), Marina Rosas-Carbajal (1), Pierre Agrinier (1), Anne Le Friant (1), Marc Chaussidon (1)

(1) Université de Paris, Institut de physique du globe de Paris, CNRS, F-75005 Paris, France

(2) Observatoire volcanologique et sismologique de Guadeloupe, Institut de physique du globe de Paris, F-97113 Gourbeyre, France

(3) Université Clermont Auvergne, CNRS, IRD, OPGC, Laboratoire Magmas et Volcans, F-63000 Clermont-Ferrand, France

(4) Institut des Sciences de la Terre - Institut de Recherche pour le Développement - BPPTKG - PVMBG Badan Geologi, Yogyakarta, Indonesia

(5) Géosciences Rennes UMR 6118 - Univ. Rennes I, Rennes, France

(6) Istituto Nazionale di Geofisica e Vulcanologia sezione di Bologna, via Donato Creti, Bologna, Italy

Corresponding Author: Roberto Moretti | email: moretti@ipgp.fr

**Abstract** - After 25 years of gradual increase, volcanic unrest at La Soufrière of Guadeloupe reached its highest seismic energy level on 27 April 2018, with the largest felt volcano-tectonic (VT) earthquake ( $M_L$  4.1 or  $M_W$  3.7) recorded since the 1976-1977 phreatic eruptive crisis. This event marked the onset of a seismic swarm (180 events, 2 felt) occurring after three previous swarms on 3-6 January (70 events), 1<sup>st</sup> February (30 events, 1 felt) and 16-17 April (140 events, 1 felt). Many events were hybrid VTs with long-period codas, located 2-4 km below the volcano summit and clustered within 2 km along a regional NW-SE fault cross-cutting La Soufrière. Elastic energy release increased with each swarm whereas inter-event time shortened. At the same time, summit fractures continued to open and thermal anomalies to extend. Summit fumarolic activity increased significantly until 20 April, with a maximum temperature of 111.4 °C and gas exit velocity of 80 m/s,

before declining to  $\sim 95^{\circ}\text{C}$  and  $\sim 33\text{m/s}$  on 25 April. Gas compositions revealed increasing C/S and  $\text{CO}_2/\text{CH}_4$  ratios and indicate hydrothermal P-T conditions that reached the critical point of pure water. Repeated MultiGAS analysis of fumarolic plumes showed increased  $\text{CO}_2/\text{H}_2\text{S}$  ratios and  $\text{SO}_2$  contents associated with the reactivation of degassing fractures ( $T=93^{\circ}\text{C}$ ,  $\text{H}_2\text{S}/\text{SO}_2\approx 1$ ). While no direct evidence of upward magma migration was detected, we attribute the above phenomena to an increased supply of deep magmatic fluids that heated and pressurized the La Soufrière hydrothermal system, triggering seismogenic hydro-fracturing, and probable changes in deep hydraulic properties (permeability) and drainage pathways, which ultimately allowed the fumarolic fluxes to lower. Although this magmatic fluid injection was modulated by the hydrothermal system, the unprecedented seismic energy release and the critical point conditions of hydrothermal fluids suggest that the 2018 sequence of events can be regarded as a failed phreatic eruption. Should a similar sequence repeat, we warn that phreatic explosive activity could result from disruption of the shallow hydrothermal system that is currently responsible for 3-9 mm/y of nearly radial horizontal displacements within 1 km from the dome. Another potential hazard is partial collapse of the dome's SW flank, already affected by basal spreading above a detachment surface inherited from past collapses. Finally, the increased magmatic fluid supply evidenced by geochemical indicators in 2018 is compatible with magma replenishment of the 6-7 km deep crustal reservoir feeding La Soufrière and, therefore, with a potential evolution of the volcano's activity towards magmatic conditions.

**Key words:** volcanic unrest; hydrothermal systems; phreatic eruptions; degassing ; hydrofracturing and hydroshearing

## 1. Rationale

Andesitic volcanoes develop hydrothermal systems that hamper a direct interpretation of the subterranean magma state and evolution from the physical and chemical signals measured at the surface. This limitation contributes enormously to the dilemma of whether observed volcanic unrest has a magmatic origin ("magma on the move") or a non-magmatic origin from a change in the hydrothermal system ("fluids that are not magma on the move") (Pritchard et al., 2019) and produces major uncertainties in the short-term forecasting of an imminent eruption. Such uncertainties are severe also for the short-term eruption hazard from non-magmatic unrest, as andesitic volcanoes may develop explosive phreatic eruptions (e.g., Barberi et al., 1992). Characterized by the absence of juvenile magmatic material, phreatic eruptions are triggered by the injection of fluids and heat of magmatic origin into the hydrothermal system, which becomes

strongly overpressured (Barberi et al., 1992; Mastin et al., 1995; Rouwet et al., 2014 and references therein). In many cases phreatic eruptions are precursors to magmatic eruptions of both explosive or effusive nature, or could serve as the decompression mechanism prior to phreatomagmatic eruptions (Rouwet et al., 2014). However, the input of mass and heat into the hydrothermal system challenges monitoring systems, being often a short-term and too low amplitude event that does not result in clear precursory signals within the time frame of monitoring (Barberi et al., 1992; Rouwet et al., 2014). If on one hand the hydrothermal system tends to buffer and mask the inputs of deep hot fluids, on the other side secondary mineral precipitation and the presence of low-permeable elemental sulphur can seal hydrothermal systems in localized, shallow and overpressured portions that can rapidly reach the threshold to phreatic eruptive activity (Salaun et al., 2011; Rouwet et al., 2014). Therefore, it is of the outmost importance to track and understand the anomalies in observation data that are related to the input of deep hot magmatic fluids into the hydrothermal system. The ongoing unrest at La Soufrière explosive andesitic volcano, on the island of Guadeloupe (French West Indies), well represents the aforementioned issues and offers us this possibility.

## **2. Introduction and volcanological background**

La Soufrière de Guadeloupe is located in the Lesser Antilles arc under which the Northern Atlantic ocean plate is subducting beneath the Caribbean plate at a rate of ~2 cm/year (Feuillet et al., 2002, 2011). La Soufrière belongs to the Grande Découverte volcanic complex, built during the past 445000 years and comprising three stratovolcanoes: Grande Découverte, Carmichael and Soufrière (Komorowski et al., 2005). La Soufrière is the most recent volcanic edifice and its eruptive history began about 9150 years ago. It is an active explosive volcano that has experienced magmatic and non-magmatic "phreatic" eruptions, in the past (Komorowski et al., 2005; Feuillard et al., 1983; Legendre, 2012). The most recent major magmatic eruption dates from 1530 AD and began with a collapse of the volcanic edifice causing a landslide that reached the coast 10 km away. The explosive eruption that followed resulted in ash and pumice fallout on southern Basse-Terre, the outpouring of pyroclastic flows (incandescent avalanches of gas, ashes and rocks) that reached distances of 5-7 km from the volcano, and mudflows (Boudon et al., 2008; Komorowski et al., 2008). It ended with the formation of the present Soufrière dome. This magmatic eruption is representative of the hazards caused by an explosive eruption of medium magnitude, although more intense eruptions have been identified in the last 10,000 years (Komorowski et al., 2005; Legendre, 2012). Recent studies suggest that a smaller magmatic eruption took place in 1657 (Legendre, 2012; Hinks et al., 2014).

Since that time the historical activity of La Soufrière has been characterized by persistent hydrothermal manifestations (fumaroles, solfataras, hot springs) culminating into intermittent non-

magmatic steam-driven (phreatic) eruptions. Major phreatic eruptions occurred in 1797-1798, 1797-1798, 1812, 1836-1837, 1976-1977, and minor ones in 1690 and 1956 (Lherminier 1937a-c, Komorowski et al., 2005; Legendre, 2012; Hinks et al., 2014).

Fumarolic degassing was initially concentrated at the Cratère Sud (hereafter CS, **Figures 1,2**), but gradually extended along the Napoleon fracture (1997) and to the Tarissan crater lake (1998). In 1998, the sudden onset of chlorine-enriched degassing from the CS fumaroles marked a significant change in the behaviour of the magmatic-hydrothermal system (Komorowski et al., 2001; Komorowski et al., 2005; Villemant et al., 2005, 2014). In parallel, boiling ponds of extremely acid water formed in 1997 at CS (mean pH of -0.1 and  $T^{\circ}\text{C} = 88.8 \pm 8.6$  between 1998 and 2001; OVSG-IPGP data and Rosas-Carbajal et al., 2016), and since 2001 at the bottom of the Cratère Tarissan (mean pH of -0.2 in 2014) (Komorowski et al., 2005, Villemant et al., 2005; Komorowski, 2001; OVSG-IPGP, 1999-2019) (**Figures 1,2**). Whereas the acid pond at the CS persisted for seven years, leaving place to an intense fumarolic degassing in 2003 (Komorowski et al., 2005), the acid thermal lake in the Cratère Tarissan continued to be active until now (OVSG-IPGP, 1999-2019).

After 2007, fumarolic activity also propagated to Gouffre 56 (the explosion pit formed during the 1956 phreatic eruption, hereafter G56; Jolivet, 1958 and **Figures 1,2**) then to the nearby Lacroix fracture (late 2011) and more eastward to the Breislack crater (2013; **Figures 1,2**). The so-called Breislack fracture cutting the lava dome was involved in 4 of the 6 historical non-magmatic phreatic explosive eruptions of La Soufrière in 1797-1798, 1836-1837, 1956 (October), and 1976-1977 (eruption onset on 8 July 1976) (Komorowski et al., 2005; 2017; Rosas-Carbajal et al., 2016). The degassing area continued to expand on top of the lava dome, with the appearance of a new fumarole (Napoleon Nord, hereafter NAPN; **Figures 1,2**) in July 2014, and of new vents (Napoleon Est 1 and Napoleon Est 2, hereafter NAPE1 and NAPE2) that opened further east (**Figures 1,2**) between 8 and 10 February 2016 with a very small steam blast (in the sense of Mastin, 1995) with hot mud projections over a distance of 5-10m radius.

The high concentration of hydrochloric and sulphuric acid plumes accompanied by high gas flows and a steady trade wind regime has destroyed the vegetation on the southwest flank of La Soufrière, contributing to small landslides of the degraded slopes, and to gas smell nuisances potentially harmful to people's health and felt since December 1997 by the population living downwind the volcanic plume (OVSG-IPGP, 1999-2019).

This reactivation ongoing since 1992 has required the implementation of an alert level scale set as of 1999 at the yellow level (i.e., vigilance), on a four-level scale (green, yellow, orange and red; OVSG-IPGP, 1999-2019). However, concern further increased recently owing to an accelerating unrest phase that developed in February-April 2018 and culminated with a magnitude

4.1 seismic activity peak, of same magnitude as the strongest earthquake recorded during the 1976-77 phreatic crisis (Feuillard et al., 1983).

In this study, we report and discuss the geophysical and geochemical features we observed to be associated with this recent peaking activity. Based on various data types, we attempt to interpret the triggering mechanism (magmatic versus hydrothermal) of this event and its significance within the unrest sequence initiated since 1992 at La Soufrière. Specifically, we try to decipher whether the observed phenomena may involve or not changes in a deep magmatic source and how unrest observables relate to the vigorous circulation and interaction of water, steam and hot gases in the porous and fractured host rocks.

### 3. Monitoring data: observations and preliminary assessments

In this section we present the data and observations resulting from our networks and measurements campaigns. A preliminary assessment is also given for each class of observation (seismic, geodetic, thermal, geochemical; see also Supplementary Table 1) with reference to the existing literature, in order to highlight the information to be extracted and then discussed quantitatively in section 4.

#### 3.1 Seismic activity

As mentioned above, after a brief repose period that followed the 1976-77 eruptive crisis, volcanic seismicity at La Soufrière renewed in 1992 (**Figure 3**), concomitantly with the degassing unrest. Since then more than 14000 earthquakes of volcanic origin were recorded (**Figure 3**). Most of them were of low local magnitude  $M_L$  ( $< 1$ ) and clustered in swarms lasting from a few days to a few weeks. Seventeen of all these volcanic earthquakes were strong enough to be felt locally, including five in 2013, one in 2014, and the most recent ones on 1 February, 16 April and 27 April 2018 (OVSG-IPGP, 1999-2019). After a relative minimum in both energy and number of events in 2016, the volcanic seismicity increased drastically since 2017 (**Figure 3**). Compared to previous years, this increase can only partly be explained by improvements in the resolution of the seismic network. Thereafter, we describe the temporal and energy pattern of recent seismicity (from 1<sup>st</sup> January 2017 to 30 July 2018). First of all, we list here the main features of observed waveforms (**Figure 4**):

- volcano-tectonic (VT) signals, showing a high-frequency content (5-20 Hz) (**Figure 4a**);

- long period (LP) signals, characterized by a low frequency (1-5 Hz), often appearing as nearly monochromatic signals (**Figure 4b**) and associated with resonance phenomenon of the hydrothermal fluids in cracks (Ucciani, 2015a);
- hybrid (HY) signals, showing the high-frequency content typical of VT events, most often at the beginning of the waveforms and accompanied by a low frequency content which often appears at the signal onset and is observed to the end of the event, in the signal coda (Ucciani, 2015a; **Figure 4c**);
- nested volcanic (VE) signals, appearing as small seismic packets in which events occur on the coda of the previous one (**Figure 4d**), and which are not concomitant or precursor to a particular phenomenon. VE events differ from spasmodic burst defined in Hill et al. (1990) and consist in a sequence of several seismic events with very short inter-times, with very often more than 6 seismic events in a short sequence (~ 10s; Ucciani, 2015a).

During 2017, the OVSG identified a total of 1432 volcanic earthquakes (**Figure 5a**), all with local magnitude  $M_L < 0.9$ , except for three events  $M_L$  1 -to 1.3 on 13 December. Seventy-two of the recorded events were of the LP type, whereas the majority (1360) were HY-type, with few VTs, and were similar to the seismic activity of dominantly volcanic origin observed in the previous years, implying a temporal continuity of seismic sources and processes (Ucciani, 2015a,b). HY events are produced by fracturing and reservoir resonance phenomena related to the propagation of fluids. Some of these events (250 in 2017) are nested (VE-type), thus representing multiple closely-spaced ruptures within a patchy fractured medium. Given the superficial distribution of the hypocenters (mainly at depths between -0.8 km and 0.8 km below sea level – b.s.l.) (**Figures 5b,6a**) such a low-energy micro-seismicity attests to the vivacity of hydrothermal circulations within the shallow part of La Soufrière edifice (Ucciani, 2015a,b; OVSG-IPGP, 2017). The 2017 activity released a total of 48.5 MJ of seismic energy (**Figure 5c**)

The overall seismicity measured at La Soufrière in the first half of the year 2018 (**Figures 5a-c,6b**) will be here discussed for four different relevant periods (January, February-March, April, May to July) that were chosen to provide a clear explanation of the sequence of observed key events, which are illustrated in **Supplementary Figures S1-S5**. In January 2018, 78 earthquakes of volcanic origin were detected and located essentially under the dome of La Soufrière, at less than 0.5 km depth b.s.l., with the exception of an event (**Figure 5b, Supplementary Figure S1**). Most of them occurred concentrated in a swarm between January 2 and 5 (key event 1). The total energy released was about 3 MJ (**Figure 5c**). A stronger seismic swarm of > 30 earthquakes (key event 2) then succeeded on 1<sup>st</sup> February 2018 between 12:55 local (16:55 UT) and 15:31 local. All hypocenters were located between 0.5 and 1 km b.s.l. (2 and 2.5 km deep under the dome summit) (**Figure 5b, Supplementary Figure S2**). The swarm started with events of very small magnitude but showed an

increasing energy that ended with three earthquakes of magnitude  $\geq 1.4$ , among which a felt one ( $M_L$  2.1, depth 1 km b.s.l., intensity III in the Saint-Claude commune (OVSG-IPGP, 2018a). The seismic energy released reached about 130 MJ (**Figure 5c**). Between 2 February and 31 March the seismicity continued with 170 VT and hybrid-type earthquakes. An intensification of the activity can be observed since mid-March (**Figure 5a**); Earthquakes were located under the dome of La Soufrière, at less than 0.5 km depth b.s.l. (**Figure 5b**), and of very low magnitude, releasing a total seismic energy of 14.7 MJ from 2 February to 31<sup>st</sup> March (**Figure 5c**).

During April 2018, 545 volcanic earthquakes occurred beneath but also also around the dome of La Soufrière, within a depth interval extending from -1 to 5.7 km b.s.l. The most prominent seismic activity concentrated in two swarms: on 16-17 April (key event 3: > 140 VT and hybrid earthquakes in 48 hours; **Figure 5a,b, Supplementary Figure S3**) and 27-28 April (key event 4: > 180 earthquakes in 24 hours; **Supplementary Figure S4**). The first swarm was located under the SW base of the volcano (between -0.5 and 2.6 km b.s.l.). Twelve events had a magnitude  $\geq 1.0$  and hypocenters between 1 km and 1.6 km b.s.l. (or 2.5 to 3.1 km of depth below the summit). The main earthquake, at 18h59 local on 17 April 2018 ( $M_L$  2.1 and depth 1.2 b.s.l.) was very slightly felt by the inhabitants of St Claude (weak macroseismic intensity, II; OVSG-IPGP, 2018b).

The second seismic swarm was instead located about 2 km north-northwest of La Soufrière summit dome. Two-thirds of the earthquakes occurred in the first two hours of activity and were of very small magnitude, with foci distributed between 1.0 and 3.1 km b.s.l. (or 2.5 to 4.6 km below the summit, **Figure 5b**). However, at 20:15 (local) on 27 April a strong shock with  $M_L$  4.1 occurred, becoming the strongest volcanic earthquake recorded at La Soufrière for 42 years. Located 1.9 km below sea level, this earthquake was largely felt throughout Guadeloupe. In the nearest affected areas, a macroseismic intensity of V was estimated (OVSG-IPGP, 2018c). These two swarms in April 2018 released about 200 MJ and 90,000 MJ, respectively (**Figure 5c**), the majority of which during the  $M_L$  4.1 earthquake on 27 April. Interestingly, the 27-28 April swarm is characterized by purely VT events, not showing any long-period coda (**Figure 4b**). However, between 18 and 25 April, it was preceded by ~30 hybrid events that occurred in a zone surrounding the hypocentral region of the 16-17 April swarm.

During May, June and July 2018, 195 VT and particularly HY earthquakes of weak magnitude ( $\leq 1$ ) occurred, beneath (between -1 and 2 km depth b.s.l.) and around the dome of La Soufrière (**Figure 5a,b, Supplementary Figure S5**). Seismic activity in May-July released 10 MJ of seismic energy and marks a period of relative seismic calm after the highly energetic 27-28 April swarm.

### 3.2 Ground deformation

### 3.2.1 GNSS data and patterns of deformation'

**Figure 7** presents the velocity field determined by Global Navigation Satellite System (GNSS) continuous and campaign measurements of La Soufrière network, with respect to the Guadeloupe archipelago (de Chabalier et al., in preparation). The network has evolved significantly since the first measurements in 1995 and the two first permanent stations in 2000 (HOUE and SOUF). The most important step occurred around 2015, with deployment of new permanent stations (CBE0, MAD0, PAR1, FNG0, AMCO, PSA1, TAR1) and more frequent reiteration campaigns. Therefore, velocity uncertainties depend mainly on the observation timespan and vary from less than 0.5 mm/yr for the oldest stations with about 20 years of data recording, to several mm/yr for stations installed recently. Stations located on the flanks of La Soufrière massif (HOUE, MAD0, CRB0, CBE0, FNG0, MATO, and PAR1 in **Figure 7a**) show velocities that vary from 0 to 1.5 mm/yr. The time series of these stations display remarkably steady state rate suggesting no significant variations of processes at depth during the last twenty years. In particular, the general pattern of the deformation is not consistent with any inflation/deflation at depth.

To estimate the sensitivity of the network, we computed the Green's functions of a simple isotropic point source model using the varying-depth method to take the topography into account (Williams and Wadge, 1998) to determine the volume variations,  $\Delta V$ , in a 3-D grid (not shown) that can induce a maximum of 1mm of displacement on the GNSS stations at the surface, considered here as an arbitrary threshold (de Chabalier et al., in preparation). For a source located at 10 km of depth below the dome, the detectability threshold of  $\Delta V$  decreases from 800.000 m<sup>3</sup> in 1995 to about 500.000 m<sup>3</sup> after 2015. We also conclude that since 2015 the maximum depth of detection for a  $\Delta V \approx 100.000$  m<sup>3</sup> reaches 4-5 km. The deformation field of the flanks of the volcano does not reveal significant intrusion during the period of observation but we can not exclude small intrusions, especially at depth larger than 6-7 km and in any case below the brittle-ductile transition. Nevertheless, the Basse-Terre deformation field can then be chosen as a reliable reference to determine the volcanic deformation of La Soufrière dome.

At the scale of the La Soufrière volcano, there is little deformation (less than 2mm/yr on horizontal components) on the peripheral (greater than 0.5 km) sectors (NEZ2, AMCO, AMC1, RCB1, RCL2 in **Figure 7b**), except in the southwestern one. On the summit lava dome, the deformation signal is globally radial and reaches 3 to 7 mm/yr. Large displacement vectors (up to 9 mm/yr) toward the southwest point to a sliding zone downslope to the Bains Jaunes site, 1.3 km away from the top of the dome (**Figure 7**).

In first approximation the horizontal components of GNSS velocities show that the pattern of the dome deformation is radial and centered on the Cratère Tarissan and Cratère Napoleon. Such

a pattern, however, is disturbed by major faults and fractures crossing through the dome (North, Napoleon-Gouffre 56-Breislack system and the Dolomieu system, **Figure 1**), resulting in three well identified blocks: a western block, an eastern block and a southern block (**Figure 7b**). The aforementioned spreading to the south and southwest further superimposes on this pattern. The single exception in above pattern is the point ECH1, on top of a scoria cone (**Figure 7b**), which slides downslope at a rate of 3.4 mm/yr to the north-northwest.

The thin orange zone in **Figure 7b** highlights the dome sector where the strongest azimuthal direction gradients occur, together with important deformation. It corresponds to the Napoleon-Breislack fracture where fumaroles reactivated most recently between 2006 and 2014. This is the main extension zone whose opening reflects the combined effect of both hydrothermal flow (Rosas-Carbajal et al., 2016) and the south-west flank sliding of the dome. The other gradient zones (yellow-dashed in **Figure 7b**) are scarcely or not at all marked by fumarolic activity and fracturing, but are characterized by diffuse soil degassing (Komorowski et al., 2013; **Figure 1**).

### 3.2.2 Extensometry

One-dimensional extensometry measurements are taken on fractures 0.4 to 20 m wide. Since the installation of the extensometry network in 1995, measurements showed a general tendency of opening of the faults and fractures in the active fumarolic zones, as well as along the dome fracture that formed during the phreatic eruption of 30 August 1976. Gouffre Napoleon (NAP1 in **Figure 8**) is the site affected by the largest extension and shows that extensional movements occurred with different rates in different periods (**Figure 8b**). Specifically, we recognize four consecutive periods (1995-1999, 1999-2003, 2003-2016, 2016-to date), the second marked by quiescence and the others by extension, with the most recent period characterized by the largest extension rate.

In general, fracture opening at some sites appears to be partially compensated by local closing of other, adjacent, fractures located outside or on the margins of the active fumarolic zone. This behaviour strongly suggests that the shallow stress field is determined at the depth of the hydrothermal system by a mechanism similar to simple shear (Buck et al., 1988). The opening trend at almost all fractures observed since mid-2016 is thus compatible with a pressure increase in the hydrothermal source, determining the displacement field and the switch to conditions close to pure shear (Buck et al., 1988).

Interestingly, a closer inspection of data between 9 March and 25 April 2018 shows a reversal in this opening trend (**Figure 8a**), implying a slight closure of the active fumarolic zones on the top of the dome except for one point along Gouffre Dupuy (DUP1, **Figure 8a**). Such a reversal thus indicates a hydrothermal pressure drop. Instead, subsequent measurements in June and August

2018 reveal a renewal of the generalized extensional trend (**Figure 8a**), suggesting a new overpressure phase of the hydrothermal source of deformation.

### 3.3 Fumarole thermal data

CS fumaroles (CSS, CSC, CSN; **Figure 2**) show generally high flow rates and large deposits of solid sulphur. A decrease in the discharges was observed after the passage of hurricane Maria (mid-September 2017), probably in response to the huge amount of water infiltrated into the subsoil and thus into the shallow hydrothermal system (the measured rain water level on top of the dome was 440mm in 24 hours due to the hurricane's passage, 2017; OVSG-IPGP, 2017). Starting in November 2017 fumarole fluxes have begun to increase to pre-hurricane values.

Driven by the interaction between hot magmatic fluids and the hydrothermal system, La Soufrière manifestations develop a number of sites where heat is preferentially transported to the surface, as commonly observed at many volcanoes in hydrothermal stage (e.g. Chiodini et al., 2001; Harris, 2013, Sigurdsson et al., 2015). Convection of water vapour transports heat from depth to the surface. Vapour travelling through the most porous conduits leads to fumaroles (e.g. CS). Near-surface steam condensation leads to large temperature gradients, conduction of heat to the surface forming thermal anomalies (e.g. Faille de la Ty, FTY; **Figure 1**). Condensed water escapes laterally, mixing with meteoric water and forming hot springs. At La Soufrière the latter contribute marginally to the overall heat budget (Allard et al., 2014; Gaudin et al., 2016) and we will not discuss them further. Moreover their chemistry and temperature have remained stable over the last 10 years (Villemant et al. (2005, 2013; Ruzié et al., 2012, 2013; OVSG-IPGP, 1999-2019). Accordingly, thermal monitoring in the form of (discrete) manual temperature measurements have been carried out over the last 20 years, roughly one per month. More recently, continuous measurement stations utilising PT100/PT1000 resistance temperature detectors have been installed at several key fumarolic sites with acquisition rates of 1s. At the time of the 2018 crisis, the CS fumaroles (central, north and south, labelled CSC, CSN, CSS, respectively; see **Figure 2** for location) had been instrumented with continuous measurements commencing on 14 April, and were routinely measured manually (for CSC, CSN and NAPN). Additionally, vent speed measurements were made using a Pitot tube instrument at CSC, CSN, CSS and NAPN though, especially in the case of CSS which requires specialised roped-access techniques, these were done less frequently.

The historical temperature record shows that fumarolic vents typically have temperatures corresponding to saturated steam vapour at the pressure of the summit (~95 °C) (**Figure 9a**). Fumaroles CSC and CSN have shown short-lived fluctuations up to 140 °C (cf. June-1999 to Feb-2000 at CSN) and longer-duration increases up to 110 or 120 °C (cf. Sept-2011 to Mar-2013 at CSC). Early during the April-2018 unrest phase, the fumarole temperatures rose again, attaining maxima of

111.4°C at CSC on 3<sup>rd</sup> April, and 109.7 °C at CSN on 23<sup>rd</sup> March (according to the manual measurements). We also note the remarkably constant temperature at NAPN at around 95 °C since its appearance in 2014 (**Figure 9b**). After the aforementioned maxima, temperatures dropped rapidly to 104°C (19 April 2018) and then to the background saturated vapour value (96 °C, 28 April 2018). The rapid temperature drop in the CS area is well detailed by the continuous measurements at CSC and CSN (**Figure 9b**) which demonstrates that the saturated steam temperature was reached on 26 April, one day prior the  $M_L$  4.1 earthquake. Indeed, the continuous measurements indicate that the temperature decreased in several stages, the temperature decreasing by 2-4 degrees at each stage. From these data, we conclude that during the early 2018 unrest phase, fumarolic fluid at CS was superheated with respect to the temperature of boiling water at the elevation (**Figure 9**).

In parallel, venting gas speeds measured at CSC and CSN dropped from 80 and 53 m/s, respectively on 6<sup>th</sup> April to 20 and 33 m/s, respectively, on 25<sup>th</sup> April. Following the  $M_L$  4.1 earthquake fumarolic flow rates decreased, becoming so low that, on 29<sup>th</sup> April, it was not possible to reliably measure gas speeds from vents located at any of the CS vents. Fumarole heat flux, which is globally proportional to vent speed, thus also decreased by a factor of four from around  $20.0 \pm 4.5$  MW to around  $5.0 \pm 1.1$  MW (see **Figure 10**; for details of these calculations, please refer to Supplementary Material). These vent speeds and the temperature measurements noted above suggest that the total steam flux at CS dropped from a maximum of around  $8.0 \pm 1.0$  kg/s at the beginning of April to about  $3.5 \pm 0.5$  kg/s soon after the 27 April. This latter value is of same order as CS steam fluxes previously estimated from MultiGAS traverses in 2006 (0.87 kg/s), 2012 (1.72 kg/s) and May 2016 (0.52 kg/s) (Allard et al., 2014; Tamburello et al., in 2019), indicating a slow but significant over the past decade or so. Instead, our values of steam and enthalpy flux are substantially lower than those of Gaudin et al., (2016), who estimated the CS steam and enthalpy fluxes (thermal camera data collected in 2010) to be  $19.5 \pm 4.0$  kg/s and  $48.0 \pm 9.8$  MW, respectively. We note that Gaudin et al. (2016) estimated the fluxes at some distance from the vent and did not correct for the effect of entrainment of ambient air into the plume and the resulting increase in plume volume. As such, it is peculiar, even given the fluctuating though increasing activity at La Soufrière, that the 2010 survey found such large values for both steam and enthalpy flux, particularly with respect to the 2006 and 2012 MultiGas-based estimation. It may be the case that the approximations made during their study affected their results more than was anticipated, potentially doubling the measurement uncertainty, in which case their values fall more in line with those found here. A complete inventory of the heat flux discharged by the dome (particularly its partitioning between fumarolic, soil diffuse and hot spring fluxes) is currently missing. Its temporal evolution since the 2010 estimate (Gaudin et al., 2016) is thus uncertain. However, we must suspect a thermal flux increase since 2010, because of the reactivation of many emission sites (e.g., G56, Lacroix Superieur, NAP; see below), the emergence of new sites

(NAPN, NAPE1, NAPE2) and the concurrent increases in soil temperatures and extent of vegetation decay in soils with degassing at the summit (OVSG bulletins).

### 3.4 Fluid Geochemistry

#### 3.4.1 Fumarole chemistry

For fumarolic sampling and gas analysis at La Soufrière the OVSG-IPGP Observatory uses the "Giggenbach"-type soda bottle methodology (e.g., Giggenbach and Goguel, 1989; see Supplementary Material). This method permits to obtain the complete, internally consistent, chemical composition of the fumarolic fluid, with an accuracy and precision that could not be attained by previous chemical routines, essentially based on  $P_2O_5$ -filled sampling bottles (Fabre and Chaigneau, 1960). The reader may refer to Allard et al. (2014) and particularly to Villemant et al. (2014) for the database of gas samples obtained with this latter sampling technique. Since November 2017, the procedures for gas sampling and analysis were improved at OVSG-IPGP. For consistency, we here report and discuss only the data obtained from that date. **Figure 11** shows the temporal evolution of major chemical indicators (molar ratios for gas/steam, C/S,  $CO_2/CH_4$ , He/ $CH_4$ ,  $H_2/H_2O$  and  $CO/CO_2$ ) in the CSC fumarole, the most accessible and surveyed fumarole on top of La Soufrière (see **Table 1** for chemical analyses). For comparative thermodynamic calculations (see section 4.2), we also include the other available and fully consistent soda-based data from summit emissions, sampled in 1997 by Brombach et al. (2000) and in July 1976 by Chevrier et al. (1976).

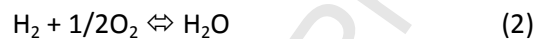
Since water vapour in La Soufrière fumaroles is essentially of meteoric (rainwater) origin whereas the major gas components have a magmatic derivation (Brombach et al., 2000; Villemant et al., 2014; Allard et al., 2014), variations of gas/steam ratio essentially reflect changes in the proportion of the deep, magma-derived, gas with respect to the meteoric component in the hydrothermal system. This ratio can increase due to either the arrival of magmatic gases or/and the condensation of water vapour. Instead, increased boiling will make it decreasing because of steam addition. As regards the C/S ratio, it can increase either due to either the uprise of deep magmatic gas (often associated with a temperature increase), because  $CO_2$  in magmas is much less soluble than sulfur-bearing gas species and then degasses much earlier (e.g., Moretti et al., 2003 and reference therein) or a loss of sulphur in the hydrothermal system (scrubbing of  $SO_2$  and  $H_2S$ , as well as precipitation of sulfides and/or native sulphur; Allard et al., 2014; Villemant et al., 2005; Tamburello et al., 2019), this latter process being often associated with a decrease in temperature.

Methane is absent in hot magmatic gases and is a typical component of low-temperature or/and reduced hydrothermal fluids (Giggenbach, 1987). The  $CO_2/CH_4$  ratio is thus a powerful

indicator of magma degassing episodes because it is orders of magnitude higher in magmatic gases than in hydrothermal fluids. Accordingly, an increase of  $\text{CO}_2/\text{CH}_4$  in fumaroles clearly indicates an enhanced supply of  $\text{CO}_2$ -rich oxidized and hot magmatic gas whose effect will be to oxidize and potentially warm the base of the hydrothermal system, thereby limiting the conversion of  $\text{CO}_2$  in  $\text{CH}_4$  at low temperature (Chiodini, 2009). Depending on the extension of the hydrothermal system and the intensity of the magmatic gas injection, there may be a time delay between the gas arrival and the observation of a  $\text{CO}_2/\text{CH}_4$  peak anomaly at the surface (Chiodini, 2009).

Similarly, peak increases of the  $\text{He}/\text{CH}_4$  ratio point to the arrival of deeply derived gases of either magmatic (e.g., Chiodini et al., 2015) or crustal origin, which can be discriminated on basis of the  $^3\text{He}/^4\text{He}$  isotopic ratio. At La Soufrière, helium present in both fumaroles and hot springs has been shown to be of pure MORB-type magmatic origin (e.g. Allard, 1983; Ruzié et al., 2012, 2013; Jean-Baptiste et al., 2014). Owing to their much lower mass than  $\text{CO}_2$ , both  $^3\text{He}$  and  $^4\text{He}$  can diffuse much faster than  $\text{CO}_2$  over the ascent path of fluids, so that deep gas inputs into a hydrothermal system should be first detected by increasing  $\text{He}/\text{CH}_4$  and later on by increasing  $\text{CO}_2/\text{CH}_4$ .

$\text{CO}$  and  $\text{H}_2$  are fast reactive species obeying the following equilibria



Owing to the fast kinetics of these two reactions, both the  $\text{CO}/\text{CO}_2$  and  $\text{H}_2/\text{H}_2\text{O}$  ratios are insensitive indicators of late-stage gas re-equilibration upon ascent and changing oxidation environment ( $f\text{O}_2$ ). Increasing  $f\text{O}_2$ , at a given  $T$ , favors the oxidized molecule (either  $\text{H}_2\text{O}$  or  $\text{CO}_2$ ). The geothermal literature has shown that along typical unspecified hydrothermal mineral buffers of the type  $\log f\text{O}_2 = a - b/T(\text{K})$  (with  $a$  and  $b$  being positive constants) both  $\text{H}_2/\text{H}_2\text{O}$  and  $\text{CO}/\text{CO}_2$  ratios increase with increasing  $T$ , hence  $f\text{O}_2$  (e.g., D'Amore and Panichi, 1980; Giggenbach, 1980; Chiodini and Marini, 1998). In addition,  $\text{H}_2/\text{H}_2\text{O}$  values can also reflect the occurrence of secondary phenomena, such as boiling and steam condensation from separated and equilibrated single vapours (Chiodini and Marini, 1998; Brombach et al., 2000; see also section 4.2). On the other hand, the  $\text{CO}/\text{CO}_2$  ratio is not affected by secondary effects, so that its increase is more directly associated to the heating of the hydrothermal system (Chiodini and Marini, 1998; Chiodini et al., 2015). It is worth recalling that coexistence of water vapour and the liquid (boiling pure water or brines) implies that heating and pressurization are associated, determining the joint increase of both temperature and pressure fixed along the liquid-gas univariant equilibrium.

We note that the gas/steam ratio did not change appreciably in concomitance with seismic swarms, though it did increase by a factor of four (**Figure 11a**) on 2 June, before rapidly returning to previous value on 21 June. The present-day gas/steam ratios, except the peak values, are in line with those measured in 1997 (Brombach et al., 2000) and also 1976 (Chevrier et al., 1976). The C/S ratio

fluctuates around a mean value of 4 (**Figure 11b**), within the range of 1976 values (Chevrier et al., 1976). This is however well below the 1997 data, that were recorded after the dome summit re-activation, when the “dry” gas was essentially made of CO<sub>2</sub> (Brombach et al., 2000), prior to the sulphur enrichment and the appearance of HCl in 1998 (Komorowski et al., 2005; Villemant et al., 2014). No change of the C/S ratio is recorded before, during or after the seismic swarms. The rise in the CO<sub>2</sub>/CH<sub>4</sub> ratio (**Figure 11c**) appears to occur gradually throughout the period of observation (from 100000 in November 2017 to 150000 on 30 July 2018) and is characterized by an increase on late April, followed by a peak at 260000 on 2 June. We note also that Brombach et al. (2000) did not report CH<sub>4</sub> emanating from the summit fumaroles in 1997, which suggests that the activity of the summit hydrothermal system was at its early stage, developing under the forcing of deep magmatic gases.

The behavior of gas/steam and CO<sub>2</sub>/CH<sub>4</sub> indicators is likely related to the increasing influx of a deep gas component, heavily discharged at the surface on 2 June, and bearing a magmatic signature particularly evidenced by the CO<sub>2</sub>/CH<sub>4</sub> ratio. Nevertheless, we cannot exclude that secondary effects such as steam condensation upon cooling, and the consequent scrubbing of soluble components, play a role in determining the observed values, especially for sulphur species and so the C/S ratio. This effect is well known to have been important at La Soufrière de Guadeloupe (Brombach et al., 2000), and has certainly contributed to the development of the shallow hydrothermal system. However, its role is presently subordinate and the chemical variations shown by the hydrothermal fluids are dominated by primary compositional variations due to degassing of the source. This is in fact well testified by 2 June samples, for which steam condensation cannot explain why they also have the largest CO<sub>2</sub>/CH<sub>4</sub> value, given the much larger solubility of CO<sub>2</sub> with respect to CH<sub>4</sub> in condensed steam (Giggenbach, 1980).

These elements, along with the temperature increase, confirm that the hydrothermal system was infiltrated by a major pulse of deep gas. This pulse determined also the rise in He/CH<sub>4</sub>, H<sub>2</sub>/H<sub>2</sub>O, and CO/CO<sub>2</sub> ratios, all peaking around 28 April and 2 May (**Figure 11d-f**). The He/CH<sub>4</sub> ratio (**Figure 11d**) increases between November 2017 and late July 2018 by a factor of three, showing the increasing contribution of a deep gas, likely of magmatic origin (e.g., Chiodini et al., 2015). A sharp peak in He/CH<sub>4</sub> is observed on 28 April 2018, right after the M<sub>L</sub> 4.1 earthquake, which anticipates any other peak, including the CO<sub>2</sub>/CH<sub>4</sub> peak (**Figure 11c**). Both H<sub>2</sub>/H<sub>2</sub>O and CO/CO<sub>2</sub> show sharp peaks on 2 May (0.00013 and 0.000015, respectively; **Figure 11e**) consistent with the onset of more oxidized conditions and the heating up of the hydrothermal system upon the arrival of hot and oxidized deep gases (e.g., Chiodini and Marini, 1998). Contrary to the He/CH<sub>4</sub> ratio, both ratios do not show an increasing baseline, as shown by the fact that after the peak phase the both attained their lowest values on 30 July 2018. H<sub>2</sub>/H<sub>2</sub>O peak values overlap with 1976 (Chevrier et al., 1976) values but plot

below 1997 data, which were much higher than those observed nowadays because of important steam condensation (Brombach et al., 2000). On the contrary, CO/CO<sub>2</sub> values compare very well with 1997 data but are much lower than those of 1976, suggesting that 2018 heat inputs are well below those involved in the 1976 phreatic eruption.

### 3.4.2 MultiGAS measurements

The OVSG-IPGP uses routinely a portable MultiGAS station (Aiuppa et al., 2005; Shinohara, 2005) to measure the concentration of gas emitted by major craters and structures, and also perform gas flux measurements along traverses through main fumarole plumes (e.g., Allard et al., 2014; Tamburello et al., 2019).

From 2012 to 2016, gas fluxes increased by a factor  $\sim 3$  and  $\sim 2$  at CS and Tarissan, respectively, while gas fluxes from G56 have varied from below detection limit to values that are comparable to those from Tarissan (e.g., Allard et al., 2014; Tamburello et al., 2019). Since 2016, measurements show constant gas fluxes at Tarissan and South Crater, with mean values of  $5.7 (\pm 1.6)$  and  $7.5 (\pm 1)$  t/d, respectively. Taking into account the high error ( $\sim 40\%$ ) on the flux determination (Tamburello et al., 2019), the gas fluxes at Gouffre 56 can be also considered constant, despite a noticeable variability ( $4.7 \pm 2.6$  t/d). Gas concentrations measured on the dome (**Figure 12a**) show that a strong chemical perturbation started in March 2018, characterized by increasing CO<sub>2</sub>/H<sub>2</sub>S and SO<sub>2</sub>/H<sub>2</sub>S ratios. In details, the C/S ratio is constant at Cratère Sud, as observed with the Giggenbach bottle. The average C/S value returned by MultiGAS is however  $\sim 2$  (**Figure 12a**), instead of 4 for the data from Giggenbach bottles (**Figure 11**). From March 2018, the C/S MultiGAS ratio increased at Tarissan and Napoléon Nord, but not at Cratère Sud and G56. At the same time, the SO<sub>2</sub>/H<sub>2</sub>S ratio increased slightly at Napoléon Nord and significantly at Cratère Sud reaching a maximum value of 0.18 (**Figure 12b**). This is the highest SO<sub>2</sub>/H<sub>2</sub>S ratio, by at least a factor 2, measured at La Soufrière since the start of MultiGAS measurements in 2012. After 2 May 2018, this ratio returned to previous values, even below detection limit. Furthermore, a MultiGAS survey was also carried out between 16 and 23 March 2018 in the surroundings of the NAPN vent, at a site around twenty meters away from the NAPN vent (**Figure 2b**) that does not show a proper fumarolic activity (i.e. a visible flux of steam) but was reactivated with a dry gas emission. Measurements yielded values up to  $T = 94$  °C, SO<sub>2</sub>/H<sub>2</sub>S = 1.4 and CO<sub>2</sub>/H<sub>2</sub>S > 50. In addition, OVSG-IPGP also operates a network of three permanent MultiGAS stations at the summit (Cratère Tarissan, G56 and Cratère Sud). Nevertheless, this network, that was partly re-installed after September 2017 hurricanes, suffered further damages by hostile conditions. Therefore, the only reliable measurement in the period of interest is the concentration of SO<sub>2</sub> detected in the plume at Cratère Sud. Data available until 20 April 2018 show a net anomaly starting in early March 2018 and culminating at 1.9 ppm of SO<sub>2</sub> on 7 April 2018 (**Figure 12b**). This

early start of chemical perturbation is also observed in data from in-situ Giggenbach gas sampling on 23 March 2018, especially for He/CH<sub>4</sub> and to a lesser extent for CO<sub>2</sub>/CH<sub>4</sub> (**Figure 11**). It is important to note that the MultiGAS measurements show that the chemical perturbation is not only present at Cratère Sud but on the entire dome. These relatively high SO<sub>2</sub> levels at the Cratère Sud occur at the time when the aforementioned SO<sub>2</sub>-rich signals were found in the periphery of the NAPN site (on 18-23 March 2018) and are correlated with portable MultiGAS data.

#### 4. Data elaboration and discussion

##### 4.1 Magmatic vs hydrothermal sources and the origin of overpressures: seismic and geodetic assessment

**Figure 5a** shows the occurrence of clusters of seismicity increasing in frequency and rate until the 27-29 April swarm. Nevertheless, the seismicity until February 2018 is superficial, being in average observed down to a depth of 1 km b.s.l. (**Figure 5b**), thus very distant from the supposed depth of the magma chamber (about 4.5 to 5.5 km b.s.l., or 6 to 7 km of depth below the summit; Pichavant et al., 2018, Villemant et al., 2014). This seismicity comes from the interactions between the flow of heat and gas from the magma at great depths and the presence of superficial phreatic groundwater layers in the volcano. Multiple factors (changes in fracturing, changes in pressure, flow, and temperature of gases, variation in the proportion of liquid water and gas, variation in the interaction depth between gases and liquid water) locally generate overpressures that favor an accumulation of deformation until the rock breaks. The corresponding waveforms are of hybrid-type, generally with a long period coda (**Figure 4**). It is therefore the activity of the (shallow) hydrothermal system in the broad sense that seems to be at the origin of the typical La Soufrière seismicity, which translates into a weak total dissipated energy (**Figure 5**) and does not testify to a deep reactivation of the volcano or to major modifications of its geomechanical response.

Values of the compressional to shear wave velocity, Vp/Vs, were estimated by the slope of P and S arrival time differences as a function of P arrival time (Wadati, 1933) and plotted versus the time to evaluate variations of the medium properties (**Figure 13**). The red line in figure represents a moving average of 50 consecutive seismic events. Although an average Vp/Vs value of 1.74 (**Figure 13b**) can be estimated, in agreement with the regional value of 1.73 reported by Bazin et al. (2010), **Figure 13** displays major Vp/Vs fluctuations differentiating the 2017 activity from that of January to July 2018. The 2017 activity is in fact characterized by Vp/Vs ratios up to 1.8, whereas two major negative Vp/Vs anomalies (Valley 1 and Valley 2 in **Figure 13**) can be observed from December 2017 to the end of February 2018 and from the end of March 2018 to the beginning of June 2018. Highest

values in 2017 occur when activity is lowest, i.e. prior to September 2017 (see also **Figure 5a**). A significant decrease in the Vp/Vs ratio is observed since the early January 2018 seismic activity peak (V1 in **Figure 13**; see also **Figure 5a** and **Supplementary Figure S1**) giving rise to a negative anomaly in concomitance to the February 2018 seismic swarm (Valley 1, with lowest Vp/Vs at 1.64; **Figure 13**), which occurred within the hydrothermal system below the dome. High Vp/Vs ratios are recovered in March 2018, but a strong decrease is then observed since the last week of March 2018, which gives rise to a second negative anomaly (Valley 2, with lowest average Vp/Vs at 1.61; **Figure 13**) that lasts until the end of June 2018 and that includes the off-axis seismic swarms that started on 16 April and 27 April 2018. The beginning of this second anomaly is related to the intensification in seismicity observed before the 16 April 2018 swarm (V2 in **Figure 13**; **Figure 5a**) and occurs when fumarole steam fluxes were highest (**Figure 10**) and temperature peaks were measured at Cratère Sud fumaroles (23 March, **Figure 9**) and in the dry vent surrounding the NAPN fumarole, along with increased SO<sub>2</sub> contents (**Figure 12**).

The observed Vp/Vs ratios are representative of the volcanic highly fractured, fluid-filled, rocky medium. Vp/Vs variations are then related to the mechanical reaction of the volcanic medium to pore fluid flow, hence to the joint effects of hydrothermal dynamics and hydrological forcing. The two negative Vp/Vs valleys reflect the fact that rock saturated with water at a temperature near water-steam transition would result in a large change in Vp, a small change in Vs, and a large change in Vp/Vs, as reported in Sanders et al. (1995) and shown by experiments conducted by Spencer and Nur (1976) and Ito et al. (1979). This is consistent with the evidence that high hydrothermal activity, is the main cause of the velocity anomalies (low Vp, low Vs, and low Vp/Vs) beneath active volcanoes (Chatterjee et al., 1985; Walck 1988; Nugraha et al., 2019), also favored by the large aspect ratio (~0.1) of water-filled cracks (Nakajima et al., 2001).

Therefore, it seems that the observed seismicity reflects the weakening of the rocky medium due to fluid infiltration and hydrofracturing, determined by the increase of pore pressure (e.g., Nakamura 1977; Miller et al., 1996; Miller and Nur, 2000; Sibson, 2000; Terakawa et al., 2010). Pore pressure increase on infiltration is not necessarily homogenous, and when it is localized into a narrow source, seepage forces originate that modify locally the stress-state (Morgues and Cobbold, 2003; Rozhko et al., 2007). However, recovery of the Vp/Vs ratio, hence of nominal rock properties, was rapid after the 1<sup>st</sup> February swarm, whilst it was much slower after the 27-28 April 2018 swarm and still incomplete in July 2018. This is related to the high energy of the 27 April M<sub>L</sub> 4.1 earthquake (**Figure 5c**), with the involvement of a much larger seismogenic volume.

Geodetic data in the Basse Terre sector show that, down to a depth of 8 km b.s.l., the measured inflation is not associated with large intrusions. In addition, the nearly radial shape of the (shallow) dome deformation (**Figure 7a**) suggests that deformation is associated to fluid

overpressures within the hydrothermal system (e.g., Battaglia et al. 2006). The pattern of dome radial spreading is however perturbed by the detachment of the southwestern sector over 1.3 km of distance at a speed of 5-7 mm/year. This is consistent with imaging by electrical-resistivity tomography (Rosas-Carbajal et al., 2016), and with the superposition of three major fracture systems (Northern Fault, the Napoléon-56-Breislack system, and the Dolomieu system; **Figure 1**) which divide the whole dome in three major blocks. In agreement with extensometric data (**Figure 8**), rapid pressure fluctuations of the hydrothermal system may determine a differential response of each block, particularly the emergence of a mechanism of simple shear, more superficial and important during low-pressure phases when the perturbation to the radial, symmetric, deformation is largest and produces the closure of some fractures (**Figure 8**).

One might expect that observed deformations and seismicity are related to the switch from drained to undrained conditions of the boiling hydrothermal system and of shallow phreatic fluids circulating through the porous medium. Under undrained conditions, rapid pore pressure build-up takes place until the occurrence of hydraulic fracturing breaks the host rock; as testified by the low  $V_p/V_s$  values observed in April 2018 (**Figure 13**). Nakamura (1977) first suggested that hydraulic fracturing is an important process in generating volcano-hydrothermal seismicity and in the case of La Soufrière de Guadeloupe this argument was invoked by West et al. (1978). Hydraulic fracturing of a rock occurs when the effective fluid pressure overcomes the tensile strength of the rock and any confining pressures. This is expressed as  $P_b = 3\sigma_3 - \sigma_1 + T - P_0$  where  $P_b$  is the formation breakdown pressure of rock of tensile strength  $T$  at a pore pressure  $P_0$  in a compressive stress field with  $\sigma_3$  and  $\sigma_1$  the minimum and maximum principal stresses, respectively, on the plane orthogonal to the infiltrating fluid stream (Kehle et al., 1964). Only fluids with a low viscosity, such as steam, have a great ability to influence the pore pressure  $P_0$  and reducing the pressures necessary for fracturing. In addition, low viscosity fluids can open existing fractures even if their orientation is other than parallel to the maximum principal stress (Zoback et al., 1977). This is the reason why some fractures and faults of the summit (including the 8 Juillet and Napoléon faults) behave very dynamically, as observed via extensometric measurements.

It must be noted that the rate of pressurization also affects the breakdown pressure, a high rate of pressurization resulting in an anomalously high breakdown pressure (Haimson and Zhao, 1991; Schmitt and Zoback, 1992). As the rate of pressurization increases, in a volcano, the mode of deformation may change from viscous to plastic and then to elastic, at high rates of pressurization (West et al., 1978). We then definitely hypothesize that the rapid pressurization determined by the onset of undrained conditions led to the  $M_L$  4.1 (or  $M_w$  3.7) earthquake of 27 April. Indeed, its focal mechanism and features (see Supplementary Material and Supplementary Figure 6) identify a NW-SE

normal fault dipping  $\sim 40^\circ$  to the NE (**Figure 14**), coherent with active regional faults (Feuillet et al., 2011). Shallowly dipping faults in extensional tectonic regimes are known to be reactivated by elevated fluid pressure (e.g., Collettini and Barchi, 2002; Sibson, 1990, 2000; Micklethwaite and Cox, 2006; Cox, 1995; Terakawa et al., 2010) and variations of fluid pore pressure related to hydrothermal fluid circulation are known to explain seismic activity in volcanic environments (e.g., Ventura and Vilaro, 1999 and references therein). A good analogy is offered by the seismic activity of Mount Vesuvius (Italy), particularly its 9 October 1999 earthquake ( $M_L=3.6$ ), for which no significant departure of the fault mechanism from a double-couple source can be inferred (Del Pezzo et al. 2004, Zollo et al., 2002).

The epicentres of 16-17 and 27-29 April 2018 swarms, although separated by an aseismic segment (**Figure 6b, Supplementary Figures 3,4**), define a structure whose direction is that of all the active regional faults that cut the volcanic arc and cross the Basse-Terre through the La Grande Decouverte-Soufrière complex (**Figure 1**). A fault of the same orientation has so far not been mapped in this area, perhaps because hidden by recent volcanic deposits. We suggest that the hybrid waveforms of the 16-17 swarm and especially of the subsequent  $\sim 30$  hybrid events, point to invading high-pressure fluids along the shallowly dipping NW-SE structure, which may have locally weakened the fault through the rapid reduction (on the scale of days) of the effective normal stress acting on the fault plane (e.g., Collettini and Barchi, 2002; Sibson, 1990; Terakawa et al., 2010, Rozhko et al., 2007). We also suggest that the lack of spatially continuous seismicity between 16-17 and 27-29 April swarms can be explained by a change in dilatation and pore pressure polarity (contraction at the 27-29 April site, expansion in the 16-17 April one, near the La Soufrière de Guadeloupe dome), in line with the explanation provided by Miller et al. (2010) for the lack of seismicity observed in 1995 at Montserrat along the structure connecting the Soufrière Hills volcano and the St. George Hills.

Feuillet et al. (2011) have studied the collocation of active and recent volcanic vents (e.g., La Soufrière of Guadeloupe and Soufrière Hills, Montserrat) and faults in the Lesser Antilles arc, and have shown that faulting and volcanism are organically connected and likely interact, through coupling mechanisms determined by static or dynamic stress changes (e.g., Brodsky et al., 1998; Nostro et al., 1998; Linde and Sacks, 1998; Hill et al., 2002; Marzocchi, 2002; Troise, 2001; Walter and Amelung, 2007 and references therein). It appears in fact that such coupling mechanisms can lead to unrest or eruptions within few days, months, and perhaps years at neighbouring volcanoes (Nostro et al., 1998; Watt et al., 2009).

## 4.2 *Magmatic vs hydrothermal sources and the origin of fluid pressures: geochemical assessment*

### 4.2.1 *Gas end-members and secondary processes*

The elements shown and listed so far clearly point out an indirect forcing of deep hydrothermal and/or magmatic origin. A first increase in  $\text{SO}_2$  content and in  $\text{SO}_2/\text{H}_2\text{S}$  via MultiGAS (**Figure 12**), and in fumarolic  $\text{CO}_2/\text{CH}_4$  and  $\text{He}/\text{CH}_4$  (**Figure 11c,d**), was in fact seen on 23 March. The further sharp evolution leading to the peaks in the  $\text{He}/\text{CH}_4$ ,  $\text{H}_2/\text{H}_2\text{O}$  and  $\text{CO}/\text{CO}_2$  ratios (Figure 11d-f) that occurred in concomitance with the 27 April 2018 highly energetic earthquake ( $M_L$  4.1), suggests that a direct link exists between the heating and overpressurization of the hydrothermal system and the rock failure process. This is very likely in relation with the thermal and pressure perturbation of hydraulic boundaries at depth due to the arrival of deep gas pulse(s). This produced an enhancement of boiling, which however contrasts with the very low fluxes observed at CS fumaroles, CSC particularly, since late April, and the concomitant temperature drop to values consistent with water boiling at the local atmospheric pressure ( $\sim 95^\circ\text{C}$ ). This(these) gas pulse(s) was(were) released until 2 June 2018 at least, when maxima in the gas/steam and  $\text{CO}_2/\text{CH}_4$  ratios were observed (**Figure 11a,c**).

In order to discriminate between the different gas end-members (e.g., meteoric, hydrothermal, magmatic) and understand more how they do interact, we first look at the covariation of compositional indicators (e.g.  $\text{CO}_2/\text{He}$ ,  $\text{He}/\text{CH}_4$ ,  $\text{CO}_2/\text{CH}_4$ ) which are not appreciably affected by secondary hydrothermal phenomena (steam condensation, boiling, component scrubbing, remobilization, precipitation). The relative effect of these secondary phenomena can then be assessed by enlarging the approach to indicators such as  $\text{S}/\text{CH}_4$  and  $\text{H}_2\text{O}/\text{CH}_4$ . On this basis, **Figure 15a,b** shows that fumarolic fluids prior to the  $M_L$  4.1 event of 27 April 2018, follow a mixing line (dashed lines in all panels), characterized by a  $\text{CO}_2/\text{He}$  ratio evolving from 150000 (November 2017 and 31<sup>st</sup> January 2018 samples) to 87000 (28 April 2018 sample). Along this mixing line, increasing  $\text{CO}_2/\text{CH}_4$  reflects an approach towards the hot and oxidized conditions typical of the deeper hydrothermal component, which then boils off in the roots of the volcanic dome upon interaction with the oxidized, nearly  $\text{CH}_4$ -free, magmatic gases. This is accompanied by the  $\text{CO}_2/\text{He}$  decrease (**panel a**) and  $\text{He}/\text{CH}_4$  increase (**panel b**), which point to a He-rich deep hydrothermal component. The helium enrichment of the local deep hydrothermal system can be ascribed to the long-term interaction of the deep hydrothermal fluid with magmatic rocks and the accumulation of radiogenic He, as well as to the contribution of a basal flux mostly determined by a contribution of background andesitic magma degassing. On the other hand, the shallow hydrothermal component is enriched in the very He-poor meteoric component.

We do not know hitherto the chemical composition of the hydrothermal liquid phase that contributes to the groundwaters circulating in the volcanic complex (Ruzié et al., 2012, 2013; Villemant et al., 2005, 2014) and, that underneath La Soufrière dome, boils off the fumarolic fluids discharged at the volcano summit. However, it is highly probable that the deep hydrothermal fluid is a NaCl aqueous solution (Brombach et al., 2000; Villemant et al., 2014). These fluids readily form in

active volcanic environments through (1) the absorption of  $\text{SO}_2$  and HCl-rich magmatic gases in deeply circulating groundwaters and (2) neutralization of these initially acidic groundwaters by reaction with wall rock containing minerals capable of neutralizing acids, such as feldspars, micas, and other silicates (Giggenbach, 1988, 1997; Reed, 1997. Chiodini et al., 2001). The (deep) NaCl-rich hydrothermal aquifer in its portion surrounding the dome is boiled off upon receiving a considerable input of fluids from a degassing magma body (4.5 to 5.5 km b.s.l., or 6-7 km deep below the dome summit; Pichavant et al. 2018). It then mixes with fast circulating meteoric waters having an average residence time of three months (Bigot et al., 1994). This results in the shallow-to-deep local hydrothermal trend of **Figure 15**.

**Figures 15a,b** show the presence of another mixing line (red dashed lines in all panels), which we identify as that trending to the more magmatic end-member characterized by the high  $\text{CO}_2/\text{CH}_4$  ratios (2 June samples, see also **Figure 11c**), but also  $\text{CO}_2/\text{He}$  and  $\text{He}/\text{CH}_4$  ratios higher and lower, respectively, than those of the gas discharged on 28 April (assumed representative of the deep hydrothermal component). This new gas of magmatic origin is different from the one typically interacting with the hydrothermal system because it is characterized by a much larger  $\text{CO}_2/\text{He}$  ratio, consistent with degassing from a deeper or more compressed magma as  $\text{CO}_2$  solubility is lower than He solubility in basaltic and andesitic magmas (Nuccio and Paonita 2000; Caliro et al., 2014). The release of this new gas component becomes evident in the 2<sup>nd</sup> May sample and reaches its maximum in the 2 June samples, which were particularly steam-poor and  $\text{CO}_2$ -rich (Table 1; **Figure 11a,c**). Using the steam-poorest composition from June 2<sup>nd</sup> sampling as the new gas end-member and the 28 April one for the hydrothermal end-member, we estimate 85 % of the 02/05 sample consists of the hydrothermal component (**Figure 15a,b**).

Hence, the behavior of  $\text{CO}_2/\text{CH}_4$ ,  $\text{CO}_2/\text{He}$  and  $\text{He}/\text{CH}_4$  ratios suggests that a magmatic gas deeper than that usually soliciting the hydrothermal system has intervened and led to the unrest episode recorded between February and late April 2018. Therefore, this gas, discharged after the seismic peak of 28 April, heated up and then pressurized the hydrothermal system prior to becoming detectable at the fumaroles. This mechanism explains the  $\text{He}/\text{CH}_4$ ,  $\text{H}_2/\text{H}_2\text{O}$  and  $\text{CO}/\text{CO}_2$  peaks (**Figure 11d-f**) roughly concomitant with the  $M_L$  4.1 earthquake and should imply increasing boiling of the hydrothermal system feeding summit fumaroles. **Figure 15a,b** also highlights that after having discharged the “anomalous” deep magmatic gas, fluid compositions returned along the hydrothermal mixing line (21 June and 30 July samples). However, pre-crisis conditions (e.g. November 2017) are not fully regained and sample position along the trend (close to the 28 April values) suggests an important residual deep hydrothermal component.

The  $\text{He}/\text{CH}_4$  vs  $\text{H}_2\text{O}/\text{CH}_4$  covariation in **Figure 15c** shows both negative and positive departures from mixing trends identified in **Figure 15a,b**. Negative departures represent steam

condensation, and affect early samples (November 2017, 31 January 2018) as well as the 21 June one, which marks the return of the fluid system along the hydrothermal trend. On the other hand, positive departures of the H<sub>2</sub>O/CH<sub>4</sub> ratio mean increased boiling with respect to the hydrothermal trend. These are observed for 23 Mars 2018 (when fumarole temperature reached 111°C, **Figure 9a**), 19 April 2018, but also for 30 July samples. However, the most important boiling effects are seen for the 2 May composition, especially considering that this results by mixing with the “anomalous” magmatic gas that started to be discharged after the seismic peak. It must be noted that the evolution of any hydrothermal system from depth to surface is most likely characterized by a multi-step sequence of secondary processes such as boiling and steam condensation. These are nearly invariably present at La Soufrière’s summital fumaroles, in light of the vent temperature normally buffered by coexisting liquid and vapour at the local atmospheric pressure (**Figure 9a,b**). Nevertheless, the information provided by **Figure 15c** summarizes the dominant secondary effect with respect to the current standard conditions occurring along the trends identified in **Figure 15a,b**.

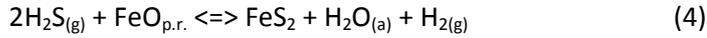
Similarly, **Figure 15d** allows us to evaluate that secondary effects influencing sulphur concentration (scrubbing versus remobilization of the stored hydrothermal sulphur. It shows that hydrothermal sulphur was remobilized on 19 April, and particularly on 23 March, when anomalous temperatures and degassing were measured in the surrounding of the NAPN site (**Figure 1**), with the dry emission of H<sub>2</sub>S and SO<sub>2</sub> in nearly equal amounts measured by Multigas (**Figure 12**). This likely resulted from the start of the heating cycle due to the arrival of relatively high-temperature fluids, which led to the local remobilization of the earlier deposited elemental sulphur (S<sub>e</sub>) according to the following reaction (Mizutani and Sugiura, 1982; Giggenbach, 1987):



In addition, the difference in C/S ratios measured by MultiGAS between CS and G56 on one side, and Tarissan and NAPN on the other one (**Figure 12a**), is likely the result of the larger sulphur scrubbing operated by the acid lake (Tarissan) and the shallow circulating groundwaters (NAPN) with respect to CS and G56 sites.

In **Figure 15d**, the 2/5 fluid composition appears to be enriched in sulphur with respect to the mixing trend of deep local hydrothermal and magmatic components, in agreement with the boiling effect described in **Figure 15c**. Instead, the position of datapoints from 21/6 and 30/7, close to each other and along the mixing trend of deep local hydrothermal and magmatic components, contrasts with the findings of **Figure 15c** (steam condensation and boiling dominant on 21 June and 30 July, respectively). It also appears that their S/CH<sub>4</sub> ratios is akin to the one due to the mixing of the deep local hydrothermal gas and the “anomalous” one of deep magmatic origin. Following Giggenbach (1980), it is in fact possible that the many secondary reactions involving sulphur modify the simple picture associating boiling to sulphur remobilization and steam condensation to sulphur scrubbing.

Following the approach described in Moretti et al. (2013a, 2017), the occurrence of perturbations on the hydrothermal equilibrium involving total sulphur as H<sub>2</sub>S can be identified by considering the following equilibrium:



in which FeO<sub>p.r.</sub> refers to a generic oxide component of divalent iron in the pyroclastic rocks, FeS<sub>2</sub> is the pyrite component of sulfide solid phases of the hydrothermal system and the superscripts (a) and (g) refer to aqueous solution and gas, respectively. By considering that activities of FeO<sub>p.r.</sub> and FeS<sub>2</sub> can be considered constant because fixed by average rock compositions of the hydrothermal systems and that H<sub>2</sub>O activity is constant and also close to unity for the system of interest, the equilibrium constant reduces to:

$$\log K_4 = \log \frac{[\text{H}_2]}{[\text{H}_2\text{S}]^2} + \text{const.} \quad (5)$$

A hydrothermal system not perturbed by anomalous heating and oxidation phenomena, for example related to the arrival of magmatic gases, should display constant logK<sub>4</sub> with time. **Figure 16** then suggests that the usual hydrothermal equilibrium conditions recorded at the CSC fumarole (logK<sub>4</sub> ≈ 0 in **Figure 16**) appear being definitely perturbed in concomitance with the 16-17 April 2018 swarm. An increase of logK<sub>4</sub> is in fact observed until 2 May, implying that the hydrothermal system experiences a relative increase of H<sub>2</sub> due to the temperature raise and boiling. The perturbation becomes negative on 2 June, reflecting the arrival of the deep “anomalous” gas (corresponding to the gas/steam and CO<sub>2</sub>/CH<sub>4</sub> peaks, **Figure 11a,c**), which injects additional sulphur and oxidizes the system. On late June 2018 the perturbation on logK<sub>4</sub> has disappeared.

#### 4.2.2 Thermal and baric evolution of the hydrothermal system

To understand more about the thermal (T) and baric (P) anomalies associated with the progressive arrival of the deep gas, the thermochemistry of discharged fluids must be considered, in order to calculate the P-T conditions of the boiling hydrothermal reservoir. From the chemistry of fumarolic gases, we then compute the P-T conditions of the boiling hydrothermal system feeding summit fumaroles following Chiodini and Marini (1998) (**Figure 17**). This method is based on the sum of log ratios between pairs of species making up redox exchanges in the gas phase and accounts for the fact that multiple oxidation states may be active within the hydrothermal system and that all species (H<sub>2</sub>O-CO<sub>2</sub>-CH<sub>4</sub>-CO-H<sub>2</sub>) attain the condition of chemical equilibrium (Chiodini and Marini, 1998; Moretti et al., 2017).

From the 1997 data (Brombach et al., 2000) appearing in the diagram of **Figure 17**, but for which methane was undetected, we estimated a detection limit concentration of 0.1 μmol/mol, based on the data from the Authors. The vertical error bars cover two orders of magnitude in CH<sub>4</sub>

concentration (0.01 to 1  $\mu\text{mol/mol}$ ) and show the low-weight that this species has on  $3\log(\text{CO}/\text{CO}_2)+\log(\text{CO}/\text{CH}_4)$  (Chiodini and Marini, 1998). Similarly, 1976 data (Chevrier et al., 1976) were plotted by considering, conservatively, a  $\text{CH}_4$  detection limit of 1  $\mu\text{mol/mol}$  and a vertical error bar covering two orders of magnitude (0,1 to 10  $\mu\text{mol/mol}$ ). Note that vertical error bars for CSC samples include data dispersion on concentration measurements from replicate samples. Therefore, they are highly conservative and greatly exaggerate the purely instrumental error, which is contained within symbol size.

**Figure 17** shows that CS samples plot within the two-phase field, and that fluids sampled on 28 April 2018 (few hours after the earthquake) and 2 May 2018 fall very close to the critical point of pure water (CP; 374°C, 220 bar). Within the two-phase field, boiling occurs and the gas separates from the liquid, theoretically by an isenthalpic process of single-step vapour separation (svss, Chiodini and Marini, 1998). Under this approximation, each sample represent a vapour which falls on a svss line related to the original temperature and pressure of the corresponding boiling liquid on the saturated liquid line (**Figure 17**)

This does not mean that the rising hydrothermal fluid does not experience multiple sequential secondary processes, such as vapour gain or loss and multi-step vapour condensation and separation. However, when falling within the two-phase field, measured data are in agreement with an isenthalpic single step vapour separation, which includes all intervening secondary effects and implies that boiling is the dominant one. We notice that the fluid system points to an original boiling liquid normally at 340°C and that since November 2017 the conditions of gas separation have shifted towards the saturated vapour line, i.e. very close to the P-T condition of the original boiling liquid. Assuming the simple scenario of single-step isenthalpic vapour separation, we find that the P-T peak is recorded by the 2 May sample, which represents a vapour separated at 350°C from a liquid phase originally at 370°C and 210 bar. The fraction of separated steam from the boiling liquid is 21 mol%. Afterwards, the hydrothermal system relaxes, experiencing a P-T decrease, until 30 July samples, when pre-crisis P-T conditions seem to be restored. **Figure 17** thus confirms the hypothesis that the boiling hydrothermal system was thermally solicited up to the critical point of water. Because of the low sampling frequency, we do not know if the critical point of water was finally exceeded, as was seen for July 1976 samples (Chevrier et al., 1976), but this is likely to have occurred. However, the supercritical excursion recorded by 1976 data might also reflect separation from a NaCl-brine, whose critical point would be located along the saturated vapour line at temperatures higher than that of pure water (Chiodini et al., 2001). Under both hypotheses (supercritical excursion of pure water vs boiling of a brine), it is supposed that the hydrothermal reservoir feeding the 1976 eruption was much more sealed than the present one (Boichu et al., 2011; Komorowski et al., 2005; Villemant et al., 2014), such that it could either rise in temperature and pressure more easily than currently, or let

much less meteoric component to be introduced and to dilute the locally boiling liquid (water or brine). In all cases, the hydrothermal system has clearly evolved since 1997, when steam condensation upon cooling (i.e.; high  $H_2/H_2O$  ratios in 1997, **Figure 11e**) was the dominant secondary process, as demonstrated by datapoints falling on the left of the saturated vapour line (**Figure 17**). Steam condensation thus favoured the growth of the very shallow hydrothermal system, accompanying the formation of acid ponds (Komorowski et al., 2005). Nevertheless, the continuous forcing of magmatic gases, has in time favoured boiling, progressively embracing circulating shallow groundwaters of meteoric origin.

**Figures 11, 15, 16 and 17** show that at the end of June 2018, the hydrothermal system seems to return to the pre-crisis situation observed in late 2017. Given the infiltration of magmatic gases into the hydrothermal system, as well as the high temperatures and pressures inside the hydrothermal system, we believe that the volcanic system was at that time being recharging and was accumulating energy. Additionally, **Figure 17** suggests that the present-day hydrothermal system is in a pre-1976 condition, such that additional overpressure peaks associated with deep pulses of magmatic gas may destabilize the hydrothermal system and lead to phreatic explosive activity, such as in 1976.

At present, we cannot establish exactly the origin of the deep “anomalous” gas and the mechanism determining its release and ascent into the hydrothermal system. Nevertheless, two reasonable hypotheses can be formulated given our analysis of conjugated chemical indicators based on conservative gas species in the discharged fumarolic fluids:

- 1) the deep “anomalous” magmatic fluid is stored at mid-to low-crustal depths and when a relevant amount is reached, it is transported upward via buoyancy-driven or pressure-driven flow mechanisms (Norton and Knight, 1977; Connolly, 1997). This takes place through a surrounding ductile medium, the brittle-ductile transition being likely located at around 1.5 km b.s.l. (3 km below the Soufrière summit) based on the geochemical conceptual model of Villemant et al. (2014). This deep upstreaming gas fluxes the shallow cooling and crystallizing magma body remnant of the 1530 eruption through cyclic mechanisms rejuvenating its exsolution behaviour (Boichu et al., 2008, 2011; Moretti et al., 2013a,b).
- 2) The deep “anomalous” magmatic fluid is released in pulses each related to episodes of fresh injections of basaltic magma in the long-lived (up to thousand years) andesitic chamber located at 4.5 km b.s.l. (6 km depth below the summit, Semet et al., 1982; Touboul et al., 2007. Poussineau, 2005; Pichavant et al., 2018). However, such inputs are likely, too small to be detected by the current geophysical instruments. Notably,  $^3He/^4He$  determinations in fumarolic and hot spring gases and considerations on the thermal evolution of springs, together with the observation of contrasting halogen behaviour in spring waters and

fumarolic condensates, point to recurrent injection of fresh basaltic magma (Ruzié et al., 2012; Villemant et al., 2014). Archetype examples of these fresh magma injections would be the one triggering the 1976-77 phreatic crisis, and another one, of smaller size that marked the onset of the long-lasting current unrest around year 1992 (Villemant et al., 2014).

It is of course possible that observed deep magmatic pulses are related to a combination of these two scenarios. Nevertheless, as far as the unrest sequence observed in 2018 were to reoccur, this might escalate to a magmatic phase following the initial phreatic activity, due to the availability of either *a*) rejuvenated magma in the shallow, 1.5 km b.s.l. deep, magma chamber (Villemant et al., 2014), or *b*) deep-sourced ( $\geq 4.5$  km b.s.l.) fresh magma which in the future could directly supply the shallow reservoir.

#### 4.3 Why the 2018 unrest episode must be regarded as a failed phreatic eruption

The evidence that hot springs do not record significant thermal and chemical variations, contrary to summit fumaroles, implies that the hydrothermal system is disconnected from shallower aquifers in the area surrounding the dome. In fact, summit vents are located along a dome axial zone of high vertical permeability due to faults and deep fractures. This allows the rapid ascent of the steam separated by one or more boiling aquifers whereas hot springs discharge from an outer zone, where groundwaters are heated through conduction or addition of small amounts of hot saline liquids coming from deeper hydrothermal aquifer(s) (Brombach et al., 2000; Ruzié et al., 2012, 2013; Villemant et al., 2014; Rosas-Carbajal et al., 2016), which are too small and readily absorbed.

For simplicity, we assume that the deep hydrothermal system below and surrounding the La Soufrière dome represents a continuum. Consequently, we relate the observed phenomena to the flow of water and steam, thus to the resulting competition between drained and undrained hydraulic conditions, which at the different sites is determined by existing hydrological boundaries (mainly permeability). Therefore, we propose that the P-T variations of the hydrothermal continuum yielded rapid pore pressure increase and undrained conditions particularly along the NW-SE fault structure activated during the 16-17 April and 27-29 April swarms, outside the La Soufrière dome. On the other hand, the fractures connecting the actively degassing dome summit area (a free-surface boundary condition) with the deep overpressured source at the base of the dome, allow the ascending fluids to be discharged and to remain at nearly hydrostatic pressure (Miller et al., 1996; Miller and Nur, 2000; Terakawa et al., 2010), thus approximating a drained condition. On this basis, **Figure 18** provides a conceptual model for the La Soufrière system and summarizes the main current features of the La Soufrière magmatic and hydrothermal system, as well as the temporal evolution through the recent

unrest episode (see Supplementary Figure 7 for a comprehensive picture of various changes and their timing).

In the representation of **Figure 18**, we locate the pressure source below the dome by considering the P-T conditions of the hydrothermal liquid and right above the sealing cap marking the top of the brittle-ductile transition zone inferred at about 1.5 km bsl (Villemant et al., 2014). This sealing cap separates the lower plastic region where magma-derived fluids accumulate from the upper hydrothermal region, where fluids at hydrostatic pressure circulate through the brittle rock and maintain permeability via persistent seismicity (Fournier et al., 2007). The depth at which we place the sealing cap agrees with observations indicating that the brittle–plastic transition commonly occurs at about 370–400°C within presently active continental hydrothermal systems (Fournier, 2007). Considering that the high-magnitude VT seismicity is associated with breaching of the self-sealed zone (Fournier, 2007), we constrain the geometry of the brittle-ductile transition zone outside the volcanic axis by considering hypocentral depths of 16 and 27 April events just on top of it. A crystal mush extending downward from depths of 5 km bsl is pictured as the source of heat and deep fluids.

Boiling of the hydrothermal liquid separates the vapour responsible of the upward fluid circulation feeding the fumaroles and nurturing the shallow seismicity and deformation. Because the temperature of such a liquid is normally 340°C (see **Figure 17**), fluid pressure is 146 bar and liquid density 611 kg/m<sup>3</sup> (NIST, 2018). Hydrostatic conditions are then established with the free-surface at the top of the dome. Considering at first approximation a constant fluid density in response to the convective homogenization, we can calculate ( $z = P/[g\rho]$ ) a source depth of 0.9 km b.s.L (or 2.4 km below the summit). This corresponds very well to the hypocentral depth of three most energetic earthquakes of 1<sup>st</sup> February (1 km b.s.l.; OVSG-IPGP, 2018a). Based on 28 April and 2 May gas samples, which separate from a liquid originally at 370°C (**Figure 17**), we infer that this source was overpressured until reaching the critical point of pure water on 27 April 2018. Because the critical point occurs at  $P = 220$  bar (NIST, 2018), an overpressure of 64 bar was attained in the source below the dome. Nevertheless, this overpressure in the dome roots was released aseismically. It is now worth recalling that the seismicity along fracture/fault planes infiltrated by fluids is produced by the instantaneous switch to large permeability values at the onset of cracking (Miller and Nur, 1996; 2000; Miller, 2015). Below the dome this process occurred evidently on February 1<sup>st</sup>, but on 27 April the volcanic dome was able to restore aseismically the hydrostatic gradient because the overpressured source was already tapped by a network of structures with high vertical permeability and already critically stressed (i.e. the fractures and faults activated or created during the 1976 phreatic eruption, which modified the dome and reactivated since the 1992 onset of volcanic unrest; Komorowski et al., 2005; Ruzié et al., 2012; Villemant et al., 2014). These structures then lowered the

tensional state of the volcanic edifice by discharging the accumulated overpressure. The latter is testified by the episodic locking of fractures measured in April 2018 (**Figure 8b**), as well as by the behavior of fumarolic temperatures and heat fluxes. These were in fact rapidly increasing since the beginning of the year and then started decreasing right after the 16-17 April swarm (**Figure 9**), showing that the heat flux is not stored in different aquifers but is evacuated through the main fractures.

The “usual” La Soufrière hybrid micro-seismicity concentrated within the dome, between -1 and 0.5 km of depth b.s.l. (**Figures 5b;6a,b**; see also Ucciani, 2015a,b). This depth range is likely determined by the mechanic interplay of volcano loading with the non-homogenous distribution of the permeability within the shallow network of fractures. This network, upon fluid circulation, continuously evolved being characterized by patches of opening cracks, and patches of sealing cracks, with the sudden recovery of permeability (Miller et al., 1996; Miller and Nur, 2000; Fournier, 2007; Miller 2017). Nevertheless, one major question is why this shallow microseismicity was not observed for a long time following the late April 2018 swarm. Diffuse hybrid seismicity (see for example December 2017 and early January 2018 swarms; **Figure 5a,b** and **Supplementary Figure S1**) was expected to be triggered, but it did not occur simply because the flux of liquid water phase migrating upward in the shallow hydrothermal system lowered considerably as demonstrated by the subsequent net decrease of fumarolic fluxes and the drop in vent temperatures (**Figures 9,10**). After the 16-17 April, the water was drained away, outside the dome, likely penetrating along the NW-SE regional structure further activated in late April 2018. Thus, pore pressure was released to areas away from the paths leading to the dome-hosted and steam-rich shallow hydrothermal system and to the summit fumarolic zone. Therefore, only gases, enriched in the “anomalous” magma-related component, could flow upward after separating from the deep hydrothermal system. Vapour separation, i.e. the mechanical decoupling of gas and liquid, occurs very likely when when boiling water soon abandon undrained conditions, experiencing at depth a significant horizontal displacement (Arnorsson and Gunnlaugsson, 1985) due to deep lateral drainage outside the dome, along the NW-SE fault segment that was seismically activated on 16-17 April 2018 (**Figure 18**). This mechanism is testified for by the samples from 23 March 2018 to 2 June 2018 in **Figure 17**, which plot following along the vapour separation curve at 300°C and 80 bar. This suggests that the vapour separation process was deeper - hence closer to the overpressure boiling source - than before 23 March and after 2 June.

Along the NW-SE fault structure, the same temperature rise (from 340°C to the critical point, 374°C, or from 613 K to 647 K) inferred from fumarolic fluid compositions (**Figure 17**) determined a dramatic rise of overpressures. This can be estimated by considering the isochoric build-up of

thermal pressure, that is, the fluid pressure increase caused by heating a single finite fluid-filled pore volume (e.g., Delaney et al., 1982; Norton, 1984; Turcotte and Schubert, 1982; Ganguly, 2009):

$$\Delta P = \int_{613K}^{647K} \frac{\alpha}{\beta} dT \quad (6)$$

in which  $\alpha$  is the isobaric thermal expansivity and  $\beta$  is the isothermal compressibility, their ratio being unity at the water critical point because both parameters tend to converge. Given the T-dependence of the  $\alpha/\beta$  ratio in the T-range of interest by fitting NIST steam tables (NIST 2018), equation (6) gives an overpressure of 175 bar, that is, a pore pressure of 321 bar at the hypocenter of the 27 April, M 4.1, earthquake (2 km b.s.l. or 3.1 below the local ground-level; **Figure 18**). This value is remarkably higher than the 220 bar inferred for an open system in which high-permeable fractures released the overpressure accumulated at 1 km b.s.l. (2.5 km depth below the volcano summit). These numbers are useful to give an idea of how the pore pressure increase along the same isotherm can affect rock behaviour. However, we cannot push further the argument as a precise treatment of thermoelastic effects and rock failure at the different sites would first demand the reconstruction of the local variations of the thermal field, and should include how fluid flow and resulting seepage forces modify the effective stresses (Morgues and Cobbold, 2003; Rozhko et al., 2007).

Nevertheless, given the current state of the dome, a thermally-driven build-up of overpressures comparable to the one reported in this study can lead to important rock failure and a phreatic eruption only when 1) self-sealing phenomena occur to confine fixed-fluid volumes, hence overpressure sources, sufficiently developed in the shallow hydrothermal system (rather than at 1 km b.s.l., i.e. 2.5 km below the summit), particularly in the sector currently responsible of measured deformations, and/or 2) the flow rate of the ascending hot fluids exceeds considerably both vertical and horizontal permeability-driven drainage through the deep dome fractures, thus impeding the pressure drop to nearly hydrostatic conditions. In this study we show evidence that this second scenario was initiated during the February-late April unrest phase, but could not reach its critical stage because water was effectively drained 2 km NW the dome axis through rock sectors of the NW-SE fault structure already solicited by the 16-17 swarm. This however produced 3 km NW away of the dome the M<sub>L</sub> 4.1 seismic episode, which is related to the sudden release of fluid overpressure initiating rock brecciation (Fournier, 2007; Sibson, 1986; Sillitoe, 2010) and can then be seen as a “failed phreatic” eruption.

As reported of the end of section 4.2, one highly possible origin for the infiltration of deep magmatic gases is replenishment of the deep ( $\geq 4.5$  km b.s.l.) magma chamber. In our view, the sudden 30°C heating inferred from February to late April 2018 at depth  $> 0.5$  km b.s.l. can only be achieved by the sudden arrival of a magma batch transferring its heat to the surrounding crustal fluids and triggering the thermoelastic effects that lead to undrained conditions (Delaney et al., 1982,

1984; McTigue, 1986), rapid overpressure build-up and rock failure. It is outside the scopes of the present study to provide a thorough treatment of this matter, which would also demand to account for the role played by tectonic stresses, but we can refer to the model developed by White and McCausland (2016) who have shown that distal volcano-tectonic (dVT) earthquakes are usually the earliest known precursor to eruptions at long dormant volcanoes. It is worth noting that the database in the work includes also the 1976 subsequent phreatic explosions of La Soufrière de Guadeloupe. The same may be said for the seismic swarms described here as dVT locations are disconnected spatially from the LP/hybrid (micro)seismicity beneath the volcano crater. The dVTs occur typically in swarm-like pulses of seismicity, characterized by large non-double component to the focal mechanism and with peaks in both event rate and average magnitude about the time of the initial (either magmatic or phreatic) activity. Coherent with the observations reported in our study, swarm-like dVT seismicity ramps up in number and magnitude over weeks. As pulses of magma intrude, they gradually over-pressurize the aquifers and lubricate the local tectonically pre-stressed fault, allowing more and larger patches to slip (White and McCausland, 2016). We suggest that this activity may thus have peaked up with the 28 April M 4.1 earthquake although this initiated a typical main shock/aftershock swarm, rather than be the major event during a ramping up sequence, as in principles required for distal VT earthquakes swarms described by White and McCausland (2016). By using the Authors' relation cumulative seismic moment with the magma intruding volume ( $\text{Log}_{10}V = 0.77 \times \text{Log}_{10}M_0 - 5.32$ , with volume  $V$  in cubic meters and moment  $M_0$  in Nm; White and McCausland, 2016), we see that an intrusion of  $2.7 \times 10^6 \text{ m}^3$ , corresponding to a sphere of only 173 m in diameter, may have emplaced between February and late April 2018. Based on the sensitivity of our GPS network (section 3.2.1) and in line with the physico-numerical findings in Coulon et al. (2017) on distal pressure changes triggering dVT seismicity, we conjecture that such a small intrusion might have emplaced well below the brittle-ductile transitions.

#### 4.4 Lessons learnt: implications for volcanic surveillance and the monitoring strategy

Geophysical and geochemical data of this study show that a phreatic eruption at La Soufrière volcano did not occur during the 2018 unrest because of the high degree of fracturing and permeability of the volcanic dome, whose mechanical state has deeply changed after the 1976 eruption (Komorowski et al., 2005; Rosas-Carbajal et al., 2016). However, episode of deep magmatic degassing point to the likely replenishment of the magma storage zones. This increases the probability for a future eruption to start with a sudden phreato-magmatic phase anticipated by a very short-lived phreatic phase. For the very same reasons, seismic activities and unrest episodes like the one recorded in February-April 2018 must be seen on one side as failed phreatic eruptions, and

on the other side as episodes prodromal to even major energy releases implying the destabilization of the hydrothermal system within the dome or the rise of magma batches.

The system has been evolving toward reactivation since 1992, as evidenced by geochemical data pointing to the 1976 (supercritical) cluster of points. The presence of acid species (HCl and SO<sub>2</sub>) and the lack of important sealing, active in 1976, should not mask the arrival of deep magmatic gas inputs prior to any future eruption. However, we cannot yet exclude that this may be preceded by a short phase in which fumarole chemistry becomes more hydrothermal. This can be also suggested by the composition of gases discharged around 28 April 2018, in concomitance with the locking episode of summit fractures (**Figure 8**). A similar, but far more important behavior, was in fact observed at Galeras, because of pre-eruptive sealing phenomena (Brombach et al., 2000; Fisher et al., 1997). In the case of La Soufrière, sealing could lead to fluid accumulation and rapid pore pressure build up under undrained conditions, and destabilize the shallow hydrothermal pressure source, leading the system to explosive activity. In addition, it can also favour the sliding of the volcano south-west flank, subject to a basal gravitational spread, because of the reduction of the coefficient of friction and the increase of pore pressure along mechanically weak areas in the dome. A rapidly escalating unrest could in fact trigger slope instability and partial collapse of the south-western flank as suggested by Komorowski et al. (2005) and Rosas-Carbajal et al. (2016) and modelled by Peruzzetto et al. (under review).

This scenario and, particularly, the fact that we could not forecast the 227 April 2018 event (intended as a phreatic eruption) call upon the need for the *in-situ* high-frequency collection and full analysis of the fumarolic fluids, in order to track the short-lived P-T transients of the hydrothermal system (Barberi et al., 1992; Rouwet et al., 2014; Stix and De Moor, 2018). This strategy, elsewhere successfully implemented via *in-situ* mass spectrometry (e.g., Campi Flegrei; Fedele et al., 2017), at La Soufrière presents many challenges related to intrinsic limits (high required power supply, instrumental fragility, costs and also logistics) and its hostile environment (rainy and windy conditions in a tropical environment, difficult accessibility, exposition to corrosion and unstable working conditions). At La Soufrière, it is however necessary to couple a full analysis including minor species (e.g., H<sub>2</sub>, CO, CH<sub>4</sub>, He) to the plume continuous measurements already operated via Multigas stations. Moreover, at La Soufrière Multigas sensors cannot provide the same levels of accuracy as at other volcanic sites where the sampled plumes emit superheated steam, much less affected by humidity than at La Soufrière (Aiuppa et al., 2011, 2018; De Moor et al., 2016).

In light of the strong role played by fluid release, hence by advective heat transport, it is then priority to improve our monitoring systems and surveillance protocols to 1) detect rapid hydrothermal transients in heat flux, 2) map and track variations in the distribution of deep isotherms. We want to stress here that joining thermal calculations based on energy conservation

(e.g., Di Renzo et al., 2016) to the deformation modeling adopted here would be a strict test for magma plumbing models as well as for sources responsible of observed rapid deformations, because they considerably narrow the domain of solutions to a set that are very similar (temporal similarity) and congruent (spatially similar). In this respect, a reasonable development of geothermal activity in the La Soufrière surroundings could represent a major contribution to track the evolution of deep temperatures, as well as anomalous chemical signatures of deep fluids. In addition, a detailed survey of spring water chemistry and isotope chemistry, extended to dissolved gases, will provide the necessary basis to model the chemical and hydraulic interaction between deep volcanic gases, the hydrothermal system and groundwaters, also contributing to the identification of possible high-pressure groundwater pathways.

On the geophysical side, the likely occurrence of rapid deformation pulses warns of the possibility of contamination of the broadband seismic signal due to tilt change, especially for long-period signals (Aoyama et al., 2008; Pino et al., 2011), and suggests that effective tiltmetric measurements should be performed, also considering the role played by aseismic slip along the deep fractures cutting the dome. These should be accompanied by permanent gravity measurements, as well as dilatometric measurements (e.g., Scarpa et al., 2007), in order to track the evolution of the 6 km deep magma chamber and its refilling. These measurements would also help understanding better the mass transfer-stress-strain relationships occurring on La Soufrière and accompanying distal seismicity, which has the potential for estimating intrusive volumes and forecasting eruptions (White and McCausland, 2016; Coulon et al., 2017). Hence, future accurate assessments should also add to scrutiny the seismic swarms periodically occurring in the Les Saintes archipelago, located km SE of La Soufrière between the Guadeloupe and Dominica (see also Bazin et al., 2010; Feuillet et al., 2011 and references therein) and often characterized by important non-double component.

In light of the small volume of magma emplaced (see section 4.3) and the short timescales between mafic recharge and eruption, which for the 1530 AD eruption span from tens of days to tens of hours (Pichavant et al., 2018), the improvement of the observatory capability to detect and interpret subtle variations related to the refilling of the 6-7 km deep magma chamber is obviously a major task. As shown here, as well as in other critical volcanic-hydrothermal areas (e.g. Campi Flegrei, Italy; Troise et al., 2019), such a task can be accomplished only through accurate joint consideration and analysis of geophysical and geochemical data (Supplementary Figure S7 and Supplementary Table 1).

## 5. Conclusions

The La Soufrière of Guadeloupe unrest attained on 27 April 2018 its relative maximum since 42 years, i.e. after the 1976-1977 phreatic eruption. Recorded events include:

- 1 felt earthquake M 2.1 on 1<sup>st</sup> February 2018 in a sequence of 30 earthquakes located at 1 km bsl (2.5 km depth below the volcano summit);
- 1 felt earthquake M 2.1 on 16-17 April in a sequence of 140 earthquakes located up to 1 km NW away of the dome, with most energetic events (  $M > 1$  ) at a depth between 1 to 1.6 km bsl (2.5 and 3.1 km below the volcano summit);
- 2 felt earthquakes on April 27, including that of magnitude  $M_L$  4.1 in a sequence of 180 earthquakes located at about 2-3 km NW away from the dome, , with most energetic events (  $M > 2$  ) at a depth of 2 km bsl (3 km below the local ground-level).

This level of volcanic seismicity, unprecedented since 1976, has been associated with

- 1) a clearly magmatic signature of "pulses" of gases rich in  $\text{CO}_2$ , HCl,  $\text{H}_2\text{S}$ , and  $\text{SO}_2$  in significant concentration around the vents;
- 2) the emission of hot hydrothermal fluids discharged by a hydrothermal system heated and pressurized ( $\Delta P$  between 64 and 175 bar) from the deep areas of the volcanic system due to arrival of a major magmatic gas pulse;
- 3) horizontal deformation velocities around the dome (<1 km) up to 9 mm / year between 1995 and 2018 that are related to the shallow pressurization of the system hydrothermal as well as the gravitational spreading of the south-west flank of the dome.
- 4) renewed phases of fracture opening on the dome;

Geochemical analysis, and its thermodynamic interpretation, show that there has been a rise in fluids of deep origin (magmatic). This caused transient phases of overpressure and overheating at the base of the hydrothermal system, particularly in a source volume that we locate 2.5 km deep below the volcano summit. This excess fluid pressure was responsible for the 2018 considerable increase of volcanic seismicity on the Grande Découverte-Soufriere massif. The seismicity recorded along the NW-SE regional fault crossing the volcanic massif presents elements compatible with a process of hydrofracturing and/or hydroshearing. Nevertheless, at the scale of the dome, overpressure was dissipated either upward, through the highly permeable vertical fractures dissecting the dome, and laterally, by triggering slip along the NW-SE fault. This sequence of events preserved the stability of the shallow hydrothermal system, whose currently small pressure source at about 0.5 km depth is responsible for the radial component of the deformation observed at the summit.

Comparison of thermochemical features of current fumarolic discharges with 1997 and July 1976 data indicates that the hydrothermal system, reactivated since 1992, has increased its vigor, evolving from an early development phase dominated by important steam condensation (1997 data)

to a mature condition in which boiling accompanies a clear increase of hydrothermal temperature, hence heat flux, and pressure, thus re-approaching the pre-1976 state.

Drainage of the hydrothermal liquid (water) outside the dome after the 16-17 April swarm along a NW-SE regional structure, inhibited the occurrence of a phreatic eruption which points to the conclusion that the 27 April  $M_L$  4.1 earthquake represents a failed phreatic eruption. No clear evidence can indicate so far the rise of magma to depths lower than those of the andesitic magma chamber (i.e. <6-7 km below the La Soufrière summit), although He-based chemical ratios and contrasting halogen behaviour have already suggested the occurrence of refreshment and/or replenishment of such a magma chamber. Based on distal seismicity evaluations, particularly the ramp up of magnitudes, a magmatic volume of  $2.7 \cdot 10^6 \text{ m}^3$  may have intruded between February and late April 2018.

The main lesson we have learnt from this record of events is that La Soufrière of Guadeloupe has changed behaviour and is at a significantly higher level of activity than it has been over the last 40 years. Given the increase in seismic and fumarolic activity recorded since February 2018, we cannot exclude an intensification of phenomena in the future, the present-day hydrothermal system being recharging in a P-T condition corresponding to the pre-1976 one, and not dissimilar to Montserrat before the eruption that started in 1995 (Chiodini et al., 1996). Only a high-frequency joint geophysical, thermal and geochemical monitoring can disclose the rapid transient in pressure and temperature able to destabilize the hydrothermal system. Future eruptive activity may be preceded by a short phase in which fumarole chemistry becomes more hydrothermal due to sealing phenomena. This could bring to fluid accumulation and rapid pore pressure build-up destabilizing the shallow hydrothermal pressure source, leading to the (initial) phreatic explosion and favoring the sliding of the volcano south-west flank.

### Acknowledgements

We thank IPGP for general funding to *Observatoires Volcanologiques et Sismologiques (OVS)* as well as for financial support via the AO-IPGP 2018 project “Depth to surface propagation of fluid-related anomalies at La Soufrière de Guadeloupe volcano (FWI): timing and implications for volcanic unrest” (coord.: R. Moretti), CNRS-INSU for funding provided by *Service National d’Observation en Volcanologie (SNOV)*, the ANR “DIAPHANE” project (coord.: D. Gibert) and the Ministère pour la Transition Ecologique et Solidaire (MTES) for financial support. Part of the G. Ucciani’s postdoc was funded by the PREST project (INTERREG Caraïbes 5). We also thank the Parc National de Guadeloupe for logistic support and assistance during field work. Willy Aspinall is acknowledged for his helpful insights into distal seismicity. The manuscript benefited of precious suggestions by P. Bernard (IPGP) and two anonymous reviewers. This study contributes to the IdEx Université de Paris ANR-18-IDEX-0001 and is ClerVolc contribution N. XXXXXXXX.

## References

- Aiuppa, A., Federico, C., Giudice, G., & Gurrieri, S. (2005). Chemical mapping of a fumarolic field: la Fossa crater, Vulcano Island (Aeolian Islands, Italy). *Geophysical Research Letters*, 32(13).
- Aiuppa, A., Shinohara, H., Tamburello, G., Giudice, G., Liuzzo, M., & Moretti, R. (2011). Hydrogen in the gas plume of an open vent volcano (Mt. Etna, Italy). *JOURNAL OF GEOPHYSICAL RESEARCH: SOLID EARTH*, 116, 1-5
- Aiuppa, A., de Moor, J. M., Arellano, S., Coppola, D., Francofonte, V., Galle, B., ... & Tamburello, G. (2018). Tracking formation of a lava lake from ground and space: Masaya volcano (Nicaragua), 2014–2017. *Geochemistry, Geophysics, Geosystems*, 19(2), 496-515.
- Allard, P. (1983). The origin of hydrogen, carbon, sulphur, nitrogen and rare gases in volcanic exhalations: Evidence from isotope geochemistry. Chapter 25 in. *Forecasting volcanic events*, 337-386.
- Allard, P., 2006. 30 years after the 1976–77 seismo-phreatic crisis of Soufrière volcano, Guadeloupe island (FWI): revisited source mechanism(s) and implications. Abstract Presented at GARAVOLCAN International Meeting, Tenerife, Canaries, 21–27 May 2006.
- Allard, P., Hammouya, G., & Parello, F. (1998). Diffuse magmatic soil degassing at Soufrière of Guadeloupe, Antilles. *Comptes Rendus de l'Academie des Sciences Series IIA Earth and Planetary Science*, 5(327), 315-318.
- Allard, P., Aiuppa, A., Beauducel, F., Gaudin, D., Di Napoli, R., Calabrese, S., ... & Tamburello, G. (2014). Steam and gas emission rate from La Soufriere volcano, Guadeloupe (Lesser Antilles): implications for the magmatic supply during degassing unrest. *Chemical Geology*, 384, 76-93.
- Aoyama, H., & Oshima, H. (2008). Tilt change recorded by broadband seismometer prior to small phreatic explosion of Meakan-dake volcano, Hokkaido, Japan. *Geophysical Research Letters*, 35(6).
- Arnorsson S. and Gunnlaugsson E. (1985) New gas geothermometers for geothermal exploration - Calibration and application. *Geochim. Cosmochim. Acta* 49, 1307–1325.
- Barberi, F., Bertagnini, A., Landi, P., & Principe, C. (1992). A review on phreatic eruptions and their precursors. *Journal of volcanology and geothermal research*, 52(4), 231-246.
- Barenblatt, G. I., Zheltov, I. P. & Kochina, I. N. Basic concepts in the theory of seepage of homogeneous liquids in fissured rocks. *J. Appl. Math. Mech.* 24, 1286–1303 (1960).
- Barrabé, L. & Jolivet, J. (1958) Les récentes manifestations d'activité de la Guadeloupe (Petites Antilles). (French) Recent activity manifestations of Guadeloupe (Lesser Antilles) .*Bulletin of Volcanology* 19, 143–157

- Battaglia, M., Troise, C., Obrizzo, F., Pingue, F., & De Natale, G. (2006). Evidence for fluid migration as the source of deformation at Campi Flegrei caldera (Italy). *Geophysical Research Letters*, 33(1).
- Bazin, S., Feuillet, N., Duclos, C., Crawford, W., Nercessian, A., Bengoubou-Valérius, M., ... & Singh, S. C. (2010). The 2004–2005 Les Saintes (French West Indies) seismic aftershock sequence observed with ocean bottom seismometers. *Tectonophysics*, 489(1-4), 91-103.
- Becker K., R. P. Von Herzen, T. J. G. Francis, R. N. Anderson, J. Honnorez, A. C. Adamson, J. C. Alt, R. Emmermann, P. D. Kempton, H. Kinoshita, C. Laverne, M. J. Mottl & R. L. Newmark In situ electrical resistivity and bulk porosity of the oceanic crust Costa Rica Rift *Nature* volume 300, pages 594–598 (16 December 1982) |
- Bigot S, G. Boudon, M.P. Semet, G. Hammouya Traçage chimique de la circulation des eaux souterraines sur le volcan de la Grande Découverte (la Soufrière), Guadeloupe CR Acad Sci Paris, 318 (1994), pp. 1215-1221
- Boichu, M., Villemant, B., & Boudon, G. (2008). A model for episodic degassing of an andesitic magma intrusion. *Journal of Geophysical Research: Solid Earth*, 113(B7).
- Boichu, M., Villemant, B. & Boudon, G. Degassing at La Soufrière de Guadeloupe volcano (Lesser Antilles) since the last eruptive crisis in 1975{77: Result of a shallow magma intrusion? *Journal of Volcanology and Geothermal Research* 203, 102{112 (2011).
- Boudon, G., Le Friant, A., Villemant, B. & Viode, J.-P. Martinique. *Volcanic Atlas of the Lesser Antilles* 126{145 (2005).
- Brace, W. F., Permeability of crystalline and argillaceous rocks, *Int. J. Rock Mech. Min. Sci. Geomech. Abstr.*, 17, 241-251, 1980
- Brodsky, E. E., Sturtevant, B., & Kanamori, H. (1998). Earthquakes, volcanoes, and rectified diffusion. *Journal of Geophysical Research: Solid Earth*, 103(B10), 23827-23838.
- Brombach, T., Marini, L., & Hunziker, J. C. (2000). Geochemistry of the thermal springs and fumaroles of Basse-Terre Island, Guadeloupe, Lesser Antilles. *Bulletin of Volcanology*, 61(7), 477-490.
- Brothelande, E., Finizola, A., Peltier, A., Delcher, E., Komorowski, J. C., Di Gangi, F., ... & Legendre, Y. (2014). Fluid circulation pattern inside La Soufrière volcano (Guadeloupe) inferred from combined electrical resistivity tomography, self-potential, soil temperature and diffuse degassing measurements. *Journal of Volcanology and Geothermal Research*, 288, 105-122.
- Buck, W. R., Martinez, F., Steckler, M. S., & Cochran, J. R. (1988). Thermal consequences of lithospheric extension: pure and simple. *Tectonics*, 7(2), 213-234.
- Caliro, S., Chiodini, G., & Paonita, A. (2014). Geochemical evidences of magma dynamics at Campi Flegrei (Italy). *Geochimica et cosmochimica acta*, 132, 1-15.
- Chatterjee, S.N., A.M. Pitt, and H.M. Iyer, Vp/Vs ratios in the Yellowstone national park region, Wyoming, *J. Volcanol. Geotherm. Res.*, 26, 213-230, 1985

- Chevrier R.M., Dajlevic D., Le Guern F. and Rouyerr J.L. (1976) Données recueillies sur la phase gazeuse de la Soufrière (Guadeloupe) du 13 Juillet au 20 Septembre 1976. Rapport CEA, Département de protection, Novembre 1976.
- Chiodini, G., Cioni, R., Frullani, A., Guidi, M., Marini, L., Prati, F., & Raco, B. (1996). Fluid geochemistry of Montserrat Island, West Indies. *Bulletin of Volcanology*, 58(5), 380-392.
- Chiodini, G. (2009). CO<sub>2</sub>/CH<sub>4</sub> ratio in fumaroles a powerful tool to detect magma degassing episodes at quiescent volcanoes. *Geophysical Research Letters*, 36(2).
- Chiodini, G., Vandemeulebrouck, J., Caliro, S., D'Auria, L., De Martino, P., Mangiacapra, A., & Petrillo, Z. (2015). Evidence of thermal-driven processes triggering the 2005–2014 unrest at Campi Flegrei caldera. *Earth and Planetary Science Letters*, 414, 58-67.
- Chiodini, G., & Marini, L. (1998). Hydrothermal gas equilibria: the H<sub>2</sub>O-H<sub>2</sub>-CO<sub>2</sub>-CO-CH<sub>4</sub> system. *Geochimica et Cosmochimica Acta*, 62(15), 2673-2687
- Chiodini, G., Marini, L., & Russo, M. (2001). Geochemical evidence for the existence of high-temperature hydrothermal brines at Vesuvio volcano, Italy. *Geochimica et Cosmochimica Acta*, 65(13), 2129-2147.
- Collettini, C., & Barchi, M. R. (2002). A low-angle normal fault in the Umbria region (Central Italy): a mechanical model for the related microseismicity. *Tectonophysics*, 359(1-2), 97-115.
- Connolly JAD (1997) Devolatilization-generated fluid pressure and deformation-propagated fluid flow during prograde regional metamorphism. *Journal of Geophysical Research*, 102, B8, 18149-18173.
- Coulon C.A., Hsieh P.A., White R., Lowenstern J.B. and Ingebritsen S.E. (2017) Causes of distal volcano-tectonic seismicity inferred from hydrothermal modelling. *J. Volcanol. Geotherm. Res.*, 345, 98-108.
- Cox, S.F., 1995, Faulting processes at high fluid pressures: An example of fault valve behavior from the Wattle Gully Fault, Victoria, Australia: *Journal of Geophysical Research (Solid Earth)*, v 100, p. 12,841–12,859, doi: 10.1029/95JB00915.
- D'Amore, F., & Panichi, C. (1980). Evaluation of deep temperatures of hydrothermal systems by a new gas geothermometer. *Geochimica et Cosmochimica Acta*, 44(3), 549-556.
- De Moor, J. M., Aiuppa, A., Avaró, G., Wehrmann, H., Dunbar, N., Müller, C., ... & Conde, V. (2017). Turmoil at Turrialba Volcano (Costa Rica): Degassing and eruptive processes inferred from high-frequency gas monitoring. *Journal of Geophysical Research: Solid Earth*, 121(8), 5761-5775.
- Del Pezzo, Edoardo, Francesca Bianco, and Gilberto Saccorotti. "Seismic source dynamics at Vesuvius volcano, Italy." *Journal of volcanology and geothermal research* 133.1-4 (2004): 23-39.

- Di Renzo, V., Wohletz, K., Civetta, L., Moretti, R., Orsi, G., & Gasparini, P. (2016). The thermal regime of the Campi Flegrei magmatic system reconstructed through 3D numerical simulations. *Journal of Volcanology and Geothermal Research*, 328, 210-221.
- Delaney PT (1982) Rpid intrusion of magma into wet rock: groundwater flow due to pore pressure increases. *J. Geophys. Res.* 87, 7739-7756
- Delaney, P., Heating of a fully saturated Darcian half-space: pressure generation fluid expulsion and phase change. *Int. J. Heat Mass Transfer*, 27, 1327-1335, 1984.
- Dorel, J., Eschenbrenner, S., Feuillard, M., 1979. Coupes sismiques des structures superficielles dans les petites antilles—I : Guadeloupe. *Pure and Applied Geophysics* 117 (9), 1050–1069.
- Fabre, R., & Chaigneau, M. (1960). Technique de prélèvement et d'analyse de gaz de fumerolles de volcans. Exemples d'analyses de gaz prélevés à la montagne Pelée (Martinique) et à la Grande Soufrière (Guadeloupe). *Bulletin Volcanologique*, 23(1), 21-30.
- Fedele, A., Pedone, M., Moretti, R., Wiersberg, T., Somma, R., Troise, C., & De Natale, G. (2017). Real-time quadrupole mass spectrometry of hydrothermal gases from the unstable Pisciarelli fumaroles (Campi Flegrei): Trends, challenges and processes. *International Journal of Mass Spectrometry*, 415, 44-54.
- Feuillard, M. et al. The 1975-1977 crisis of La Soufrière de Guadeloupe (FWI): a still-born magmatic eruption. *Journal of Volcanology and Geothermal Research* 16, 317{334 (1983).
- Feuillet, N., Manighetti, I., Tapponnier, P., & Jacques, E. (2002). Arc parallel extension and localization of volcanic complexes in Guadeloupe, Lesser Antilles. *Journal of Geophysical Research: Solid Earth*, 107(B12), 107.B12: ETG 3-1-ETG 3-29.
- Feuillet, N., Beauducel, F. & Tapponnier, P (2011). Tectonic context of moderate to large historical earthquakes in the lesser antilles and mechanical coupling with volcanoes. *Journal of Geophysical Research: Solid Earth* (1978{2012) 116.
- Fischer, T. P., Sturchio, N. C., Stix, J., Arehart, G. B., Counce, D., & Williams, S. N. (1997). The chemical and isotopic composition of fumarolic gases and spring discharges from Galeras Volcano, Colombia. *Journal of Volcanology and Geothermal Research*, 77(1-4), 229-253.
- Fournier R.O. (2007) Hydrothermal systems and volcano geochemistry. In *Volcano deformation*. 323-341, Springer, Berlin, Heidelberg
- Ganguly, J. (2009). *Thermodynamics in earth and planetary sciences*. Springer Science & Business Media.
- Gaudin, D., Beauducel, F., Coutant, O., Delacourt, C., Richon, P., de Chabaliér, J. B., & Hammouya, G. (2016). Mass and heat flux balance of La Soufrière volcano (Guadeloupe) from aerial infrared thermal imaging. *Journal of Volcanology and Geothermal Research*, 320, 107-116.

- Giggenbach, W. F. (1980). Geothermal gas equilibria. *Geochimica et Cosmochimica Acta*, 44(12), 2021-2032.
- Giggenbach, W. (1987) Redox processes governing the chemistry of fumarolic gas discharges from White Island, New Zealand. *Applied Geochemistry* 2, 143-161.
- Giggenbach W. F. (1988) Geothermal solute equilibria. Derivation of Na-K-Mg-Ca geothermometers. *Geochim. Cosmochim. Acta* 52, 2749–2765.
- Giggenbach W. F. (1997) The origin and evolution of fluids in magmatic-hydrothermal systems. In *Geochemistry of Hydrothermal Ore Deposits*, 3rd Edition (ed. H. L. Barnes), pp. 737–796, John Wiley & Sons, New York.
- Giggenbach, W. F., & Goguel, R. L. (1989). Collection and analysis of geothermal and volcanic water and gas discharges. Report No. CD 2401. Department of Scientific and Industrial Research. Chemistry Division, Petone, New Zealand.
- Haimson, B. C., & Zhao, Z. (1991) Effect of borehole size and pressurization rate on hydraulic fracturing breakdown pressure. In *The 32nd US Symposium on Rock Mechanics (USRMS)*. American Rock Mechanics Association.
- Hanks T.C., H. Kanamori (1979). A Moment Magnitude Scale *Journal of Geophysical Research*, 84/B5, 2348-2350
- Hapel-Lachênaie, T., Peyre, A. & Fontelliau, C. (1798) Rapport fait aux citoyens Victor Hugues et Lebas, agents particuliers du directoire exécutif aux isles du vent, par la commission établie en vertu de leur arrêté du 12 vendémiaire, an 6 de la république, pour examiner la situation du Volcan de la Guadeloupe, et les effets de l'éruption qui a eu lieu dans la nuit du 7 au 8 du même mois. (An VI. Facsimile, Société d'Histoire De la Guadeloupe, Basse-Terre, 179
- Harris, A. (2013). *Thermal remote sensing of active volcanoes: a user's manual*. Cambridge University Press. 728 pp
- Hill, D.P., Ellsworth, W.L., Johnston, M.J.S., Langbein, J.O., Oppenheimer, D.H., Pitt, A.M., Reasenberg, P.A., Sorey, M.L. and McNutt, S.R. (1990). The 1989 earthquake swarm beneath Mammoth Mountain, California: An initial look at the 4 May through 30 September activity. *Bulletin of the Seismological Society of America*, 80(2), 325-339.
- Hill, D. P., F. Pollitz, and C. Newhall (2002), Earthquake-volcano interactions, *Phys. Today*, 55(11), 41–47.
- Hincks, T. K., Komorowski, J.-C., Sparks, S. R. & Aspinall, W. P. Retrospective analysis of uncertain eruption precursors at La Soufrière volcano, Guadeloupe, 1975–1977: volcanic hazard assessment using a bayesian belief network approach. *Journal of Applied Volcanology* 3, 1{26 (2014).

- Hyndman R.D., S.L. Klemperer *GEOPHYSICAL RESEARCH LETTERS*, VOL. 16, NO. 3, PAGES 255-258, MARCH 1989 LOWER-CRUSTAL POROSITY FROM ELECTRICAL MEASUREMENTS AND INFERENCES ABOUT COMPOSITION FROM SEISMIC VELOCITIES
- Hyndman R.D., P. M. Sheare *Geophys. J. Int.* (1989) 98, 343-365 Water in the lower continental crust: modelling magnetotelluric and seismic reflection results
- Ito, H., DeVilbiss, J. and Nur, A., 1979. Compressional and shear waves in saturated rock during water-steam transition. *J. Geophys. Res.*, 84: 4731--4735.
- Jean-Baptiste, P., Allard, P., Fourré, E., Parello, F., & Aiuppa, A. (2014). Helium isotope systematics of volcanic gases and thermal waters of Guadeloupe Island, Lesser Antilles. *Journal of Volcanology and Geothermal Research*, 283, 66-72.
- Jolivet, J. La crise volcanique de 1956 à la Soufrière de la Guadeloupe. (French). The volcanic crisis of 1956 at La Soufrière of Guadeloupe. In *Annales de Géophysique*, vol. 14, 305 (1958).
- Kehle R., The Determination of Tectonic Stresses Through Analysis of Hydraulic Well Fracturing, *J. Geophys. Res. Q*, 259-273 (1964).
- Komorowski, J-C. et al. L'activité éruptive et non-éruptive de la Soufrière de Guadeloupe: problèmes et implications de la phénoménologie et des signaux actuellement enregistrés. (French). Eruptive and non-eruptive activity from la Soufrière of Guadeloupe: problems and implications posed by the current phenomenology and monitoring signals. Workshop on volcanic hazards - Lesser Antilles volcanoes: from processes to signals. . PNRN (CNRS){INSU, BRGM, CEA, CEMAGREF, CNES, IRD 18(19 (2001).
- Komorowski, J. et al. Guadeloupe. In *Volcanic Atlas of the Lesser Antilles*, 65{102 (Seismic Research Unit, The University of the West Indies Trinidad, 2005).
- Komorowski, J.-C., Legendre, Y., Caron, B. & Boudon, G. Reconstruction and analysis of subplinian tephra dispersal during the 1530 AD Soufrière (Guadeloupe) eruption: Implications for scenario definition and hazards assessment. *Journal of Volcanology and Geothermal Research* 178, 491{515 (2008).
- Komorowski, J., Hincks, T., Sparks, R., Aspinall, W. et al. Improving crisis decision-making at times of uncertain volcanic unrest (Guadeloupe, 1976). In *Global Volcanic Hazards and Risk*, 255 (Cambridge University Press, 2015).
- Korenaga Jun, Peter B. Kelemen *Earth and Planetary Science Letters* 156 ( 1998) 1 – 11 Melt migration through the oceanic lower crust: a constraint from melt percolation modeling with finite solid diffusion
- Le Guern, F., Bernard, A. & Chevrier, R. (1980) Soufrière of Guadeloupe 1976-1977 eruption. Mass and energy transfer and volcanic health hazards. *Bulletin Volcanologique* 43, 577-593.

- Legendre, Y. Reconstruction de l'histoire éruptive et scénarii éruptifs à La Soufrière de Guadeloupe: vers un modèle intégrale de fonctionnement du volcan. (French) [A high resolution reconstruction of the eruptive past and definition of eruptive scénarii at La Soufrière of Guadeloupe]. Ph.D. thesis, Paris 7 (2012).
- Lherminier, F. (1837a) Sur les produits du volcan de la Guadeloupe. Comptes rendus de l'Académie des sciences. 454–455.
- Lherminier, F. (1837b) L'éruption du volcan de la Guadeloupe. La Soufrière of Guadeloupe . Nouvelles Annales de Voyage 74, 349–350
- Lherminier, F. (1837c) Note sur l'éruption du volcan de la Guadeloupe. (French). On the products from the volcano of La Guadeloupe. Comptes rendus de l'Académie des sciences. 294.
- Lesparre, N., Gibert, D., Marteau, J., Komorowski J-C., Nicollin, F., Coutant, O. (2012) Density Muon Radiography of Soufrière of Guadeloupe Volcano: Comparison with Geological, Electrical Resistivity and Gravity data. *Geophys. J. Int.*, doi : 10.1111/j.1365-246X.2012.05546.x
- Linde, A. T., & Sacks, I. S. (1998). Triggering of volcanic eruptions. *Nature*, 395(6705), 888.
- Lomax, A., Virieux, J., Volant, P., Berge-Thierry, C., 2000. Probabilistic earthquake location in 3D and layered models – Introduction of a Metropolis-Gibbs method and comparison with linear locations. In : *Advances in Seismic Event Location*. pp. 101–134.
- Manning C.E. and S.E. Ingebritsen Permeability of the continental crust: Implications of geothermal data and metamorphic systems 1999 37, 127-150 *Reviews of Geophysics*
- Marzocchi, W. (2002). Remote seismic influence on large explosive eruptions. *Journal of Geophysical Research: Solid Earth*, 107(B1).
- Mastin, L.G. (1995). The thermodynamics of steam-blast eruptions. *Bulletin of Volcanology*, 57:85-98
- McTigue, D. F. (1986). Thermoelastic response of fluid-saturated porous rock. *Journal of Geophysical Research: Solid Earth*, 91(B9), 9533-9542.
- Micklethwaite, S., & Cox, S. F. (2006). Progressive fault triggering and fluid flow in aftershock domains: Examples from mineralized Archaean fault systems. *Earth and Planetary Science Letters*, 250(1-2), 318-330.
- Miller S.A. (2015) Modeling enhanced geothermal systems and the essential nature of large-scale changes in permeability at the onset of slip. *Geofluids* 15, 338–349
- Miller S.A., Nur A., Olgaard D.A. Earthquakes as a coupled shear stress - high pore pressure dynamical system. *GEOPHYSICAL RESEARCH LETTERS*, VOL. 23, NO. 2, PAGES 197-200, JANUARY 15, 1996
- Miller S.A., Nur A. (2000) Permeability as a toggle switch in fluid-controlled crustal processes. *Earth and Planetary Science Letters* 183 (2000) 133-146
- Miller, V., B. Voight, C. J. Ammon, E. Shalev, and G. Thompson (2010) Seismic expression of magma-induced crustal strains and localized fluid pressures during initial eruptive stages,

- Soufrière Hills Volcano, Montserrat GEOPHYSICAL RESEARCH LETTERS, VOL. 37, L00E21, doi:10.1029/2010GL043997
- Mizutani, Y., & Sugiura, T. (1982). Variations in chemical and isotopic compositions of fumarolic gases from Showashinzan volcano, Hokkaido, Japan. *Geochemical Journal*, 16(2), 63-71.
- Moretti, R., Papale, P., & Ottonello, G. (2003). A model for the saturation of COHS fluids in silicate melts. Geological Society, London, Special Publications, 213(1), 81-101.
- Moretti, R., Arienzo, I., Civetta, L., Orsi, G., & Papale, P. (2013a). Multiple magma degassing sources at an explosive volcano. *Earth and Planetary Science Letters*, 367, 95-104.
- Moretti, R., Arienzo, I., Orsi, G., Civetta, L., & D'antonio, M. (2013b). The deep plumbing system of Ischia: A physico-chemical window on the fluid-saturated and CO<sub>2</sub>-sustained Neapolitan Volcanism (Southern Italy). *Journal of Petrology*, 54(5), 951-984.
- Moretti, R., De Natale, G., & Troise, C. (2017). A geochemical and geophysical reappraisal to the significance of the recent unrest at Campi Flegrei caldera (Southern Italy). *Geochemistry, Geophysics, Geosystems*, 18(3), 1244-1269.
- Moretti, R., Troise, C., Sarno, F., & De Natale, G. (2018b). Caldera unrest driven by CO<sub>2</sub>-induced drying of the deep hydrothermal system. *Scientific reports*, 8(1), 8309.
- Moretti, R., Arienzo, I., Di Renzo, V., Orsi, G., Arzilli, F., Brun, F., ... & Deloule, E. (2019). Volatile segregation and generation of highly vesiculated explosive magmas by volatile-melt fining processes: The case of the Campanian Ignimbrite eruption. *Chemical Geology*, 503, 1-14.
- Mourgues, R., & Cobbold, P. R. (2003). Some tectonic consequences of fluid overpressures and seepage forces as demonstrated by sandbox modelling. *Tectonophysics*, 376(1-2), 75-97.
- Nakajima, J., Matsuzawa, T., Hasegawa, A., & Zhao, D. (2001). Three-dimensional structure of V<sub>p</sub>, V<sub>s</sub>, and V<sub>p</sub>/V<sub>s</sub> beneath northeastern Japan: Implications for arc magmatism and fluids. *Journal of Geophysical Research: Solid Earth*, 106(B10), 21843-21857.
- Nakamura K, "Volcanoes as Possible Indicators of Tectonic Stress Orientation--Principle and Proposal," *J. Volcanol. and Geotherm. Res.* , 1-16 (1977).
- Nicollin, F., Gibert, D., Beauducel, F., Boudon, G. & Komorowski, J.-C. (2006) Electrical tomography of La Soufrière of Guadeloupe Volcano: Field experiments, 1D inversion and qualitative interpretation. *Earth and Planetary Science Letters* 244 , 709–724
- NIST (2018). *Thermophysical properties of fluid systems*. NIST Chemistry WebBook, SRD 69. National Institute of Standards and Technology. U.S.Department of Commerce (<https://webbook.nist.gov/chemistry/fluid/>) .
- Norton, D. L. (1984). Theory of hydrothermal systems. *Annual Review of Earth and Planetary Sciences*, 12(1), 155-177.

- Norton, D., & Knight, J. (1977). Transport phenomena in hydrothermal systems: cooling plutons. *Am. J. Sci.*, 277.
- Nostro, C., Stein, R. S., Cocco, M., Belardinelli, M. E., & Marzocchi, W. (1998). Two-way coupling between Vesuvius eruptions and southern Apennine earthquakes, Italy, by elastic stress transfer. *Journal of Geophysical Research: Solid Earth*, 103(B10), 24487-24504.
- Nuccio, P. M., & Paonita, A. (2000). Investigation of the noble gas solubility in H<sub>2</sub>O–CO<sub>2</sub> bearing silicate liquids at moderate pressure II: the extended ionic porosity (EIP) model. *Earth and Planetary Science Letters*, 183(3-4), 499-512.
- Nugraha, A.D., Indrastuti, N., Kusnandar, R., Gunawan, H., McCausland, W., Aulia, A.N. and Harlianti, U. (2019). Joint 3-D tomographic imaging of V<sub>p</sub>, V<sub>s</sub> and V<sub>p</sub>/V<sub>s</sub> and hypocenter relocation at Sinabung volcano, Indonesia from November to December 2013. *Journal of Volcanology and Geothermal Research*. 382, 210-223
- OVSG-IPGP, 1999-2019 monthly reports on the activity of La Soufrière de Guadeloupe and on regional seismicity, <http://www.ipgp.fr/fr/ovsg/bulletins-mensuels-de-lovsg>
- OVSG-IPGP (2017) September 2017 monthly report, [http://www.ipgp.fr/sites/default/files/ovsg\\_2017\\_bilan-annuel.pdf](http://www.ipgp.fr/sites/default/files/ovsg_2017_bilan-annuel.pdf)
- OVSG-IPGP 2018a seismic report, [http://volcano.ipgp.jussieu.fr/guadeloupe/Communiqués/2018/OVSG\\_20180202\\_SequenceSeismesVolcaniques\\_Soufrie%C3%A8re.pdf](http://volcano.ipgp.jussieu.fr/guadeloupe/Communiqués/2018/OVSG_20180202_SequenceSeismesVolcaniques_Soufrie%C3%A8re.pdf)
- OVSG-IPGP 2018b seismic report, [http://volcano.ipgp.jussieu.fr/guadeloupe/Communiqués/2018/OVSG\\_20180416\\_SequenceSeismesVolcaniques\\_Soufrie%CC%80re.pdf](http://volcano.ipgp.jussieu.fr/guadeloupe/Communiqués/2018/OVSG_20180416_SequenceSeismesVolcaniques_Soufrie%CC%80re.pdf)
- OVSG-IPGP seismic report seismic report, [http://volcano.ipgp.jussieu.fr/guadeloupe/Communiqués/2018/OVSG\\_20180428\\_SequenceSeismesSoufriere.pdf](http://volcano.ipgp.jussieu.fr/guadeloupe/Communiqués/2018/OVSG_20180428_SequenceSeismesSoufriere.pdf)
- Peyssonnel, J. A. and Maty M. (1756). Observations Made upon the Brimstone-Hill (in French La Souffriere) in the Island of Guadelupa; By John Andrew Peyssonnel, M. D. Member of the Royal Academies of Sciences of Paris and Montpellier, and of Marseilles and Rouen; The King of France's Physician and Botanist Heretofore on the Coast of Barbary, and Now in the Island of Guadelupa, F. R. S. Translated from the French by M. Maty, M. D. and F. R. S., *Philosophical Transactions*, 49, 564-579.
- Pichavant, M., Poussineau, S., Lesne, P., Solaro, C., & Bourdier, J. L. (2018). Experimental Parametrization of Magma Mixing: Application to the ad 1530 Eruption of La Soufrière, Guadeloupe (Lesser Antilles). *Journal of Petrology*, 59(2), 257-282.

- Pino, N. A., Moretti, R., Allard, P., & Boschi, E. (2011). Seismic precursors of a basaltic paroxysmal explosion track deep gas accumulation and slug upraise. *Journal of Geophysical Research: Solid Earth*, 116(B2).
- Poussineau, S. (2005). *Dynamique des magmas andésitiques: approche expérimentale et pétrostructurale; application à la Soufrière de Guadeloupe et à la Montagne Pelée* (Doctoral dissertation, Université d'Orléans).
- Pritchard, M. E., Mather, T. A., McNutt, S. R., Delgado, F. J., & Reath, K. (2019). Thoughts on the criteria to determine the origin of volcanic unrest as magmatic or non-magmatic. *Philosophical Transactions of the Royal Society A*, 377(2139), 20180008.
- Reed M. H. (1997) Hydrothermal alteration and its relationship to ore fluid composition. In *Geochemistry of Hydrothermal Ore Deposits*, 3rd Edition (ed. H. L. Barnes), pp. 517–611, John Wiley & Sons, New York.
- Rosas-Carbajal, M., Komorowski, J. C., Nicollin, F., & Gibert, D. (2016). Volcano electrical tomography unveils edifice collapse hazard linked to hydrothermal system structure and dynamics. *Scientific reports*, 6, 29899.
- Rouwet, D., Sandri, L., Marzocchi, W., Gottsmann, J., Selva, J., Tonini, R., & Papale, P. (2014). Recognizing and tracking volcanic hazards related to non-magmatic unrest: a review. *Journal of Applied Volcanology*, 3(1), 17.
- Rozhko, A. Y., Podladchikov, Y. Y., & Renard, F. (2007). Failure patterns caused by localized rise in pore-fluid overpressure and effective strength of rocks. *Geophysical Research Letters*, 34(22).
- Ruzié, L., Moreira, M., & Crispi, O. (2012). Noble gas isotopes in hydrothermal volcanic fluids of La Soufrière volcano, Guadeloupe, Lesser Antilles arc. *Chemical Geology*, 304, 158-165.
- Ruzié, L., Aubaud, C., Moreira, M., Agrinier, P., Dessert, C., Gréau, C., & Crispi, O. (2013). Carbon and helium isotopes in thermal springs of La Soufrière volcano (Guadeloupe, Lesser Antilles): implications for volcanological monitoring. *Chemical Geology*, 359, 70-80.
- Sanders, C.O., Ponko, S.C., Nixon, L.D. and Schwartz, E.A. (1995). Seismological evidence for magmatic and hydrothermal structure in Long Valley caldera from local earthquake attenuation and velocity tomography. *Journal of Geophysical Research: Solid Earth*, 100(B5), pp.8311-8326.
- Salaün A, Villemant B, Gérard M, Komorowski J-C, Michel A (2011) Hydrothermal alteration in andesitic Volcanoes: Trace element redistribution in active and ancient hydrothermal systems of Guadeloupe (Lesser Antilles). *J Geochem Expl* 111:59–83
- Scarpa R., A. Amoroso, L. Crescentini, P. Romano, W. De Cesare, M. Martini, G. Scarpato, A.T. Linde, S.I. Sacks New borehole strain system detects uplift at Campi Flegrei *Eos Trans. AGU*, 88 (18), doi:10.1029/2007EO180002, 2007

- Semet, M. P., Vatin-Perignon, N., Vincent, P. M., & Joron, J. L. (1982). Magma mixing once more: its involvement in triggering the 16th century volcanic activity at La Soufrière, Guadeloupe (FWI). *Bull. PIRPSEV*, 60, 63.
- Sheridan, M. F. (1980). Pyroclastic block flow from the September, 1976, eruption of La Soufrière volcano, Guadeloupe. *Bulletin Volcanologique* 43 (2), 397–402
- Shinohara, H. (2005). A new technique to estimate volcanic gas composition: plume measurements with a portable multi-sensor system. *Journal of Volcanology and Geothermal Research*, 143(4), 319-333.
- Schmitt, D. R., & Zoback, M. D. (1992). Diminished pore pressure in low-porosity crystalline rock under tensional failure: Apparent strengthening by dilatancy. *Journal of Geophysical Research: Solid Earth*, 97(B1), 273-288.
- Sibson, R.H. (1986) Brecciation processes in fault zones: Inferences from earthquake rupturing. *PAGEOPH* 124, 159–175 doi:10.1007/BF00875724
- Sibson, R.H., 1990, Rupture nucleation on unfavorably oriented faults: *Bulletin of the Seismological Society of America*, v. 80, p. 1580–1604.
- Sibson, R.H., 2000, Fluid involvement in normal faulting: *Journal of Geodynamics*, v. 29, p. 469–499, doi: 10.1016/S0264-3707(99)00042-3
- Sigurdsson, H., Houghton, B., McNutt, S., Rymer, H., & Stix, J. (Eds.). (2015). *The Encyclopedia of Volcanoes*. Elsevier. 1456 pp.
- Sillitoe, R.H. (2010). Porphyry copper systems. *Economic geology*, 105(1), 3-41.
- Spencer, J.W. Jr. and Nur, A., 1976. The effects of pressure, temperature and pore water on velocities in westerly granite. *J. Geophys. Res.*, 81 : 899--904.
- Stix, J., & de Moor, J. M. (2018). Understanding and forecasting phreatic eruptions driven by magmatic degassing. *Earth, Planets and Space*, 70(1), 83.
- Tamburello G, Moune S, Allard P, Venugopal S, Robert V, Rosas-Carbajal M, Ucciani G, Deroussi S, Kitou T, Didier T, Komorowski J-C, Beauducel F, de Chabaliier J-B , Lemarchand A., Dessert C., Moretti R. (2019) Spatio-temporal relationships between fumarolic activity, hydrothermal fluidcirculation and geophysical signals at an arc volcano in degassing unrest: LaSoufrière of Guadeloupe (French West Indies). *Geosciences*, 9(11) 480
- Terakawa T., Zoporowski A., Galvan B. and Miller S.A. (2010) High-pressure fluid at hypocentral depths in the L'Aquila region inferred from earthquake focal mechanisms earthquake focal mechanisms. *Geology*, November 2010; v. 38; no. 11; p. 995–998; doi: 10.1130/G31457.1;
- Touboul, M., Bourdon, B., Villemant, B., Boudon, G., & Joron, J. L. (2007). 238 U–230 Th–226 Ra disequilibria in andesitic lavas of the last magmatic eruption of Guadeloupe Soufriere, french Antilles: Processes and timescales of magma differentiation. *Chemical Geology*, 246(3), 181-206.

- Troise, C. (2001). Stress changes associated with volcanic sources: constraints on Kilauea rift dynamics. *J. Volcanol. Geoth. Res.*, 109, (191–203)
- Troise C., De Natale G., Schiavone R., Somma R. and Moretti R. (2019) The Campi Flegrei caldera unrest: Discriminating magma intrusions from hydrothermal effects and implications for possible evolution. *Earth Sci. Rev.*, 188, 108-122.
- Turcotte, D. L., & Schubert, G. (1982). *Geodynamics: Applications of continuum physics to geological problems*, 450 pp. John Wiley, New York
- Ucciani, G. (2015a). *Caractérisation spatiale et temporelle de la sismicité volcanique de la Soufrière de Guadeloupe: relation avec le système hydrothermal* (Doctoral dissertation, Sorbonne Paris Cité).
- Ucciani, G., Beauducel, F., Bouin, M. P., & Nercessian, A. (2015b). Dynamic of the volcanic activity of La Soufrière volcano (Guadeloupe, Lesser Antilles): Evidence for shallow fluid seismic sources. In *AGU Fall Meeting Abstracts*.
- Ventura, G., and Vilardo, G. (1999). Seismic-based estimate of hydraulic parameters at Vesuvius Volcano. *Geophysical research letters*, 26(7), 887-890.
- Villemant, B. et al. The memory of volcanic waters: shallow magma degassing revealed by halogen monitoring in thermal springs of La Soufrière volcano (Guadeloupe, Lesser Antilles). *Earth and Planetary Science Letters* 237, 710{728 (2005).
- Villemant, B. et al. Evidence for a new shallow magma intrusion at La Soufrière of Guadeloupe (Lesser Antilles): insights from long-term geochemical monitoring of halogen-rich hydrothermal fluids. *Journal of Volcanology and Geothermal Research* 285, 247{277 (2014).
- Wadati, K. (1933), On the travel time of earthquake waves, Part II, *Geophys. Mag.* 7, 101-111.
- Walck, M. C. (1988), Three-dimensional  $V_p / V_s$  variations for the Coso Region, California, *Journal of Geophysical Research*, 93(B3), 2047, doi:10.1029/JB093iB03p02047
- Walter, T. R., & Amelung, F. (2007). Volcanic eruptions following  $M \geq 9$  megathrust earthquakes: Implications for the Sumatra-Andaman volcanoes. *Geology*, 35(6), 539-542
- Watt, S. F. L., D. M. Pyle, and T. A. Mather (2009), The influence of great earthquakes on volcanic eruption rate along the Chilean subduction zone, *Earth Planet. Sci. Lett.*, 277, 399–407.
- White, R., & McCausland, W. (2016). Volcano-tectonic earthquakes: A new tool for estimating intrusive volumes and forecasting eruptions. *Journal of Volcanology and Geothermal Research*, 309, 139-155.
- West F.G., Heiken G.H., Homuth E.F., Peterson R.W., Crowe B.M., Wohletz (1978) Tilts Associated with Volcanic Activity Guadeloupe, French West Indies. Fall 1976. LA-7500-MS Informal Report Uc-11, Los Alamos National Laboratories.

- Westbrook, G. K., and W. R. McCann (1986), Subduction of Atlantic lithosphere beneath the Caribbean, in *The Geology of North America*, vol. M, The Western North Atlantic Region, edited by P. R. Vogt and B. E. Tucholke, pp. 341–350, Geol. Soc. of Am., Boulder, Colorado
- Williams, C. A., and G. Wadge (1998). The effects of topography on magma chamber deformation models: Application to Mt. Etna and radar interferometry, *Geophys. Res. Lett.*, 25(10), 1549-1552, doi:10.1029/98gl01136.
- Yang, D., Li, Q. & Zhang, L. Propagation of pore pressure diffusion waves in saturated porous media. *J. Appl. Phys.* 117, 134902 (2015).
- Zlotnicki, J., Feuillard, M. & Hammouya G. (1994) Water circulations on La Soufrière volcano inferred by self-potential surveys (Guadeloupe, Lesser Antilles). Renew of volcanic activity? *Journal of geomagnetism and geoelectricity* 46, 797{813 (1994).
- Zlotnicki, J., Boudon, G., Le Mouél, J.-L., (1992).The volcanic activity of La Soufrière of Guadeloupe (Lesser Antilles): structural and tectonic implications. *J. Volcanol. Geotherm. Res.* 49 (1–2), 91–104.
- Zoback M., F. Rummel, R. Jung, and C. Raleigh (1977) Laboratory Hydraulic Fracturing Experiments in Intact and Pre-Fractured Rock, *Int. J. Rock Mech. Min. Sci. and Geomech.*, 14, 49-58.
- Zollo, A., Marzocchi, W., Capuano, P., Lomax, A., and Iannaccone, G. (2002). Space and time behavior of seismic activity at Mt. Vesuvius volcano, southern Italy. *Bulletin of the Seismological Society of America*, 92(2), 625-640.

**TABLE 1**

Chemical analyses of fumarolic gases from Cratère Sud Central (CSC) fumarole. Note that the 2 May sample was taken at the Cratère Sud Nord (CSN) fumarole, which is conjugated to the CSC one. Errors on concentrations are given beneath the name of each gas species in the table heading. See Supplementary Material for details.

Date	Fumarole	H <sub>2</sub> O	CO <sub>2</sub>	H <sub>2</sub> S	H <sub>2</sub>	CH <sub>4</sub>	CO	N <sub>2</sub>	He	Ar	O <sub>2</sub>
		±2%	±8%	±7%	±5.4%	±4.5%	±4%	±2%	±5.5%	±12.5%	±58%
30/07/2018	CSC	981210	15283	3412	18	0.10	0.06	75	0.14	0.34	0.06
30/07/2018	CSC	982650	13983	3274	18	0.09	0.06	74	0.15	0.35	0.05
21/06/2018	CSC	970960	22321	6574	30	0.14	0.18	112	0.23	0.59	0.43
02/06/2018	CSC	931921	54947	12830	54	0.26	0.35	245	0.36	2.07	0.29
02/06/2018	CSC	909747	74557	15305	59	0.32	0.44	313	0.38	3.07	14.11
02/05/2018	CSN	979901	15990	3777	134	0.08	0.26	195	0.15	2.38	1.05
28/04/2018	CSC	973404	21630	4695	103	0.12	0.33	165	0.25	1.50	0.60
19/04/2018	CSC	975536	19334	4982	61	0.14	0.16	85	0.17	0.49	0.76
23/03/2018	CSC	973775	19639	6427	62	0.15	0.13	94	0.18	0.73	2.04
23/03/2018	CSC	976232	17878	5706	54	0.13	0.12	127	0.16	1.25	0.69
31/01/2018	CSC	963147	30514	6139	45	0.30	0.26	153	0.19	1.39	0.39
24/11/2017	CSC	977581	18134	4171	28	0.18	0.11	85	0.12	0.35	0.09
24/11/2017	CSC	969947	24491	5402	37	0.25	0.17	120	0.17	0.79	0.75

## FIGURE CAPTIONS

**FIGURE 1** Map of the main structures, sites of historical eruptive activity and current hydrothermal activity of the La Soufrière dome (modified after Komorowski et al., 2005; Lesparre et al., 2012; and OVSG-IPGP, 1999-2019, with data taken from Hapel-Lachenaie, 1798; Peyssonnel, 1756; Lherminier, 1815; 1837; Jolivet, 1958; Barrabé et Jolivet, 1958; Sheridan, 1980; Le Guern et al., 1980; Feuillard et al., 1983; Boudon et al., 1988; Komorowski, 2008; Nicollin et al. 2006; Feuillard, 2011; Brothelande et al., 2014; Hincks et al., 2014; Villemant et al., 2014, Allard et al., 2014; Rosas-Carbajal et al., 2016).

**FIGURE 2** Location of the principal fumaroles, extensometry sites and seismometer stations on the summit of La Soufrière. Site codes are as indicated in the text. The white star indicates the location of the highest point. Green arrows indicate directions to several volcanic seismometer stations which are off the current map view. The base image is a georectified orthophoto derived from 2010 IGN aerial photographs.

**FIGURE 3.** Seismic activity of volcanic origin from 1955 to July 2018 (yearly histogram, with exception of 2018). Grey bars are the number of events per year. Black bars represent earthquakes felt by population. The two red lines indicate the released seismic energy, following Feuillard et al. (1983) (solid line) and Hanks and Kanamori (1979) (dashed line). The Feuillard et al. (1983) seismic energy is shown only for the purposes of continuity with the historical record.

**FIGURE 4.** Typical waveforms observed on the vertical component of TAG station, La Soufrière volcano. **Panel a)** “Pure” volcano-tectonic (VT) event. **Panel b)** Hybrid (HY) event (examples from shallow hydrothermal microseismicity and from ~2 km deep events recorded between the two subsequent swarms of April 2018). **Panel c)** example of “monochromatic” long-period (LP) event. **Panel d)** Nested (VE) event, typically of hybrid nature (examples from shallow hydrothermal microseismicity and from the 1<sup>st</sup> February swarm). Note that VE events are observed by the OVSG since the 80’s; because of the absence of a specific class in the literature, the observatory decided since the 90s to name these events as nested (*Volcaniques Emboîtés* in French)

**FIGURE 5. Panel a)** Seismic events observed on a daily basis from 1<sup>st</sup> January 2017 to 31<sup>st</sup> July 2018. **Panel b)** Depths of hypocenters of seismic events observed from 1<sup>st</sup> January 2017 to 31<sup>st</sup> July 2018, based on the adoption of the 1D velocity model of Dorel et al. (1979) and the use of the NonLinLoc algorithm (Lomax et al., 2000) for hypocentral location. **Panel c)** Semi-logarithmic diagram of cumulative (daily basis) seismic energy (Hanks and Kanamori, 1979) released by volcanic activity from 1<sup>st</sup> January 2017 to 31<sup>st</sup> July 2017. Dashed lines mark the seismic swarms of 1<sup>st</sup> February 2018, 16-17 April 2018 and 28-29 April 2018. The seismic energy release is dominated by the  $M_L$  4.1 event of 27 April 2018.

**FIGURE 6.** Maps of the seismic activity recorded within, below and around the La Soufrière dome. **Panel a)** Seismic records in year 2017. **Panel b)** Seismic records from 1<sup>st</sup> January 2018 to 31<sup>st</sup> July 2018. See **Supplementary Figures S1-5** for relevant periods described in text. Blue circles refer to mid-crustal seismic (depth > 6 km b.s.l.) events which occurred off-volcanic axis and with maximum magnitude of 2.5. Results are based on the adoption of the 1D velocity model of Dorel et al. (1979) and the use of the NonLinLoc algorithm (Lomax et al., 2000) for hypocentral location.

**FIGURE 7:** GNSS horizontal velocities from 1995 to 2018 with respect to Guadeloupe archipelago (de Chabalier et al., in preparation). Error ellipses are 95% of confidence. The same scale have been used for south Basse-Terre Island (**Figure 7a**) and La Soufrière volcano (**Figure 7b**). Red box on **figure 7a** give location of **Figure 7b**.

**FIGURE 8. Panel a)** Extensometric measurements during the last year (August 2017-July 2018) at all sites. Note the enhanced dynamics shown by the NAP1 site. **Panel b)** Extensometric measurements at the NAP1 site since network installation (1995) with indication of the four periods, corresponding to different extensional velocities (see text). See **Figure 2** for location of measurement sites.

**FIGURE 9 Panel a)** Temperatures (discrete measurements) at CSC, CSN and NAPN fumarolic sites over the last 26 years. **Panel b)** Temperatures since October 2017; symbols refer to discrete measurements at fumarolic sites, the solid lines refer to continuous measurements at the CSN and CSC (CSN\_c and CSC\_c, respectively) since installation in April 2018. Vertical lines correspond to the onset of the three major seismic swarms of 2018 (1<sup>st</sup> February, 16 April and 27 April).

**FIGURE 10** Steam fluxes determined from gas exit velocities (measured by Pitot tube) from 23 March 2018 to mid-May 2017.

**FIGURE 11.** Molar ratios of relevant chemical species at CSC fumarole since November 2017. Also shown are data from the 1997 sampling in Brombach et al. (2000). Left-side diagrams (**panels a-c**) show maxima on 2 June 2018, associated with the arrival of the most magmatic gas composition. Right-side diagrams (**panels d-f**) show maxima on 28 April 2018, revealing a peak in hydrothermal pressure and temperature related with the onset of the  $M_L$  4.1 earthquake on 27 April 2018. Due to the very low flux at CSC, on 2<sup>nd</sup> May sampling was carried out at the nearby “twin” CSN fumarole. Vertical lines refer to the 2018 seismic swarms. Error bars are  $\pm 11\%$ , or within symbol size if not shown. See Table 1 for errors on concentration measurements and the Supplementary Material for additional details.

**FIGURE 12** SO<sub>2</sub> concentration and concentration ratios at major fumarolic vents (**Figures 1,2**). **Panel a)** Chronogram of the C/S ratio (portable MultiGas station) at South crater (CSC and CSS vents), NAPN, G56,

Tarissan crater lake (TAS). **Panel b**) Chronogram of SO<sub>2</sub> concentration (ppm) at South Crater (permanent MultiGas station).

**FIGURE 13** Chronogram of V<sub>p</sub>/V<sub>s</sub> ratio, calculated from the Wadati method (1933) (**panel c**). Solid lines in each panel represent moving averages of 50 events, according to the expression for seismic rate (see text).

**FIGURE 14** Focal mechanism and moment magnitude of the 27 April M<sub>L</sub> 4.1 earthquake. The 3-component displacement waveforms provided by the 7 seismic stations (indicated by triangles) were used for source parameter determination. The MECAVEL waveform-based method (see Supplementary Material) retrieves an M<sub>w</sub>=3.7 moment magnitude and a pure normal-faulting mechanism, whose strike, dip and rake (for the two possible planes) are shown on the map. The optimal epicentral location (lat=16.08, lon=-61.66) is consistent with the location determined by arrival times (lat=16.06, lon=-61.67), given the frequency range used in the inversion (0.04-0.7Hz).

**FIGURE 15.** Covariation of CO<sub>2</sub>/He with CO<sub>2</sub>/CH<sub>4</sub> (**panel a**), He/CH<sub>4</sub> vs CO<sub>2</sub>/CH<sub>4</sub> (**panel b**), He/CH<sub>4</sub> vs He/H<sub>2</sub>O (**panel c**) and He/CH<sub>4</sub> vs He/H<sub>2</sub>S (**panel d**), showing a He-rich hydrothermal component (meteoric-local hydrothermal line) mixing with a deep, magma-derived gas component. Secondary effects due to either steam condensation or boiling can be observed in **panel c**. These effects due to either scrubbing or hydrothermal sulphur remobilization can be observed in **panel d**. See Supplementary Material for discussion on error bars, which are within symbol size if not shown.

**FIGURE 16.** Chronogram of the hydrothermal sulphur equilibrium (Moretti et al., 2013a, 2017), showing the April perturbation (red ellipse). H<sub>2</sub>S is used for total sulphur.

**FIGURE 17.** Plot of the sum of chemical log-ratios within the H<sub>2</sub>O-CO<sub>2</sub>-H<sub>2</sub>-CO-CH<sub>4</sub> system. See Chiodini and Marini (1998) for details on the construction of the diagram. Present-day data plot within the field of boiling liquids and represent separated vapour phases. Note that data tend to define a baseline at 340°C, corresponding to the base temperature of the current hydrothermal liquid. Different single-step vapour separation (svss) lines are plotted for different temperatures, connecting the saturated liquid and the saturated vapour. Blue lines are common loci for vapour separation occurring at 100°C (solid line) and 300°C (dashed line). Horizontal error bars are ±11%, or within symbol size if not shown. For CSC sample, vertical error bars are ±10%, or within symbol size if not shown. In both cases, errors account for the average long-term external reproducibility on gas concentration measurements in our laboratory, by averaging measurements on replicate successive samplings. Therefore, they greatly exaggerate the purely instrumental error, which is contained within symbol size. See also Table 1 for errors on concentration measurements and the Supplementary Material for additional details. For data from Brombach et al. (2000) and Chevrier et al. (1976) error bars are given by the strong uncertainty in CH<sub>4</sub> content (see text).

**FIGURE 18.** Conceptual model of the La Soufrière of Guadeloupe and the February-April 2018 unrest episode. The conceptual model summarizes the evolution of observed geophysical and geochemical processes, including the build-up of pore pressures of thermal derivation.

Journal Pre-proof

## SUPPLEMENTARY MATERIAL

### Source characterization of the 27 April 2018 Main shock

For the source characterization of the main shock, we use the MECAVEL waveform-based technique (see previous applications in e.g. Vaca et al., 2019 or Grandin et al., 2017). As other methods (e.g. FMNEAR, Delouis, 2014; ISOLA, Zahradník et al., 2008), MECAVEL method searches for the set of source parameters leading to the optimal waveform reconstruction. Waveforms are computed with the discrete wavenumber method (Bouchon, 1981) inside a 1D velocity model. A specificity of the MECAVEL method is to optimize this 1D model simultaneously with the searched source parameters (strike, dip, and rake of the focal mechanism, centroid location, source origin time and duration, and moment magnitude). Within the MECAVEL method, the three-component displacement waveforms are bandpassed between a low frequency ( $F_{c1}$ ) and a high frequency ( $F_{c2}$ ) threshold.  $F_{c1}$  is typically chosen above the low-frequency noise that may affect the waveforms for a moderate earthquake and  $F_{c2}$  is mostly controlled by the limited accuracy of the simplified 1D structure model. Here  $F_{c1}$  and  $F_{c2}$  are taken equal to 0.04Hz and 0.07Hz, respectively.

Waveform agreement between observed and modelled waveforms is shown in **Supplementary Figure S7**. The corresponding optimal model has the following characteristics. (1) Focal mechanism (see **Figure 14**) shows a purely normal-faulting fault with a NW-SE azimuth. (2) moment magnitude is found equal to 3.65; such differences with the local magnitude ( $M_l=4.1$ ) have already been observed in this magnitude range in other contexts (e.g. Vaca et al., 2019). (3) The optimal epicentral location ( $lat=16.08$ ,  $lon=-61.66$ ) is consistent with the location determined by arrival times ( $lat=16.06$ ,  $lon=-61.67$ ), given the frequency range used in the inversion. (4) The optimal depth is shallow, equal to 3.8km. As the inversion does not take into account the topography on which the two closest stations are installed (CDE and LKG, located at an elevation of 1250m and 1374m, respectively) this depth is expected to be biased toward deeper values. The difference with the value given by the arrival times determination ( $1.9 \pm 0.5$ km) is therefore not considered significant.

### Fumarolic sampling and analysis

Gas samples were collected from fumaroles in Giggenbach flasks using the standard methods described by Giggenbach and Goguel (1989). The glass flasks were equipped with a Teflon stopcock and contained approximately 50 ml of 5N NaOH solution. The gas samples were analysed at the Gas and Water Analysis Laboratory at the OVSG-IPGP (Guadeloupe, FWI). The headspace gases ( $N_2$ ,  $O_2$ ,  $CO$ ,  $H_2$ ,  $He$ ,  $Ar$ ,  $Ne$ ,  $CH_4$ ) were analysed using a quadrupole mass spectrometer (Pfeiffer Vacuum OMNISTAR). The instrument is configured for routine analysis with accurate de-convolution of mass interferences. Concentrations are obtained by calibration with a set of standard gas mixtures. Water vapour and the acidic gas species dissolved in the alkaline solution.  $H_2O$  is determined by gravimetric weighing.  $CO_2$  was analysed by volumetric wet chemistry involving the use of acidimetric titration with 0.1 N HCl (for  $CO_2$  as  $CO_3^{2-}$ ). Total sulphur, given as  $H_2S$  (Table 1) was analysed with ion

(Dionex™) chromatography. Analytical uncertainties (see Table 1) are within  $\pm 1$ –5%. However, for error bars given in figures we also included the average long-term external reproducibility on gas concentration measurements in our laboratory, by averaging measurements on replicate successive samplings at la Soufrière CSC site. This gives  $\pm 8$  for the steam/gas ratio,  $\pm 11\%$  for C/S,  $\pm 9\%$  for  $\text{CO}_2/\text{CH}_4$ ,  $\pm 7\%$  for He/ $\text{CH}_4$ ,  $\pm 6\%$  for  $\text{H}_2/\text{H}_2\text{O}$ ,  $\pm 9\%$  for  $\text{CO}/\text{CO}_2$ ,  $\pm 10\%$  for  $\text{CO}_2/\text{He}$ ,  $\pm 5\%$  for  $\text{H}_2\text{O}/\text{CH}_4$  and  $\pm 8\%$  for S/ $\text{CH}_4$ .

## SUPPLEMENTARY FIGURE CAPTIONS

**SUPPLEMENTARY FIGURE S1.** 2-6 January 2018 swarm. Blue circles refer to mid-crustal seismic (depth > 6 km b.s.l.) events which occurred off-volcanic axis (maximum magnitude was 2.4). The 1D velocity model of Dorel et al. (1979) and the NonLinLoc algorithm (Lomax et al., 2000) were used for hypocentral location.

**SUPPLEMENTARY FIGURE S2.** 1 February 2018 swarm. The 1D velocity model of Dorel et al. (1979) and the NonLinLoc algorithm (Lomax et al., 2000) were used for hypocentral location.

**SUPPLEMENTARY FIGURE S3.** 16-17 April 2018 swarm. The 1D velocity model of Dorel et al. (1979) and the NonLinLoc algorithm (Lomax et al., 2000) were used for hypocentral location.

**SUPPLEMENTARY FIGURE S4.** 27-28 April 2018 swarm. The 1D velocity model of Dorel et al. (1979) and the NonLinLoc algorithm (Lomax et al., 2000) were used for hypocentral location.

**SUPPLEMENTARY FIGURE S5.** May-July 2018 activity. The 1D velocity model of Dorel et al. (1979) and the NonLinLoc algorithm (Lomax et al., 2000) were used for hypocentral location.

**SUPPLEMENTARY FIGURE S6:** Agreement of the 3D displacement waveforms (data are shown in black and synthetics in red) for the best source model determined by the MECAVEL method. Location of the 7 stations can be seen in **Figure 14**. The horizontal components of DHS station have not been used due to their low quality in the selected [0.04Hz-0.07Hz] frequency range.

**SUPPLEMENTARY FIGURE S7:** Chronogram summarizing data, observations and elaborations reported in main text and figures for the five periods of interest (hence since January 1<sup>st</sup>, 2018; see section 3 and Figure 5) and key seismic events (vertical gray bars). Cumulative seismic energy in **panel a**) is based on Hanks and Kanamori (1979). Mean earthquake foci depths in **panel b**) are based on a 25-event moving average. Fracture opening at NAP1 site in **panel c**) is relative to the November 2017 value. Solid black circles ( $\text{SO}_2/\text{H}_2\text{S}$ ) refer to portable MultiGAS measurements in **panel d**); fumarolic  $\text{CO}_2/\text{He}$ ; He/ $\text{CH}_4$  and  $\text{CO}_2/\text{CH}_4$  ratios and  $\log K_4$  values in the

same panel have been averaged in case of multiple samples of the same day (see Table 1). Computed overpressures and temperatures in **panel e**) refer to the two-phase hydrothermal reservoir feeding summit fumaroles, with overpressure being referred to the November 2017 value (148 bar at 340°C); the overpressure spike occurring on 27-28 April 2018 refers to the off-volcanic axis location of the 27 April earthquake (see figure 18).

### Supplementary References

Bouchon, M., 1981. A simple method to calculate Green's functions for elastic layered media, *Bull. Seismol. Soc. Am.*, 71(4), 959–971.

Delouis, B., 2014. FMNEAR: Determination of focal mechanism and first estimate of rupture directivity using near-source records and a linear distribution of point sources, *Bull. Seismol. Soc. Am.*, 104, 1479–1500.

Grandin, R., Vallée, M., Lacassin, R., 2017. Rupture process of the Oklahoma Mw 5.7 Pawnee earthquake from Sentinel-1 InSAR and seismological data, *Seismol. Res. Lett.*, 88, 994-1004.

Vaca, S., Vallée, M., Nocquet, J.-M., Alvarado, A., 2019. Active deformation in Ecuador enlightened by a new waveform-based catalog of earthquake focal mechanisms, *Journal of South American Earth Sciences*, minor revision.

Zahradník, J., Janský, J., Plicka, V., 2008. Detailed waveform inversion for moment tensors of M~4 events; examples from the Corinth Gulf, Greece, *Bull. Seismol. Soc. Am.*, 98, 2756-2771.

**AUTHOR STATEMENT**

**Roberto Moretti** Conceptualization, Investigation, Project administration, Formal analysis, Writing - Original Draft , Writing - Review & Editing, Supervision, Visualization, Data Curation, Validation

**Jean-Christophe Komorowski** Conceptualization, Project administration, Funding acquisition, Writing - Review & Editing, Supervision

**Guillaume Ucciani** Formal analysis, Visualization, Investigation,

**Séverine Moune** Visualization, Data Curation; Conceptualization, Investigation, Writing - Review & Editing

**David Jessop** Formal analysis, Data Curation, Conceptualization, Investigation, Writing - Review & Editing

**Jean-Bernard de Chabaliér** Formal analysis, Visualization, Data Curation, Investigation

**François Beauducel** Formal analysis, Software, Investigation, Visualization

**Magali Bonifacie** Formal analysis, Investigation

**Arnaud Burtin** Data Curation, Validation

**Martin Vallée** Formal analysis, Software, Visualization

**Sebastien Deroussi** Resources, Data Curation, Investigation, Validation

**Vincent Robert** Resources, Formal analysis, Data Curation, Validation

**Dominique Gibert** Data Curation, Validation

**Tristan Didier** Resources, Data Curation, Validation

**Thierry Kitou** Resources, Data Curation, Validation

**Nathalie Feuillet** Conceptualization

**Patrick Allard** Conceptualization, Writing - Review & Editing

**Giancarlo Tamburello** Writing - Review & Editing

**Tara Shreve** Writing - Review & Editing

**Jean-Marie Saurel** Data Curation, Validation

**Arnaud Lemarchand** Funding acquisition, Data Curation, Validation

**Marina Rosas-Carbajal** Writing - Review & Editing

**Pierre Agrinier** Formal analysis

**Anne Le Friant** Project administration, Funding acquisition, Supervision

**Marc Chaussidon** Project administration, Funding acquisition, Writing - Review & Editing, Supervision

Journal Pre-proof

**Declaration of interests**

The authors declare that they have no known competing financial interests or personal relationships that could have appeared to influence the work reported in this paper.

The authors declare the following financial interests/personal relationships which may be considered as potential competing interests:

Journal Pre-proof

## HIGHLIGHTS

- Distal seismicity due to pore pressure build-up and hydroshearing/hydrofracturing
- Permeability of dome fractures and faults is key for phreatic activity
- Ratios of non-condensable gases disclose involved gas end-members
- Joint geochemical and geophysical assessment mandatory to assess role of fluids
- The hydrothermal system reacts very quickly to deep fluid infiltration

Journal Pre-proof

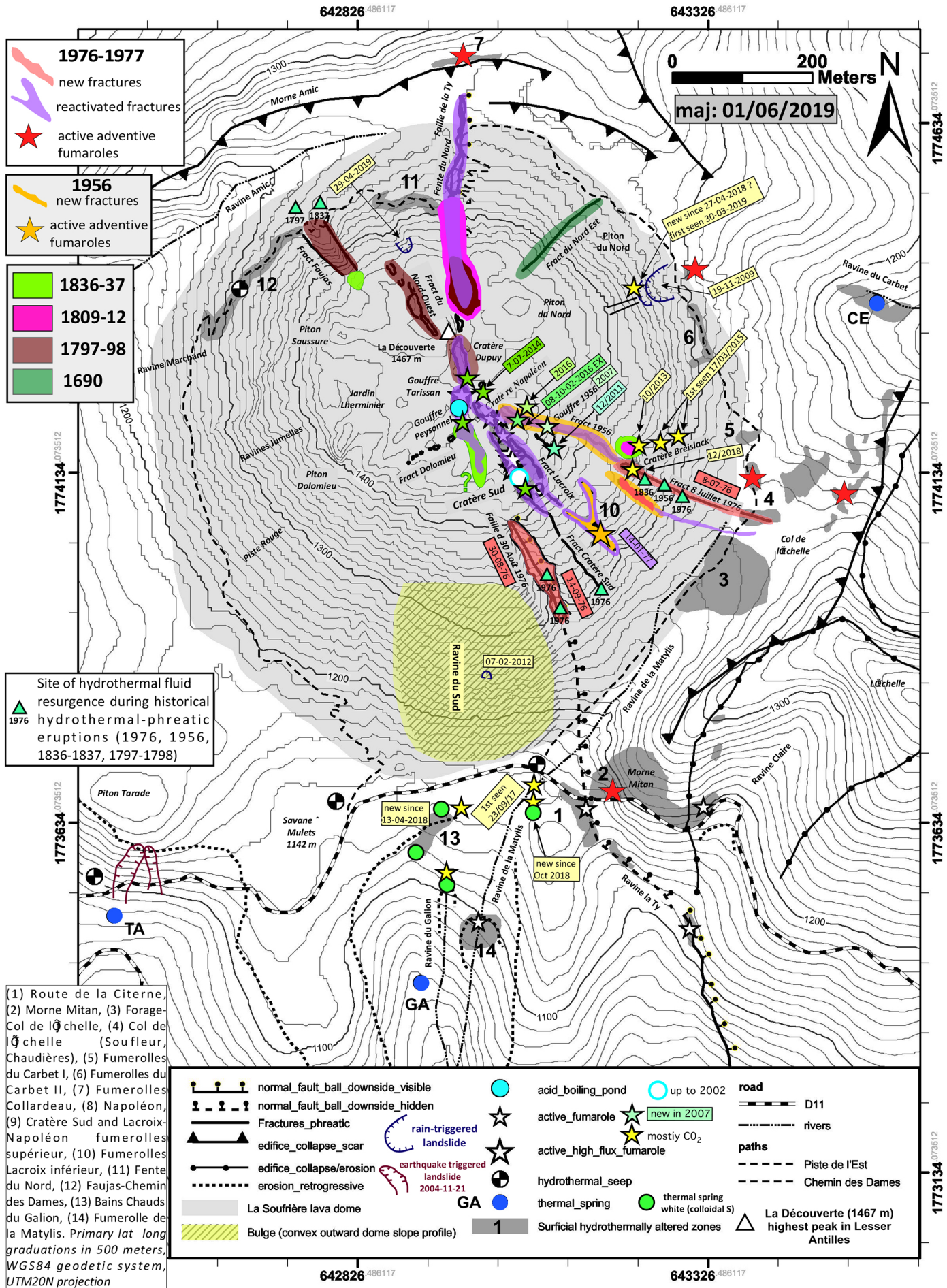


Figure 1

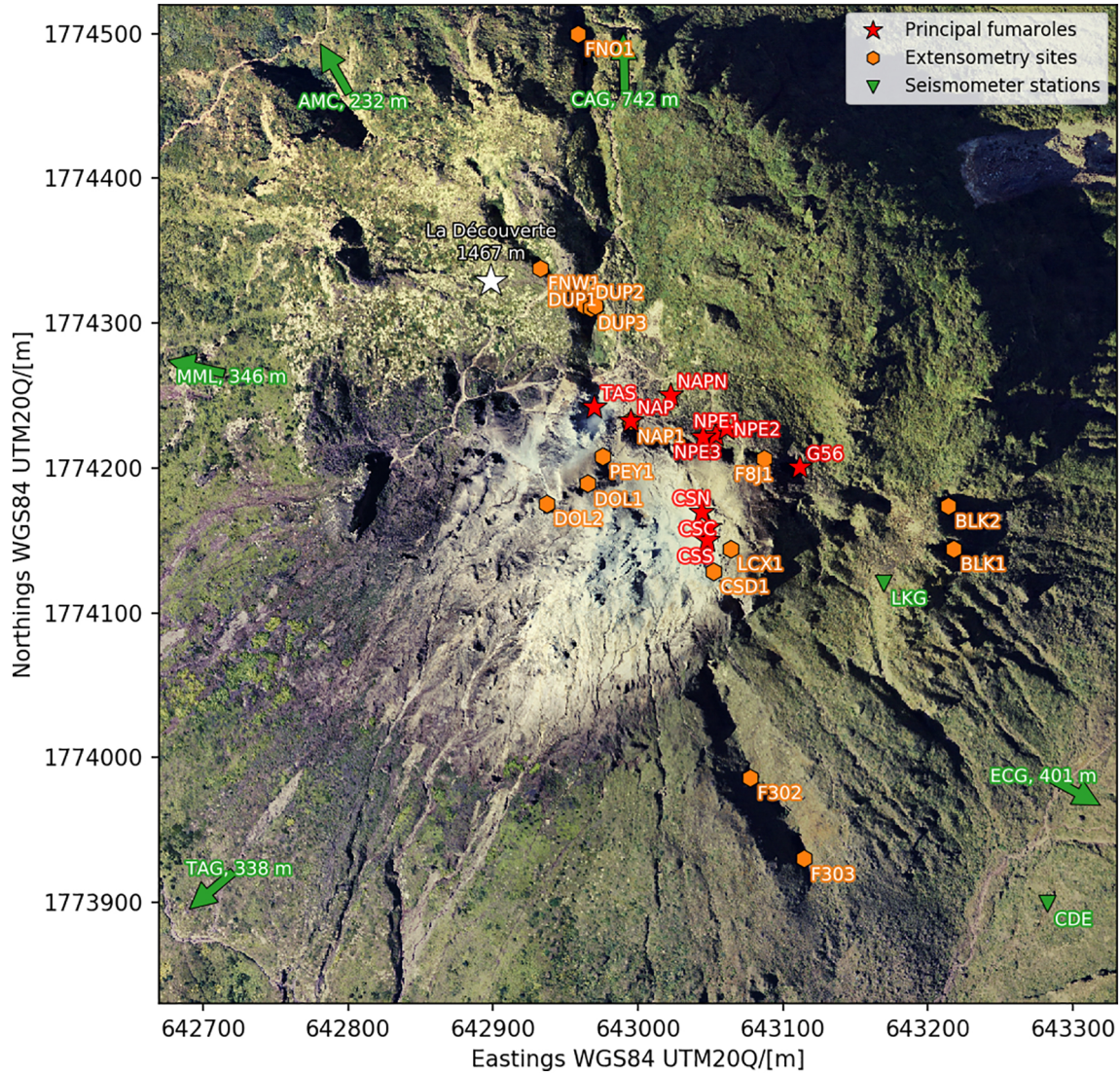


Figure 2

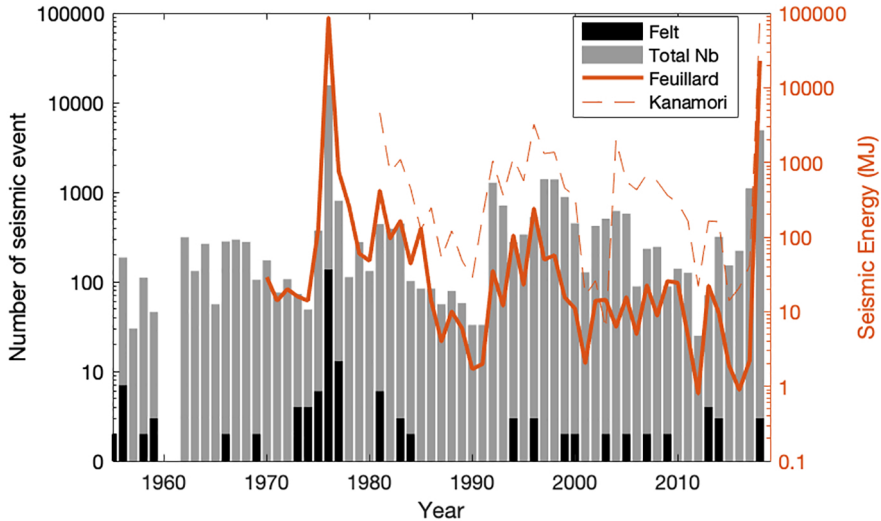


Figure 3

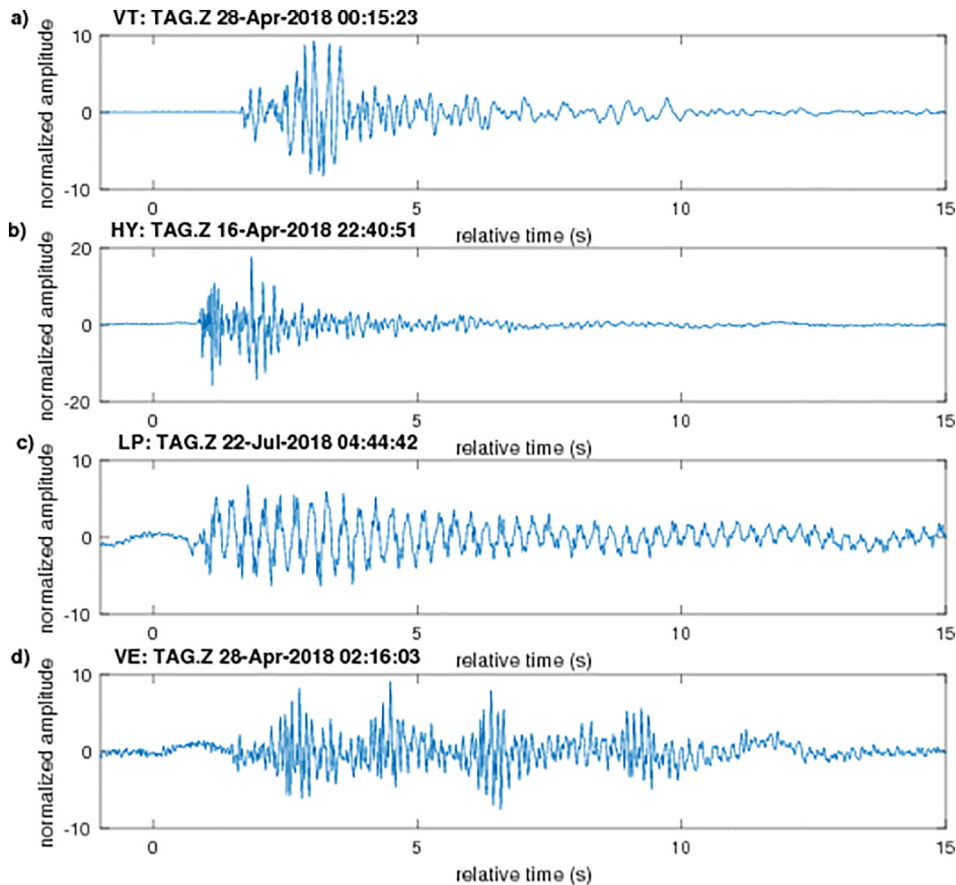


Figure 4

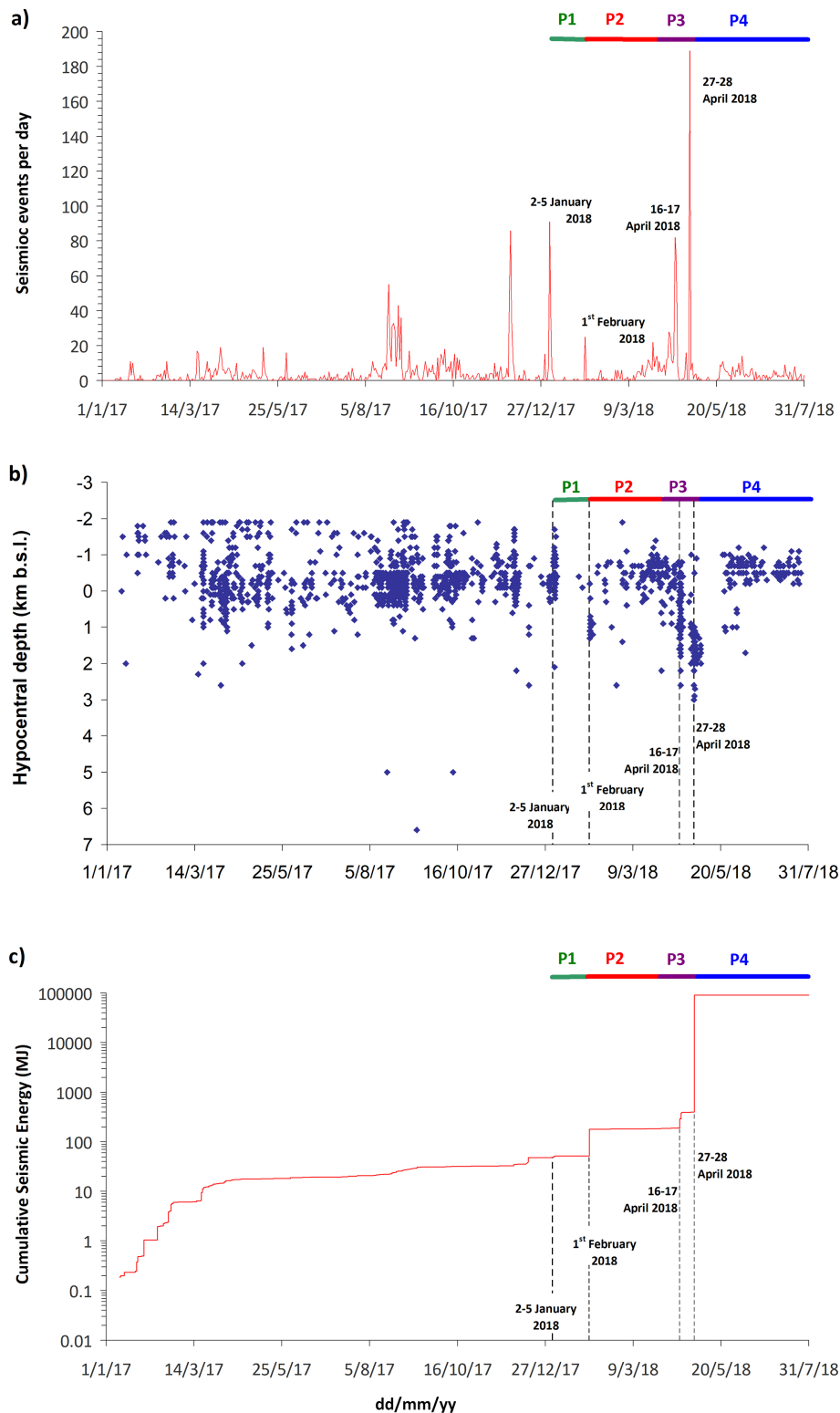


Figure 5

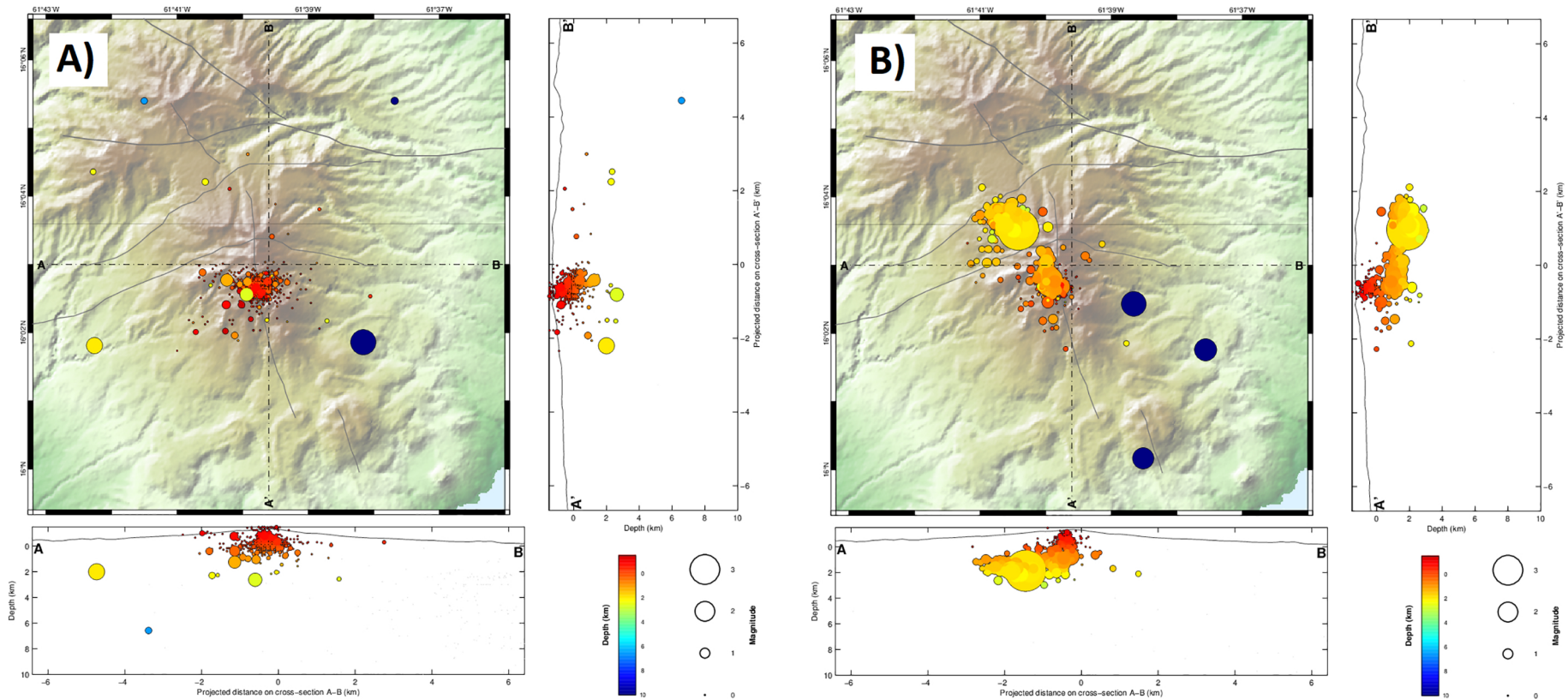


Figure 6

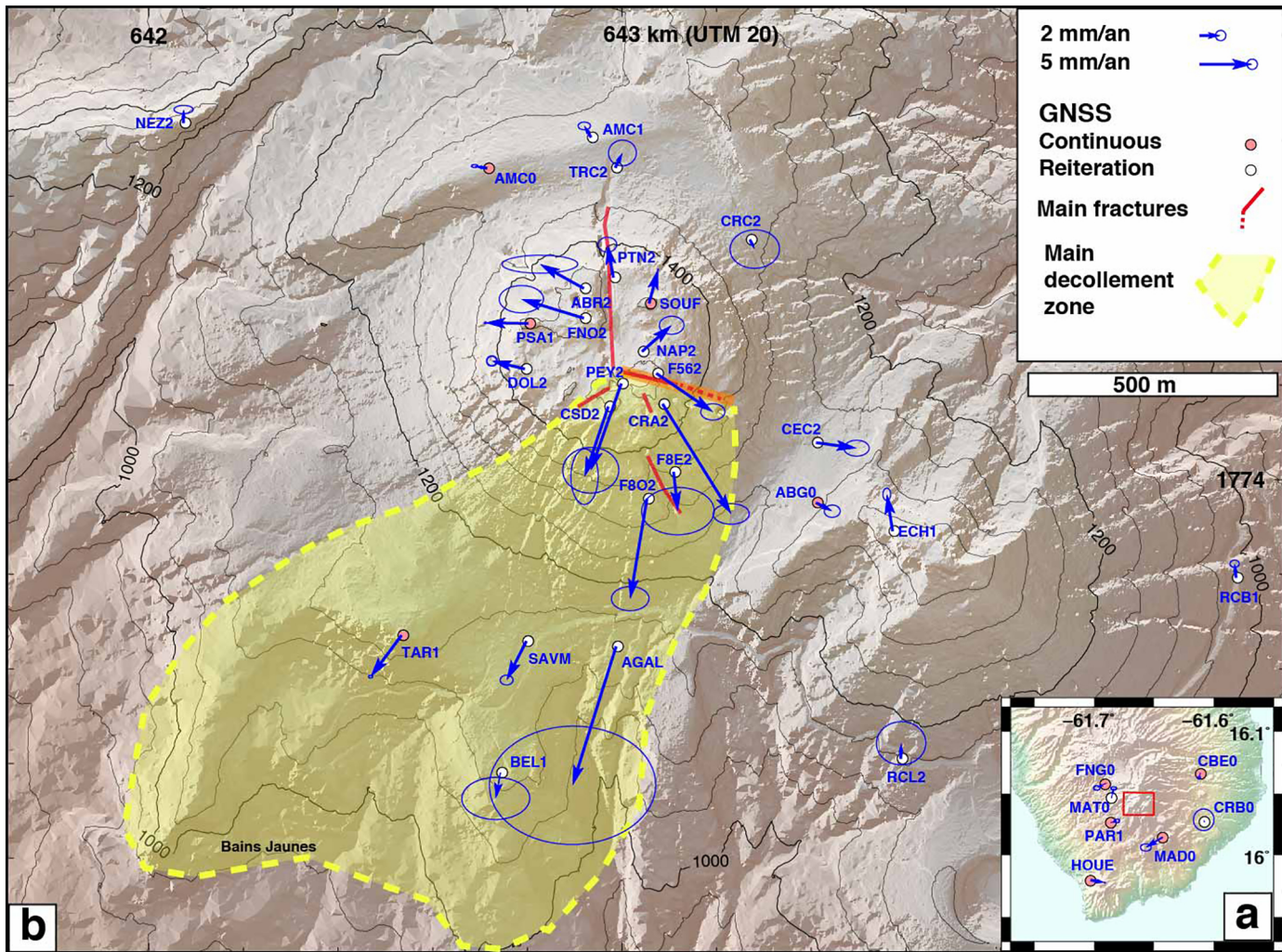


Figure 7

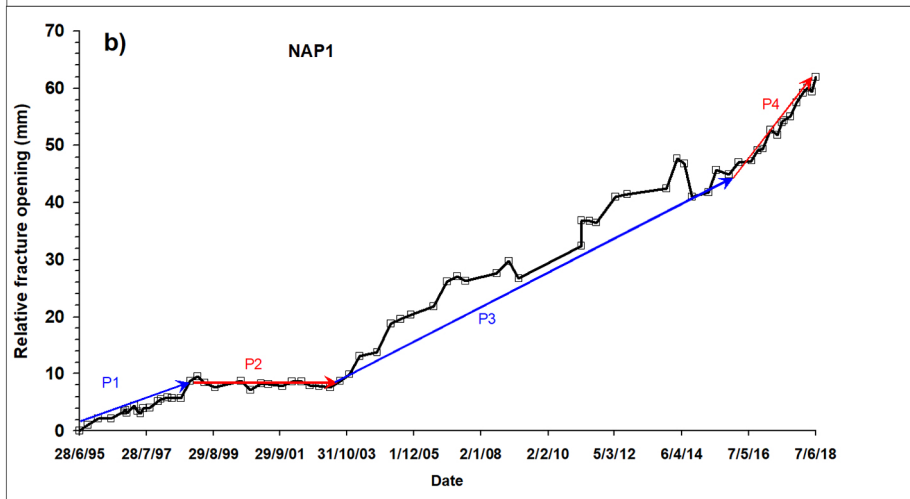
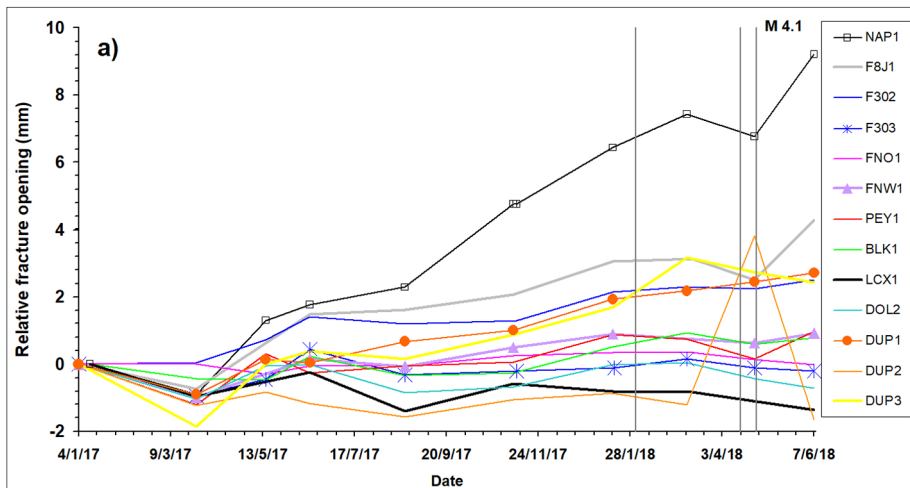


Figure 8

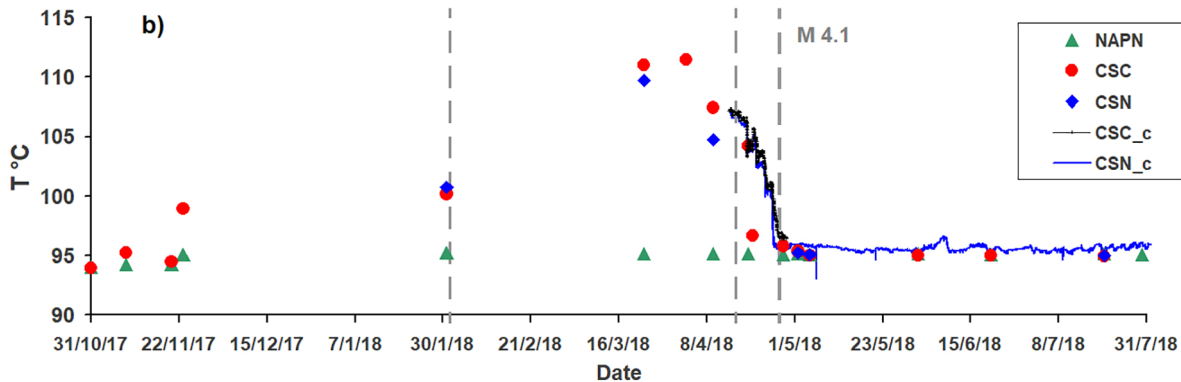
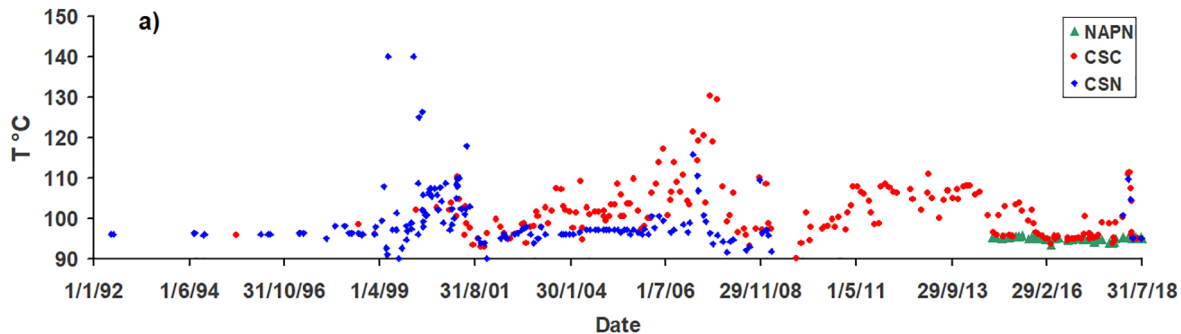


Figure 9

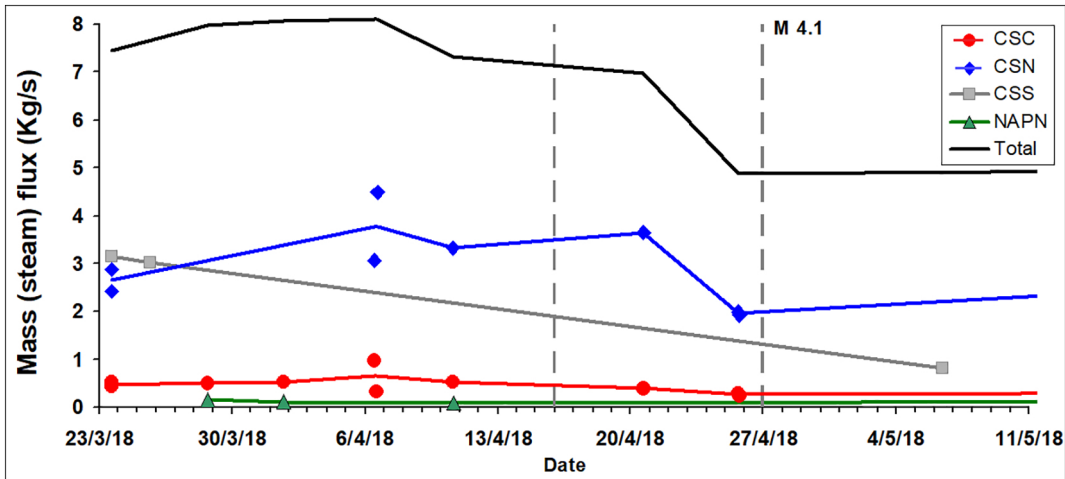


Figure 10

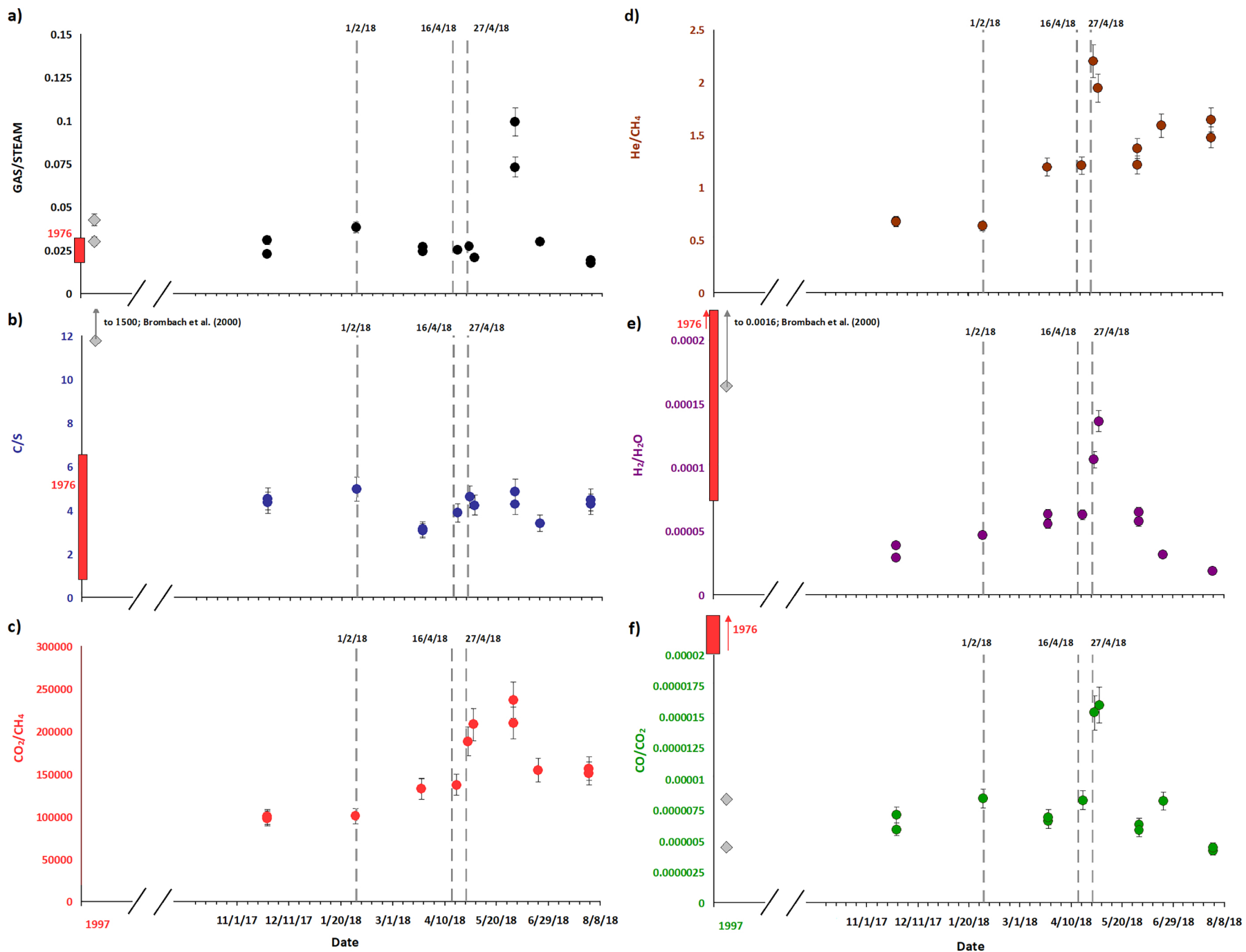


Figure 11

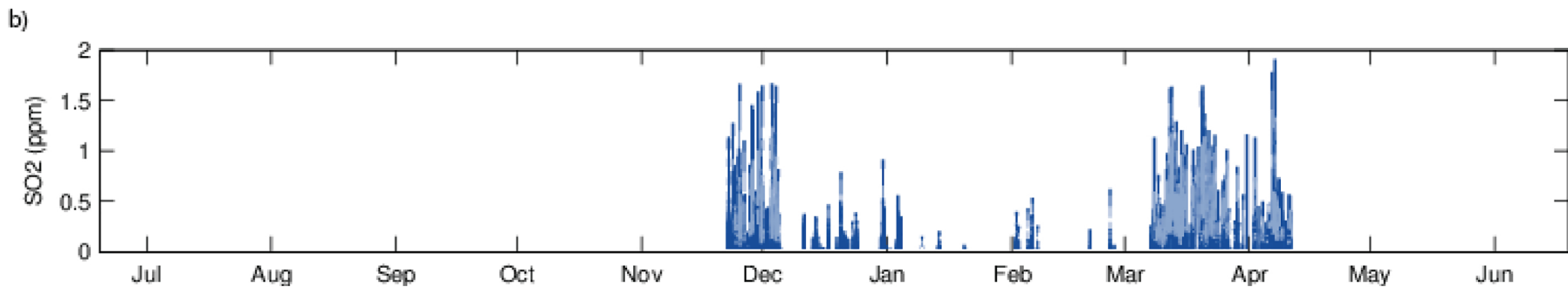
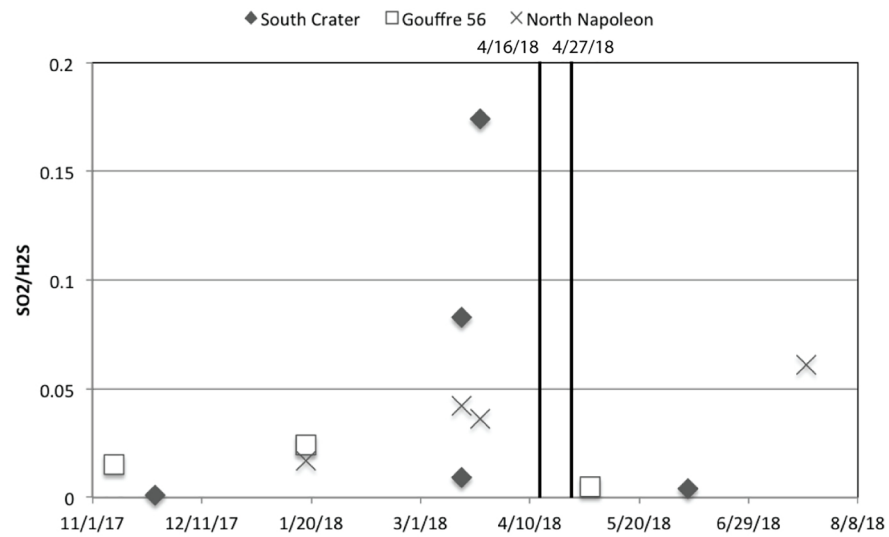
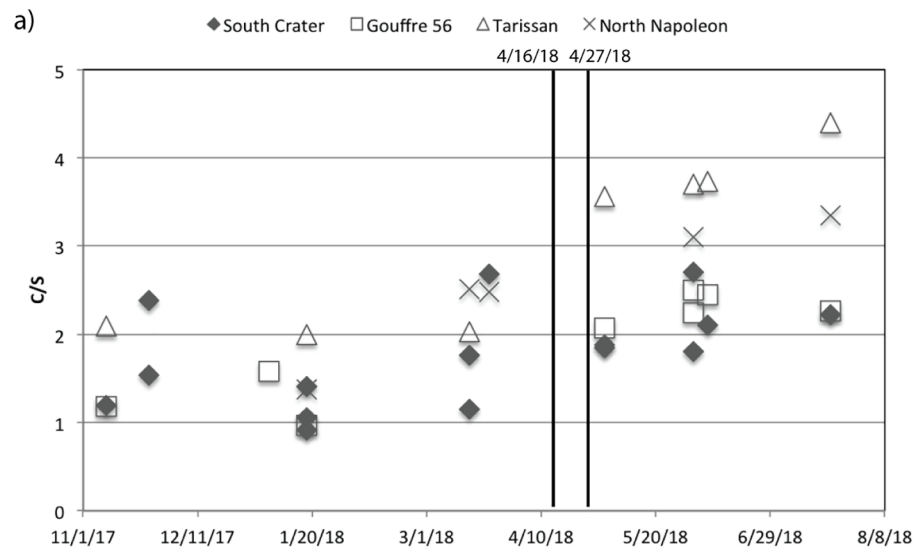


Figure 12

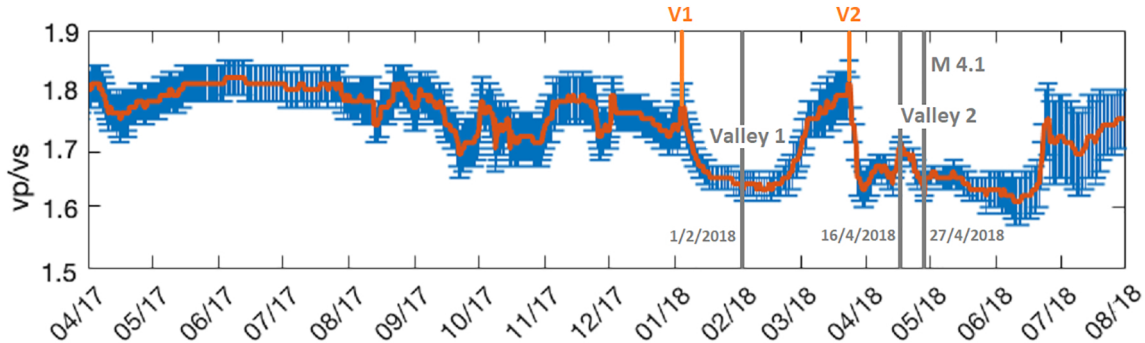


Figure 13

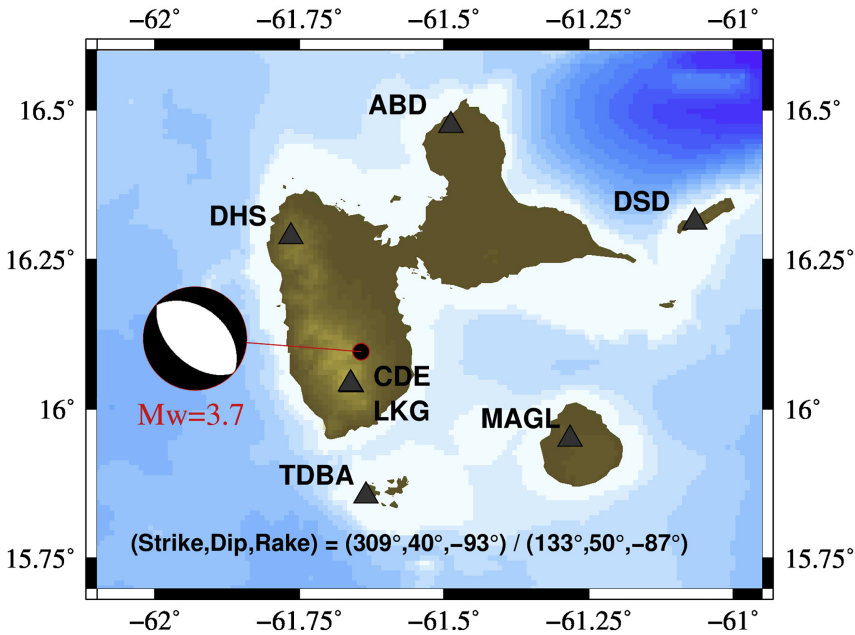


Figure 14



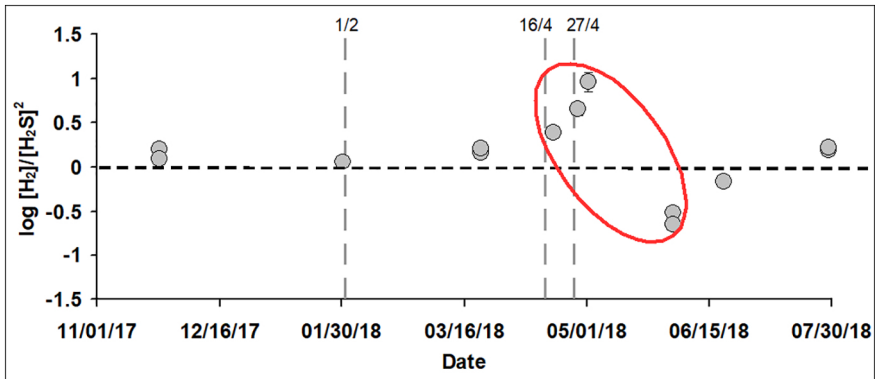


Figure 16

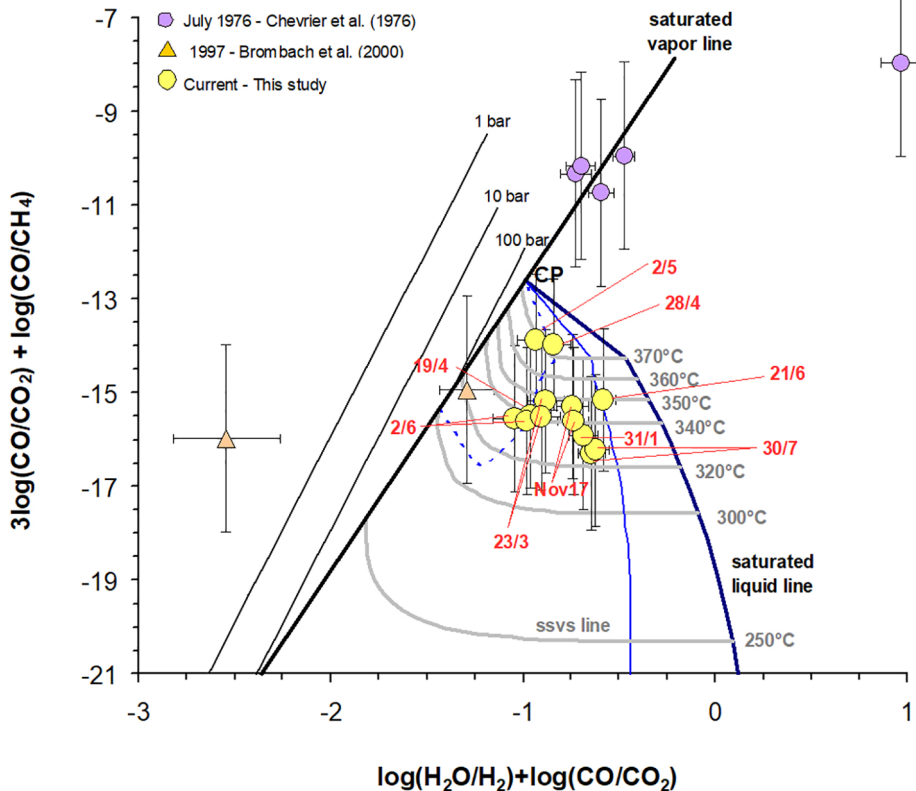


Figure 17

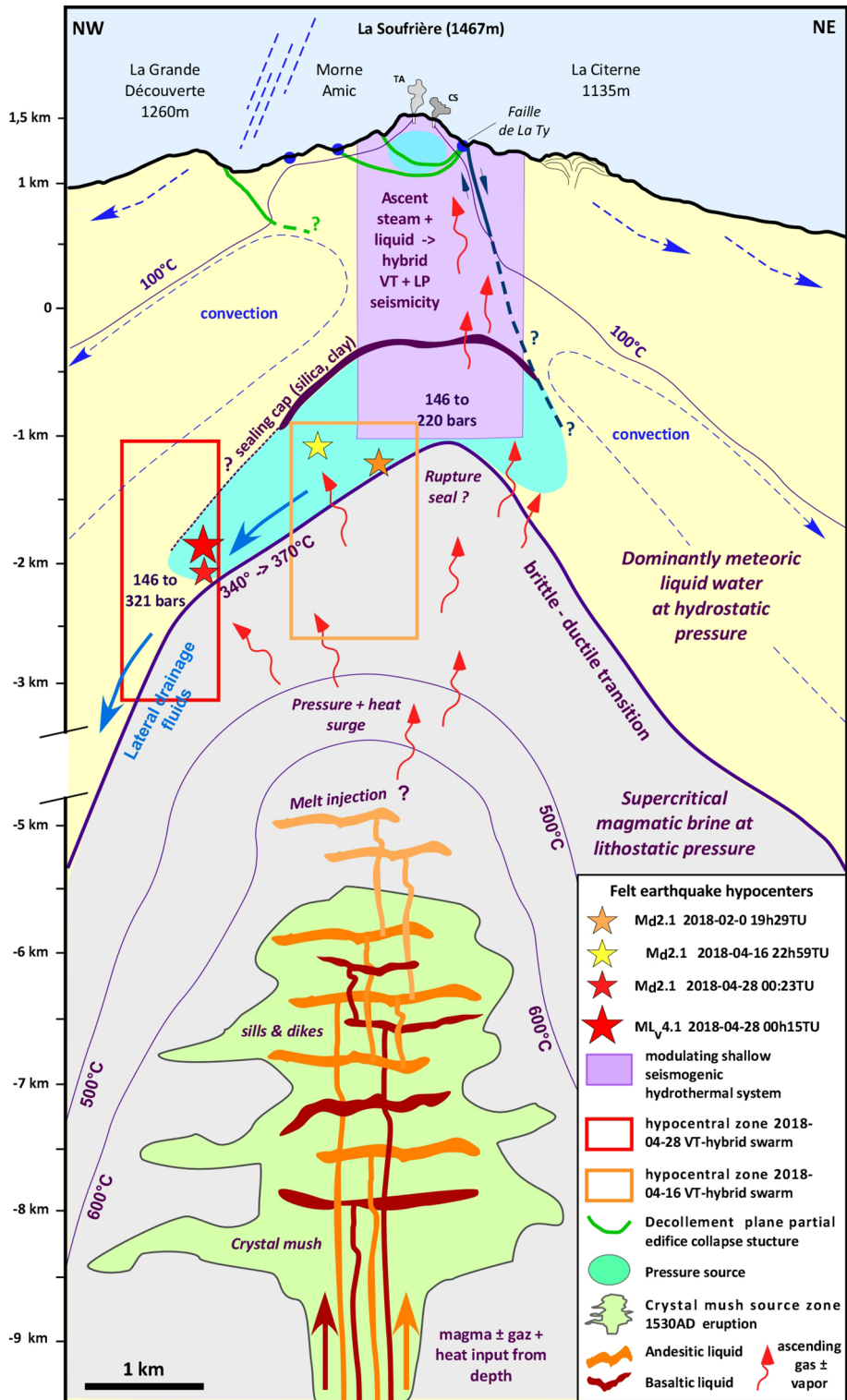


Figure 18